UC Irvine

UC Irvine Previously Published Works

Title

Improving topological cluster reconstruction using calorimeter cell timing in ATLAS

Permalink

https://escholarship.org/uc/item/8bb3q8sc

Journal

European Physical Journal C, 84(5)

ISSN

1434-6044

Authors

Aad, G

Abbott, B

Abeling, K

et al.

Publication Date

2024

DOI

10.1140/epjc/s10052-024-12657-1

Copyright Information

This work is made available under the terms of a Creative Commons Attribution-NonCommercial License, available at https://creativecommons.org/licenses/by-nc/4.0/

Peer reviewed

eScholarship.org Powered by the California Digital Library
University of California

Eur. Phys. J. C (2024) 84:455
https://doi.org/10.1140/epjc/s10052-024-12657-1

THE EUROPEAN PHYSICAL JOURNAL C

Regular Article - Experimental Physics

Improving topological cluster reconstruction using calorimeter cell timing in ATLAS

ATLAS Collaboration[⋆]

CERN, 1211 Geneva 23, Switzerland

Received: 26 October 2023 / Accepted: 10 March 2024 / Published online: 3 May 2024
© CERN for the benefit of the ATLAS Collaboration 2024

Abstract Clusters of topologically connected calorimeter cells around cells with large absolute signal-to-noise ratio (*topo-clusters*) are the basis for calorimeter signal reconstruction in the ATLAS experiment. Topological cell clustering has proven performant in LHC Runs 1 and 2. It is, however, susceptible to *out-of-time pile-up* of signals from soft collisions outside the 25 ns proton-bunch-crossing window associated with the event's hard collision. To reduce this effect, a calorimeter-cell timing criterion was added to the signal-to-noise ratio requirement in the clustering algorithm. Multiple versions of this criterion were tested by reconstructing hadronic signals in simulated events and Run 2 ATLAS data. The preferred version is found to reduce the out-of-time pile-up jet multiplicity by ∼50% for jet $p_{\mathrm{T}} \sim 20$ GeV and by ∼80% for jet $p_{\mathrm{T}} \gtrsim 50$ GeV, while not disrupting the reconstruction of hadronic signals of interest, and improving the jet energy resolution by up to 5% for $20 < p_{\mathrm{T}} < 30$ GeV. Pile-up is also suppressed for other physics objects based on topo-clusters (electrons, photons, τ-leptons), reducing the overall event size on disk by about 6% in early Run 3 pile-up conditions. Offline reconstruction for Run 3 includes the timing requirement.

Contents

1 Introduction

The ATLAS experiment [1], one of the four major experiments at the LHC [2], relies on the precise measurement of particle showers as the starting point for physics object reconstruction. Calorimeter showers are reconstructed by clustering groups of topologically connected calorimeter cells, the first step in this process involving cells with high absolute energy relative to calorimeter noise [3]. The produced clusters are referred to as *topo-clusters* and provide the input to the reconstruction of a number of physics objects, including jets, electrons, τ-leptons and missing transverse momentum ($E_{\mathrm{T}}^{\mathrm{miss}}$). The topological cell clustering algorithm is well established and performed very well during the LHC Run 1 and Run 2 data-taking periods, from 2010 to 2012 and 2015 to 2018 respectively. However, further improvement is possible, especially in view of the increased luminosity foreseen in LHC Run 3 and beyond.

At the LHC, bunches of about 10^{11} protons collide every 25 ns, giving rise to multiple pp interactions in each *bunch-crossing*.[1] Signals from particles produced in additional soft pp collisions pile up on top of those from the pp *hard-scattering* that triggered the ATLAS data-recording process. If the additional particles are produced in the same bunch-crossing that produced the recorded event's pp hard-

⋆ e-mail: atlas.publications@cern.ch

[1] The average number of pp collisions per bunch-crossing was 25 in 2016, 38 in 2017 and 36 in 2018 data-taking [4].

scattering, they are referred to as *in-time pile-up*, whereas if they are produced in the previous or next bunch-crossings they are called *out-of-time pile-up*. Calorimeter signals are sensitive to both in-time and out-of-time pile-up, which can result in the formation of additional topo-clusters, as well as spurious contributions to those originating from the hard scattering. Multiple pile-up suppression techniques have been studied in ATLAS, such as the grooming algorithms used for the reconstruction of boosted objects [5–7] or the Constituent Subtraction [8] and Soft Killer [9] methods used prior to jet reconstruction [10]. These methods, however, are all applied after topo-cluster reconstruction, whereas in this paper a low-level mitigation technique is explored with the goal of reducing pile-up contributions at cell level while building the topo-clusters.

The ATLAS calorimeters provide a measurement of the signal time, in addition to the deposited energy. In this paper, the topo-clustering algorithm is modified by applying a calorimeter time-measurement selection criterion (the *time cut* in the following) to cells with large signal-to-noise ratio in order to reject contributions from out-of-time pile-up. Multiple versions of the time cut were compared and tested on both Monte Carlo (MC) simulated events and a sample of ATLAS data events. An Upper Limit, switching off the time cut for very high energy signals, was explored and it was adopted as a safety measure to avoid rejecting potential new-physics processes which might produce out-of-time signals. The performance of the new algorithm has been tested in the context of jet reconstruction, focusing on the suppression of pile-up-initiated jets as well as its effects on jet energy calibration and resolution.

The rest of this paper is organised as follows. Section 2 describes the detector. Section 3 lists the data and MC samples used for this analysis. Section 4 describes the current topo-cluster reconstruction algorithm and Sect. 5 introduces the time cut. Section 6 discusses the time cut's performance on topo-cluster and jet kinematics as evaluated using MC samples. Section 7 discusses the time cut's performance on ATLAS data taken during Run 2 of the LHC, including checks for possible time-cut inefficiency and the cut's impact on the ATLAS event size. Conclusions are presented in Sect. 8.

2 ATLAS detector

The ATLAS detector [1] at the LHC covers nearly the entire solid angle around the collision point.[2] It consists of an inner tracking detector surrounded by a thin superconducting solenoid, electromagnetic and hadron calorimeters, and a muon spectrometer incorporating three large superconducting air-core toroidal magnets.

The inner-detector system is immersed in a 2 T axial magnetic field and provides charged-particle tracking in the range $|\eta| < 2.5$. The high-granularity silicon pixel detector covers the vertex region and typically provides four measurements per track, the first hit normally being in the insertable B-layer [11,12] installed before Run 2. It is followed by the silicon microstrip tracker, which usually provides eight measurements per track. These silicon detectors are complemented by the transition radiation tracker (TRT), which enables radially extended track reconstruction up to $|\eta| = 2.0$. The TRT also provides electron identification information based on the fraction of hits (typically 30 in total) above a higher energy-deposit threshold corresponding to transition radiation.

The calorimeter system covers the pseudorapidity range $|\eta| < 4.9$. Within the region $|\eta| < 3.2$, electromagnetic (EM) calorimetry is provided by barrel and endcap high-granularity lead/liquid-argon (LAr) calorimeters, with an additional thin LAr presampler covering $|\eta| < 1.8$ to correct for energy loss in material upstream of the calorimeters. Hadron calorimetry is provided by the steel/scintillator-tile calorimeter (*Tile calorimeter* in the following), segmented into three barrel structures within $|\eta| < 1.7$, and two copper/LAr hadronic endcap calorimeters. The solid angle coverage is completed with forward copper/LAr and tungsten/LAr calorimeter modules optimised for electromagnetic and hadronic energy measurements respectively. Electromagnetic and hadronic calorimeters based on LAr technology are collectively referred to as the *LAr calorimeter* in the following. Additional details about the timing measurements in the ATLAS calorimeters are provided in Sect. 2.1.

The muon spectrometer comprises separate trigger and high-precision tracking chambers measuring the deflection of muons in a magnetic field generated by the superconducting air-core toroidal magnets. The field integral of the toroids ranges between 2.0 and 6.0 T · m across most of the detector. Three layers of precision chambers, each consisting of layers of monitored drift tubes, cover the region $|\eta| < 2.7$, complemented by cathode-strip chambers in the forward region, where the background is highest. The muon trigger system covers the range $|\eta| < 2.4$ with resistive-plate chambers in the barrel, and thin-gap chambers in the endcap regions.

[2] ATLAS uses a right-handed coordinate system with its origin at the nominal interaction point (IP) in the centre of the detector and the z-axis along the beam pipe. The x-axis points from the IP to the centre of the LHC ring, and the y-axis points upwards. Cylindrical coordinates (r, ϕ) are used in the transverse plane, ϕ being the azimuthal angle around the z-axis. The pseudorapidity is defined in terms of the polar angle θ as $\eta = -\ln\tan(\theta/2)$. Angular distance is measured in units of $\Delta R \equiv \sqrt{(\Delta\eta)^2 + (\Delta\phi)^2}$. The rapidity $y = \frac{1}{2}\ln\left(\frac{E+p_z}{E-p_z}\right)$ can also be used for kinematic distributions instead of η, as it accounts for the particle's mass.

Interesting events are selected by the first-level (L1) trigger system implemented in custom hardware, followed by selections made by algorithms implemented in software in the high-level trigger (HLT) [13]. The first-level trigger accepts events from the 40 MHz bunch-crossings at a rate below 100 kHz, which the high-level trigger reduces in order to record events to disk at about 1 kHz. Triggers with acceptance rates that are too large are prescaled, i.e. only a fraction of the events satisfying the trigger are written to disk. The prescale factor is then applied to estimate the original rate. An extensive software suite [14] is used in data simulation, in the reconstruction and analysis of real and simulated data, in detector operations, and in the trigger and data acquisition systems of the experiment.

2.1 Calorimeter timing measurement

In addition to the energy deposited in each cell, both the LAr and Tile calorimeters can measure the time of arrival of the particle depositing the energy. LAr signals are read out using Front End Boards (FEB). They shape the signal and sample it at 40 MHz, four samples are then digitised if the event passes the L1 trigger. The shape of the LAr signal is optimised to minimise the noise contribution [15]. An example of the typical LAr calorimeter pulse shape is shown in Fig. 1. The long negative tail of the shaped LAr pulse implies that out-of-time pile-up provides a negative energy contribution on average, while the contribution from in-time pile-up is positive on average. Because of this, the average pile-up energy per event is zero. While this feature is very useful in correcting for the average pile-up energy deposition, suppression methods like the one presented in this paper are still very useful in suppressing pile-up contributions to individual physics objects.

The signal amplitude A (proportional to its energy) and timing (t) are both reconstructed using an optimal filtering algorithm [16] applied to the digitised samples S_i:

$$A = \sum_{i=1}^{n_{\text{samples}}} a_i S_i, \qquad t = \frac{1}{A} \sum_{i=1}^{n_{\text{samples}}} b_i S_i, \tag{1}$$

where the optimal filtering coefficients a_i and b_i are computed from the predicted pulse shape and measured noise. The cell time is only measured if the detected energy is above a certain configurable threshold. Typically, threshold values equal to three times the cell noise ($3\sigma_{\text{noise}}$) are used. If the reconstructed energy is below threshold, then the cell time is not computed and $t = 0$ is stored.

The LAr time measurement is synchronised with the LHC clock and fine-tuned at the FEB level [17]. Time alignment corrections are recalculated using beam-splash and early collision data [18]. The measured time is also monitored as part of the data quality assessment [19] in order to ensure its stability. The LAr time resolution is typically parameterised as the sum in quadrature of a constant term and a $\sim 1/E$ noise term:

$$\sigma_t = \frac{p_1}{E} \oplus p_0.$$

In Run 2 and after applying calibration constants obtained from data, the constant term p_0 was found to reach ~200 ps, while the noise term p_1 was $\mathcal{O}$(1 GeV ns) [18].

The Tile calorimeter signal is also shaped, amplified and sampled at 40 MHz by the front-end electronics. Unlike the LAr calorimeter, seven rather than four samples are digitised and the cell energy and time are reconstructed via an optimal filtering method as described by Eq. (1). If the signal amplitude is below 5 ADC counts,[3] then the timing is not measured and a default value of $t = 0$ is stored. Since most Tile calorimeter cells are read out by two independent channels, the average of the two times is taken as the measured cell time [20]. The Tile calorimeter uses its Laser calibration system [21] to monitor the timing of all channels during physics runs. Laser events are recorded during empty bunch-crossings in physics data-taking and the stability of the timing is monitored as part of the data quality assessment, allowing corrections for possible misconfiguration to be made in the main data processing. Channels that exhibit a large number of timing jumps are flagged as *bad timing* and are not used

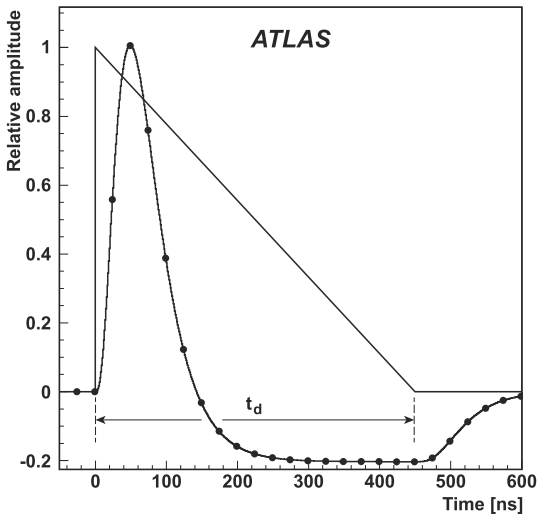

Fig. 1 Example of the LAr (central EM barrel) calorimeter pulse shape from Ref. [3]. The unipolar triangular pulse is the one generated by fast ionising particles in the liquid argon. Its characteristic time is the drift time $t_d \simeq 450$ ns in the example shown. The shaped pulse is superimposed, with a characteristic duration of $t_{\text{signal}} \simeq 600$ ns. The full circles on the shaped pulse indicate the nominal bunch-crossings at 25 ns intervals

[3] In a few Tile cells affected by higher radiation (*gap scintillators* [20]), the minimum amplitude for time reconstruction is 15 ADC counts.

for further physics object reconstruction [21]. Cells flagged as Tile *bad timing* are not considered when implementing the time cut. The Tile timing resolution is described with a functional form similar to the one commonly used for the calorimeter energy resolution:

$$\sigma_t = p_0 \oplus \frac{p_1}{E} \oplus \frac{p_2}{\sqrt{E}}.$$

In Run 2, the constant term was found to be ∼300 ps, while p_1 and p_2 are $\mathcal{O}(1\,\text{GeV ns})$ and $\mathcal{O}(1\,\sqrt{\text{GeV}}\,\text{ns})$, respectively, with variations depending on the gain [22].

3 Data and Monte Carlo samples

The time cut's performance has been studied on simulated multi-jet event samples as well as *pp* collision data from the ATLAS detector. The data sample used corresponds to one run, taken by ATLAS in 2017 during Run 2 of the LHC at a centre-of-mass energy $\sqrt{s} = 13$ TeV, with an integrated luminosity of $\mathcal{L} = 76 \pm 2\,\text{pb}^{-1}$. Because the goal of this study is only to compare jet kinematic distributions, a larger data sample is not needed. In the selected run the LHC provided collisions from bunch trains with a nominal bunch-crossing spacing of 25 ns. The recorded average mean number of interactions per bunch-crossing $\langle\mu\rangle = 38.8$ is consistent with the average $\langle\mu\rangle$ recorded during the 2017 data-taking period. Data quality requirements are applied to ensure that all detector components were fully operational [23]. Data were collected using multiple single-jet triggers (see Sect. 7). Events selected by each trigger are scaled by the corresponding trigger prescale factor. In a few *Luminosity Blocks*[4] at the beginning of the run, the prescale factors for the chosen single-jet triggers were found to be very large, resulting in an apparent loss of statistical precision due to recording few events with very large trigger weights. To avoid this issue, the Luminosity Blocks in question were excluded from the analysis. The loss of integrated luminosity due to this additional rejection amounts to 6.5%. The integrated luminosity after data quality requirements are applied is $\mathcal{L} = 71 \pm 2\,\text{pb}^{-1}$. The uncertainty in the 2017 integrated luminosity is assumed for this run; it amounts to 2.4% [4], obtained using the LUCID-2 detector [24] for the primary luminosity measurements.

Additional data samples were used to check for inefficiencies caused by time miscalibration and to test the ATLAS event size for reductions due to the time cut. For time-cut inefficiency checks, one Luminosity Block of data collected in 2018 was used, with an average number of interactions per bunch-crossing of $\langle\mu\rangle = 42.5$. The data used for the event size test also consists of one Luminosity Block, taken in 2022. The average pile-up for this run is $\langle\mu\rangle = 41.3$.

Multi-jet production was modelled using PYTHIA 8.230 [25] with leading-order matrix elements for dijet production which were matched to the parton shower. The renormalisation and factorisation scales were set to the geometric mean of the squared transverse masses of the two outgoing particles in the matrix element, $\sqrt{(p_{\text{T},1}^2 + m_1^2)(p_{\text{T},2}^2 + m_2^2)}$. The NNPDF2.3LO set of parton distribution functions (PDFs) [26] was used in the matrix element generation, the parton shower, and the simulation of the multi-parton interactions. The A14 [27] set of tuned parameters was used. The modelling of fragmentation and hadronisation was based on the Lund string model [28,29]. The effect of both in-time and out-of-time pile-up was modelled by overlaying the simulated hard-scattering event with inelastic proton–proton (pp) events generated with PYTHIA 8.186 [30] using the NNPDF2.3LO PDF set [26] and the A3 set of tuned parameters [31].

The MC events have been reweighted to account for the difference between the simulated number of interactions per bunch-crossing (μ) profile and the one from the single run used for this paper. The correction factor is defined in bins of μ, as the ratio of the data to MC sample μ spectra, normalised to unity and prior to any event selection. This reweighting is not applied when performing MC-only studies, to allow a wider μ range to be covered.

An additional MC sample was used to assess the ATLAS event size reduction due to the time cut. This MC sample describes $t\bar{t}$ production in the fully hadronic decay channel. The production of $t\bar{t}$ events was modelled using the POWHEG BOX v2 [32–35] generator at NLO with the NNPDF3.0NLO [36] PDF set and the h_{damp} parameter set to $1.5\,m_{\text{top}}$ [37]. The events were interfaced to PYTHIA 8.307 [25] to model the parton shower, hadronisation, and underlying event, with parameters set according to the A14 tune [27] and using the NNPDF2.3LO set of PDFs [26]. The decays of bottom and charm hadrons were performed by EVTGEN 2.1.1 [38].

4 The topo-cluster reconstruction algorithm

The cell time cut is introduced into the existing ATLAS topo-cluster reconstruction algorithm, a detailed description is provided in Ref. [3]. In short, ATLAS topo-clustering is based on the cell signal significance $\zeta_{\text{cell}}^{\text{EM}}$, defined as the ratio of the cell signal energy to the average expected noise (Eq. (2)). Both are measured at the electromagnetic (EM) scale, defined by

[4] A Luminosity Block (LB) is a period of time during which the instantaneous luminosity, detector and trigger configuration, and data quality conditions are considered constant. In general, one LB corresponds to a time period of 60 s, although LB duration is flexible and actions that might alter the run configuration or detector conditions trigger the start of a new LB before 60 s have elapsed. LB start and end timestamps are assigned in real time during data-taking by the ATLAS Central Trigger Processor [23].

calibrating the calorimeter energy measurement to the energy deposited by an electron or photon, without any correction for the non-compensating response of the calorimeter.

$$\zeta_{\text{cell}}^{\text{EM}} = \frac{E_{\text{cell}}^{\text{EM}}}{\sigma_{\text{noise,cell}}^{\text{EM}}}. \tag{2}$$

Topo-clusters are formed by a growing-volume algorithm, configured by three threshold parameters $\{S,\ N,\ P\}$:

$$|\zeta_{\text{cell}}^{\text{EM}}| > S \quad \text{(primary seed threshold)}, \tag{3}$$
$$|\zeta_{\text{cell}}^{\text{EM}}| > N \quad \text{(threshold for growth control)}, \tag{4}$$
$$|\zeta_{\text{cell}}^{\text{EM}}| > P \quad \text{(principal cell filter)}; \tag{5}$$

set to $\{S = 4,\ N = 2,\ P = 0\}$ in Runs 1, 2 and 3. The algorithm is seeded by cells (*seed* cells in the following) whose signal significance exceeds a threshold S (Eq. (3)) and which have not been marked as having either read-out or general signal extraction problems in the actual run conditions. Seed cells are then sorted from highest to lowest energy significance and topo-clusters are grown by adding all neighbouring cells that satisfy Eq. (5).

Two cells are considered to be neighbours if they are directly adjacent in a given sampling layer, or, if in adjacent layers, if they at least partially overlap in the plane. If a neighbouring cell has a signal significance above the threshold N in Eq. (4), then the procedure is iterated over its neighbours, while if it satisfies Eq. (5) but not Eq. (4), its neighbours are not included in the growing topo-cluster. This algorithm iterates over further neighbours until no more neighbouring cells satisfying Eq. (4) are found. Since the S, N and P thresholds are applied to the absolute significance, cells of either positive or negative energy can seed a cluster or be included in one. As discussed in Sect. 2.1, negative cell signals in the ATLAS calorimeters are often the result of out-of-time pile-up, since the residual signal trace produced by out-of-time particles is scaled by the negative tail of the LAr calorimeter signal-shaping function [15]. Only clusters with an overall positive energy are used as inputs for jet reconstruction. The algorithm described so far, however, has no limitations to how large a cluster can grow and it could potentially lead to very large, unphysical clusters. For this reason, clusters are then split around local energy maxima, as detailed in Ref. [3].

5 The cell time cut

As discussed in Sect. 2.1, both the ATLAS LAr and Tile calorimeters provide a time measurement for signals of sufficiently large energy. Figure 2 shows the distribution of the energy significance and time of calorimeter signals in real data. Calorimeter cells belonging to the LAr EM barrel region are picked as an example, but similar distributions occur in other calorimeter regions. At high energy significance, two secondary peaks at ± 25 ns are clearly visible, associated with out-of-time pile-up from the previous and next bunch-crossings. The asymmetry visible between positive and negative cell time is due to the LAr calorimeter being affected by a larger number of bunch-crossings before the current one than after it.

At lower energy significance the time resolution is poorer, and the secondary peaks cannot in general be distinguished. When limiting the study to candidate *seed* cells, i.e. those with energy significance greater than $S = 4$, the three peaks are separated well enough to justify a selection on the absolute cell time, requiring it to be within ± 12.5 ns of the midpoint between the secondary peaks. Multiple approaches to implementing a cell time cut in topo-cluster building were explored. The most relevant are detailed below.

5.1 The *Seed* time cut

The requirement for seeding a topo-cluster is modified. Seed cells must satisfy Eq. (6), i.e. have both an absolute cell signal significance larger than $S = 4$ and a cell time within ± 12.5 ns:

$$\begin{cases} |\zeta_{\text{cell}}^{\text{EM}}| > S \quad \text{(primary seed threshold, default } S = 4) \\ |t_{\text{cell}}| < 12.5 \text{ ns}. \end{cases} \tag{6}$$

The cluster growth and splitting stages of the topo-clustering algorithm are left untouched. Since this selection is exclusively applied to topo-cluster seeds, it is referred to as the *Seed cut* in the following.

5.2 The *Seed Extended* time cut

In the Seed cut implementation, a cell exceeding the signal significance threshold in Eq. (6), but failing the time cut, would be prevented from seeding a cluster. It could, however, be included in another cluster as a neighbouring cell if it falls in the vicinity of an in-time signal. Due to the high level of pile-up at the LHC, this phenomenon is not unlikely. To prevent their inclusion, a tighter version of the cut was defined, in which candidate seed cells that satisfy Eq. (3), but not Eq. (6), are vetoed from being included in growing topo-clusters. In the following, this version of the time cut is referred to as the *Seed Extended* cut.

5.3 The upper limit

Although this paper focuses on the reduction of out-of-time pile-up, delayed calorimeter signals with substantial energy can also arise from new physics, for example from the decays of slow-moving long-lived particles (LLPs) that are predicted by several theories for physics beyond the Stan-

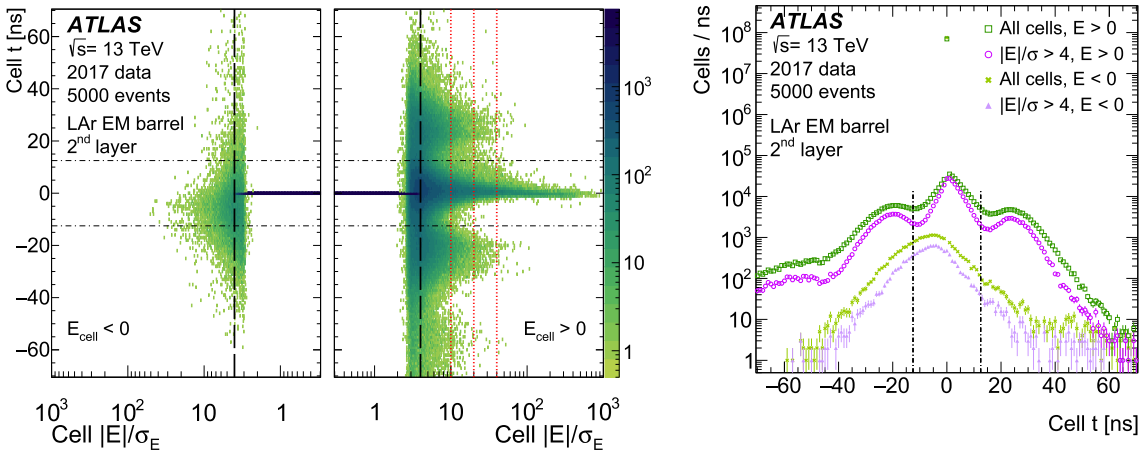

Fig. 2 Time and energy significance for calorimeter cells in the second layer of the LAr EM barrel calorimeter. **a** Shows the two-dimensional cell time vs significance spectrum. The cell time is computed if the cell energy exceeds a given threshold (typically $3 \cdot \sigma^{\mathrm{EM}}_{\mathrm{noise,cell}}$), below which a default value of $t = 0$ is stored. The dashed vertical line represents the seed candidate requirement $S = 4$ (Eq. (3)), while the horizontal lines represent the cell time rejection limits of ±12.5 ns. The three dotted vertical lines represent the three possible values considered for the Upper Limit (see Sect. 5.3). **b** Shows a comparison between the inclusive cell time spectrum and the one for seed candidates ($|E|/\sigma_E > 4$). The vertical lines represent the cell time rejection limits of ±12.5 ns

dard Model [39,40]. Optimising the time cut for LLP signals would require taking into account the many signatures considered for LLP searches and is outside the scope of this paper. A conservative approach was therefore adopted, where the time cut is not applied to signals with very large significance, thus leaving the decision of whether or not to reject such signals to a later stage of the reconstruction chain, where differentiation between standard and LLP-dedicated selections is possible.

The time cut was therefore modified by introducing an Upper Limit (UL). The time cut is turned off if the cell signal significance $\zeta^{\mathrm{EM}}_{\mathrm{cell}} = E^{\mathrm{EM}}_{\mathrm{cell}}/\sigma^{\mathrm{EM}}_{\mathrm{noise,cell}}$ is positive and larger than a given value X_{UL}, i.e. if:

$$\begin{cases} |\zeta^{\mathrm{EM}}_{\mathrm{cell}}| > S \quad \text{(primary seed threshold, default } S = 4) \\ |t_{\mathrm{cell}}| < 12.5 \text{ ns} \end{cases}$$
$$\text{OR} \quad \zeta^{\mathrm{EM}}_{\mathrm{cell}} > X_{\mathrm{UL}}.$$

A lower value of X_{UL} implies a larger phase space left untouched by the time cut. Three values $X_{\mathrm{UL}} = 10, 20$ and 40 were tested in order to estimate how low the Upper Limit can be set without reintroducing too much pile-up into the event. While the Upper Limit could in principle be combined with either the Seed cut or the Seed Extended cut, in this paper it is only studied in combination with the Seed Extended cut, as the latter appeared more promising than the Seed cut (Sect. 6). The Upper Limits $X_{\mathrm{UL}} = 10, 20$ and 40 are shown as dotted lines in Fig. 2. As expected, $X_{\mathrm{UL}} = 40$ affects a very limited number of out-of-time cells and it is expected to have a negligible effect, while $X_{\mathrm{UL}} = 10$ is expected to have the largest impact.

6 Performance of the time cut on MC simulation

The performance of the time cut was evaluated using a PYTHIA 8.230 dijet MC sample, as described in Sect. 3. The event selection is kept as loose as possible in order to observe ample ranges of cluster energy and jet energy.

6.1 Performance on topo-clusters

Since the time cut is applied in the topo-clustering algorithm, the overall number of clusters is expected to be reduced, because the applied cut leads to a smaller number of cluster seeds. It should be noted, however, that the topo-clusters built with the time cut applied are not necessarily a subsample of those built using only the cell energy significance. Excluding out-of-time signals may change the number of local maxima, prompting additional cluster splitting. Figure 3 shows the number of clusters reconstructed per event; only positive-energy topo-clusters (i.e. eligible inputs to the jet reconstruction) are shown. The number of positive-energy clusters in each event is on average ∼15% smaller when the time cut is applied, with very little difference between the different choices for the cut. The Seed and Seed Extended cuts differ only in their treatment of out-of-time signals with significant energy when these signals are included as neighbouring

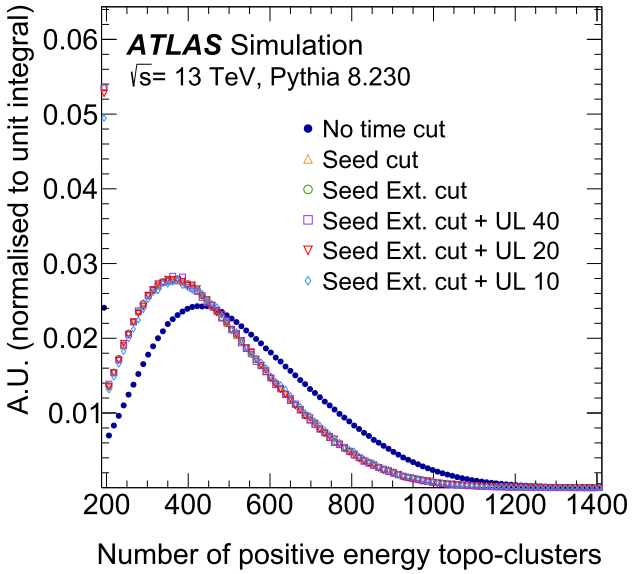

Fig. 3 Number of positive energy ($E_{\mathrm{cl}} > 0$) reconstructed topo-clusters per event: comparison between no time cut and multiple choices for the time cut. The first and last bins show the overflow and underflow

cells, and hence the two algorithms can be expected to differ more strongly in their effect on topo-cluster properties than on the number of reconstructed topo-clusters. Since the UL only truncates the relatively sparsely populated high-energy tail of the topo-cluster spectrum, its effect then becomes subdominant when considering the inclusive number of clusters.

Removing out-of-time contributions can also result in a change in the kinematic properties of the reconstructed topo-clusters. This effect is expected to be more significant when applying the Seed Extended time cut as opposed to the Seed time cut. Figure 4 shows the multiplicity of topo-clusters that have various kinematic properties, comparing the various time cut options. Each kinematic moment of the topo-clusters is defined as the weighted average of the property of interest over the cells contributing to the cluster. A full description of the topo-clusters' properties is given in Ref. [3]. An additional calibration using the local cell weighting (LCW) scheme is applied[5] to take into account the non-compensating response of the calorimeter, out-of-cluster energy deposits and energy deposited in the dead material within the detector [3]. Only the topo-clusters with overall positive energy in each event are shown. Bottom panels show the "cut/no-cut" ratio plot. Uncertainties in the ratios must take into account that the distributions with and without the time cut are obtained from the same events, and hence are correlated in a non-trivial way. To properly account for the correlations, uncertainties are computed by splitting the available sample into subsamples of approximately 10,000 events each, and the cut/no-cut ratio is recomputed for each subsample. The ratio's uncertainty is estimated from the standard deviation of the resulting distribution. The estimated uncertainty is propagated to the inclusive ratio as a relative uncertainty. This method is used to compute the uncertainties in the cut/no-cut ratio plots throughout this paper.

Figure 4a shows the cluster time. When no time cut is applied, two shoulders are clearly visible near ±25 ns, consistent with being due to out-of-time pile-up from the previous and next bunch-crossings. Once the time cut is applied, the number of clusters around ±25 ns is reduced by more than 80% by the Seed Extended time cut, smoothing out the two shoulders, while the main peak at 0 ns appears unchanged. The Seed cut has a smaller impact, reducing the two peaks by ∼70%, while the impact of the Seed Extended plus Upper Limit $X_{\mathrm{UL}} = 10$ cut lies between those of the Seed and Seed Extended cuts. Overall, topo-clusters with absolute time greater than 12.5 ns are not removed entirely, since out-of-time contributions can still occur due to predominantly low-energy cells being included in topo-clusters as neighbouring cells.

The relative effect of the time cut on the number of clusters is also found to vary with jet rapidity (Fig. 4b), the largest effect being a ∼25% reduction in the cluster multiplicity for $2 \lesssim |y| \lesssim 3.5$. The energy deposited by pile-up is expected to increase at larger absolute rapidity, but the time cut has only a ∼10% effect above $|y| \sim 3.5$ because each forward calorimeter cell covers a larger pseudorapidity interval. This geometrical effect implies that larger numbers of both in-time particles and out-of-time particles deposit energy in the same cell, thus resulting in a less effective distinction between in-time and out-of-time signals. The effect of the time cut is also seen to vary with the cluster energy (Fig. 4c). The number of clusters with energy between about 1 GeV and 100 GeV is reduced by ∼25%, with the reduction decreasing to ∼10% at both very low and very high energies. Finally, the dependence on the cluster p_{T} (Fig. 4d) provides the best way to observe the effect of the Upper Limit. As expected, $X_{\mathrm{UL}} = 40$ has hardly any effect, while $X_{\mathrm{UL}} = 20$ produces a small difference and it starts to diverge from the Seed Extended cut for clusters with $p_{\mathrm{T}} \gtrsim 15$ GeV. However, $X_{\mathrm{UL}} = 10$ has a larger impact, which starts to appear for clusters with $p_{\mathrm{T}} \gtrsim 2$ GeV. At $p_{\mathrm{T}} = 5$ GeV for instance, the Seed Extended cut reduces the number of clusters by ∼20%, while the Seed Extended plus $X_{\mathrm{UL}} = 10$ cut reduces their number by only ∼15%.

Figure 5 shows two topo-cluster moments. The topo-cluster isolation (Fig. 5a) is computed from the number of non-clustered cells on the outer perimeter of the topo-cluster [3]: an isolation value close to 1 indicates an isolated topo-cluster, while it tends to 0 when the topo-cluster is not isolated. Since the lower values of the isolation spectrum

[5] The LCW scheme is not propagated to the jets, in order to mimic the approach most commonly followed by ATLAS physics analyses.

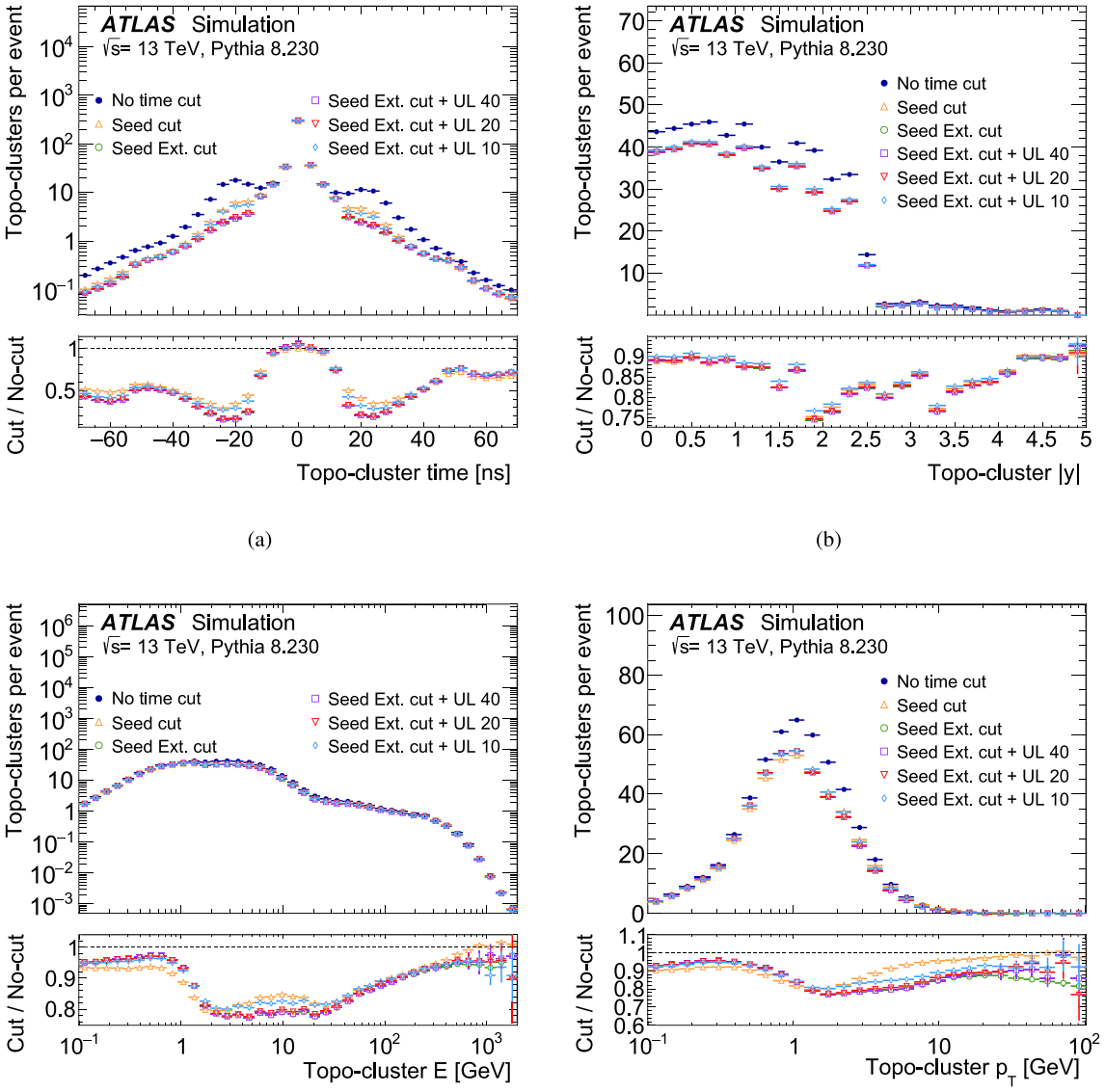

Fig. 4 Kinematics of reconstructed topo-clusters, compared between no time cut, the Seed cut, the Seed Extended cut and the Seed Extended cut combined with multiple choices of Upper Limit: $X_{\mathrm{UL}} = 40$, $X_{\mathrm{UL}} = 20$ and $X_{\mathrm{UL}} = 10$. Each kinematic moment of the topo-clusters is defined as the weighted average of the property of interest over the cells contributing to the cluster [3]. Topo-clusters with energy $E_{\mathrm{cl}} > 0$ are shown. Plots are normalised to the total number of positive-energy topo-clusters per event. Uncertainties in the cut/no-cut ratios are computed by splitting the available sample into subsamples and recomputing the cut/no-cut ratio for each subsample. The standard deviation of the distribution of the ratio is used to estimate the ratio's uncertainty

are affected the most by the time cut, it can be concluded that topo-clusters reconstructed with the time cut tend to be more isolated than those from the standard algorithm. This observation can be explained as a combination of two effects. Firstly, isolated topo-clusters are mostly produced by EM showers, and are less sensitive to pile-up because of their smaller size. Secondly, the pile-up reduction introduced by the timing cut is likely to produce more isolated topo-clusters. Specific studies are needed to further understand the interplay between these two effects. The distance λ of the cluster's centre of gravity from the calorimeter's front face [3] is shown in Fig. 5b. The region of $\lambda \lesssim 100$ mm is known to be dominated by EM clusters, while clusters located at $\lambda \gtrsim 400$ mm are predominantly hadronic [3]. In Fig. 5b very little difference is visible in the region dominated by EM clusters while a relatively uniform reduction of about 20% is visible for predominantly hadronic clusters. The area between $\lambda \sim 100$ mm and $\lambda \sim 400$ mm corresponds to a

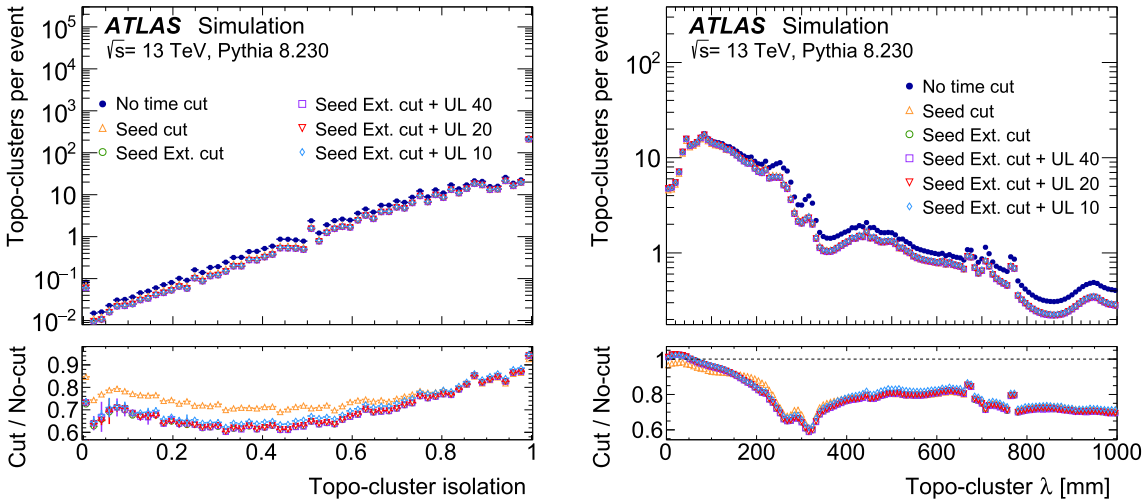

Fig. 5 Topo-cluster **a** isolation and **b** distance λ from the calorimeter front face. A comparison between no time cut, the Seed cut, the Seed Extended cut and the Seed Extended cut combined with $X_{\mathrm{UL}} = 40$, $X_{\mathrm{UL}} = 20$ and $X_{\mathrm{UL}} = 10$ is shown. Each kinematic moment of the topo-clusters is defined as the weighted average of the property of interest over the cells contributing to the cluster [3]. Topo-clusters with energy $E_{\mathrm{cl}} > 0$ are shown. Plots are normalised to the total number of positive-energy topo-clusters per event. Uncertainties in the cut/no-cut ratios are computed by splitting the available sample into subsamples and recomputing the cut/no-cut ratio for each subsample. The standard deviation of the distribution of the ratio is used to estimate the ratio's uncertainty

mixture of EM and hadronic clusters. Here, peaks are visible in the spectrum of standard clusters, while they are almost entirely removed by the time cut. This effect hints that the timing cut may increase the separation between hadronic and EM showers in the presence of pile-up.

6.2 Performance on jets

Topo-clusters serve as inputs to the reconstruction of many physics objects in ATLAS. This paper focuses on the effect of the time cut on jets reconstructed by applying the anti-k_t clustering algorithm with radius parameter $R = 0.4$ [41]. In ATLAS, jets are most often reconstructed from *particle-flow* objects [42,43], which are built by combining topo-clusters with matching inner-detector tracks. Despite it being the preferred method in ATLAS, particle flow adds a layer of complexity to the jet reconstruction: jets built directly from topo-clusters provide a more straightforward way of evaluating the time cut's performance and are hence used in this paper. Preliminary studies show that the effect of the time cut on $R = 0.4$ particle-flow jets is about the same size as the effect on those built directly from topo-clusters. Since the ATLAS tracking is performed within the triggered bunch crossing, it is reasonable to expect that most out-of-time calorimeter signals would not match tracks, so the time cut can be expected to primarily affect objects classified as neutral by the particle-flow algorithm, which in turn consist only of topo-clusters, with no track-based correction.

6.2.1 *Jet calibration*

Jets are calibrated to correct for both the pile-up contribution and the detector response. A complete description of jet calibration in ATLAS can be found in Ref. [43]. The calibration procedure consists of three stages. First, a two-step pile-up correction is made. Then a MC-based calibration factor is applied to correct for the detector response (MC jet energy scale: *MC-JES*) and improve the jet resolution by reducing the calibration's dependence on additional jet properties (*Global Sequential Calibration*). Finally, an in situ correction is applied to account for discrepancies between data and MC events.

The first stage of the calibration procedure starts with an *area-based* correction in which the average pile-up contribution is subtracted from the jet's transverse momentum:

$$p_{\mathrm{T}}^{\mathrm{area}} = p_{\mathrm{T}} - \rho \times A,$$

where p_{T} is the jet p_{T}, A is the jet catchment area and ρ is the median p_{T} density of the event. The value of ρ is calculated using jets reconstructed by applying the k_t algorithm [44,45] to positive-energy topo-clusters with $|\eta| < 2$. A residual pile-up correction is then applied to account for residual dependence of the jet p_{T} on pile-up activity in the event. Two η-dependent correction terms are derived independently by fitting the dependence of the jet p_{T} on μ and the number of reconstructed primary vertices per event, N_{PV}. In general, μ provides an estimate of the amount of out-of-

time pile-up in the event, while N_{PV} estimates the amount of in-time pile-up. The residual correction is then applied as:

$$p_{\mathrm{T}}^{\mathrm{residual}} = p_{\mathrm{T}}^{\mathrm{area}} - \alpha \times (N_{\mathrm{PV}} - 1) - \beta \times \mu,$$

where α and β are the correction factors estimated from MC simulation.

The pile-up contribution to jets is expected to be affected by the time cut. Figure 6 shows the spectrum of the median p_{T} density ρ, as well as the dependence of ρ on μ. When the time cut is applied, ρ is found to be ∼20% smaller overall, and also to increase more slowly as a function of μ. Since ρ is built from topo-clusters, the improved pile-up rejection of the time cut leads to smaller ρ values, decreasing the pile-up-dependent contribution to the jet energy. To account for possible remaining data–MC differences in the pile-up contribution to jets, not covered by the jet-area correction, the residual correction is recalculated after the application of the time cut. The standard procedure summarised above is repeated for both the Seed and Seed Extended cuts. Since the effect of the Upper Limit is smaller and limited to high-energy regions, the residual correction is not recalculated for any of the X_{UL} values, and the residual correction calculated for the Seed Extended cut is used.

6.2.2 Jet selection

Reconstructed jets are calibrated by applying the pile-up correction and the MC-JES calibration. They are then preselected, requiring them to lie within $|\eta|<4.5$ and satisfy $p_{\mathrm{T}} > 7$ GeV. Jets are also required to be isolated, i.e. there must be no other preselected jet satisfying $\Delta R(j_1, j_2) < 1.5\, R_{\mathrm{jet}}$, where j_1 and j_2 are any two reconstructed jets and R_{jet} is the jet radius parameter used in the anti-k_t algorithm (here $R_{\mathrm{jet}} = 0.4$). Since this study focuses on both signal and pile-up jets, pile-up suppression requirements such as the one using the Jet Vertex Tagger [46] are not applied.

In order to distinguish jets produced by the hard-scattering from jets originating from pile-up, reconstructed jets are matched to *truth-level jets* in MC events. Truth-level jets are reconstructed by applying the anti-k_t algorithm ($R = 0.4$) to stable final-state particles, defined as having $c\tau > 10$ mm in the generator's event record, excluding muons and neutrinos. Three types of truth jets are distinguished. First, truth jets originating from the hard scattering (*HS-truth jet*) are obtained by clustering stable particles from the simulated hard-scattering event, excluding particles from pile-up interactions. Next, two types of pile-up truth jets are obtained by clustering stable particles from the minimum-bias events which are overlaid on the hard scattering in order to simulate pile-up [47]. Jets are clustered for each minimum-bias event individually and then grouped into two pile-up jet collections: jets from in-time overlay events are included in the in-time pile-up jet collection (*IT-truth jet* in the following), while those from out-of-time overlay events are included in the out-of-time pile-up jet collection (*OOT-truth jet* in the following). The latter are built from 32 bunch-crossings before the current one and 6 after [47].

Default cuts requiring $p_{\mathrm{T}} > 10$ GeV and $p_{\mathrm{T}} > 15$ GeV are applied to IT-truth jets and OOT-truth jets respectively. HS-truth jets are also preselected by requiring $p_{\mathrm{T}} > 7$ GeV. All truth jets must satisfy $|\eta| < 5$. It should be noted that while a p_{T} match can be expected between HS-truth jets and reconstructed jets after the calibration is applied, this is less the case for OOT-truth jets: because of negative energy contributions, one might expect the reconstructed energy of an out-of-time pile-up jet to be lower than that of the truth jet. This is the reason for having a higher p_{T} selection for truth pile-up jets than for HS-truth jets. Truth-level jets are also required to be isolated: there must be no other truth jet satisfying $\Delta R(j_1, j_2) < 2.5\, R_{\mathrm{jet}}$. Here j_1 and j_2 are any two truth jets, all three truth-jet categories being considered together when computing the isolation. Reconstructed jets are matched to truth jets via a geometrical matching requirement: a reconstructed jet j_{r} is said to match a truth jet j_{t} if their separation satisfies $\Delta R(j_{\mathrm{r}}, j_{\mathrm{t}}) < 0.3$. Reconstructed jets are first checked for matches with a HS-truth jet. If no such match is found, then matches with IT-truth and OOT-truth jets are attempted.

6.2.3 Jet kinematics

Figure 7 shows the calibrated transverse momentum distributions for the jet categories described in Sect. 6.2.2. Both the reconstructed jets matching HS-truth jets and those matching IT-truth jets show only a percent-level impact from the time cut. It should be pointed out that the time cut can affect the reconstructed jet kinematics, possibly resulting in bin-to-bin migrations in the spectra shown in this subsection. Energy (and p_{T}) variations can occur in either direction, since the cell energies included in the topo-clusters can be either positive or negative. Out-of-time cells often produce negative energy signals and this explains why the ratio plots in Fig. 7a, b have values above unity in some places. The small p_{T} -dependent decrease in the fraction of jets matching HS-truth jets was found to be due to random matches. The fraction of jets that match OOT-truth jets, on the other hand, is drastically reduced by the Seed Extended cut, especially in the high p_{T} region. The Seed Extended cut reduces the multiplicity of out-of-time jets by ∼60% at $p_{\mathrm{T}} = 20$ GeV, and no out-of-time jets are found above ∼ 45 GeV. The Seed cut, on the other hand, reduces the multiplicity of the out-of-time jets by only ∼30% at 20 GeV and only ∼ 20% at 50 GeV, indicating that the Seed Extended cut rejects out-of-time pile-up more effectively. Figure 7 also illustrates the effect of the different

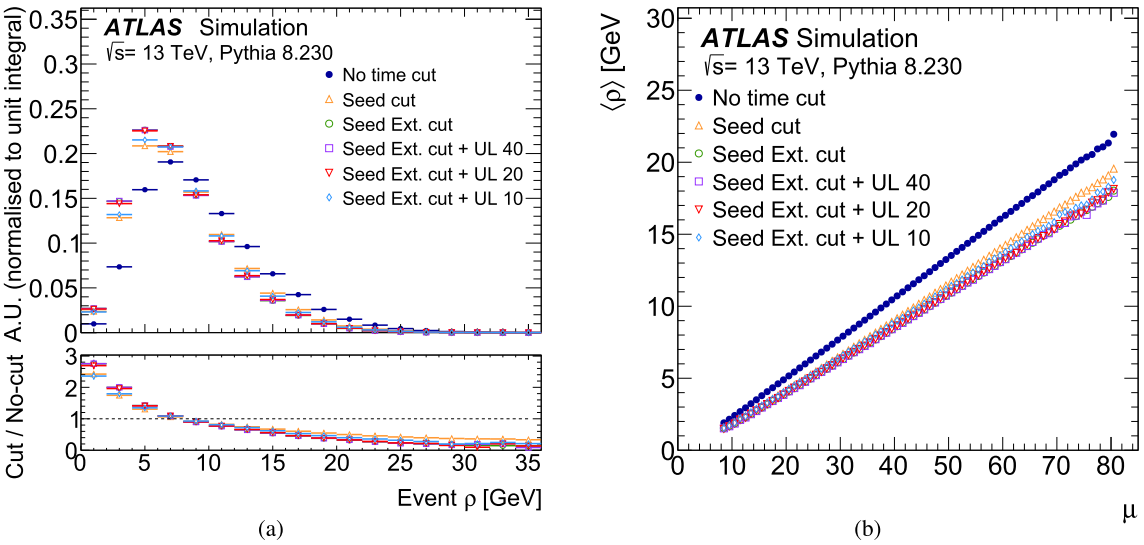

(a) (b)

Fig. 6 Topo-cluster median p_{T} density (ρ): comparison between the no time cut and the considered time cut options. **a** ρ spectrum. **b** average ρ in bins of the number of interactions per bunch-crossing (μ). Uncertainties in the cut/no-cut ratios are obtained by splitting the available sample into subsamples and recomputing the cut/no-cut ratio for each subsample. The standard deviation of the distribution of the ratio is used to estimate the ratio's uncertainty

Upper Limit values. At $p_T \sim 45$ GeV, the reduction in out-of-time jet multiplicity is ∼90% for an Upper Limit of 40, ∼70% for an Upper Limit of 20, and ∼50% for an Upper Limit of 10, confirming that lower Upper Limit values allow more pile-up in the event.

Figure 8 shows an analogous comparison for the jet rapidity. In order to limit the kinematics plots to the phase space of interest in physics analyses, an additional requirement of $p_{\mathrm{T}} > 20$ GeV is applied to the jets. Overall, all cuts except the Seed cut and Seed Extended plus Upper Limit 10 cut provide a ∼40% suppression of out-of-time jets within $|y| < 1.5$. The effect increases to a 50–60% reduction for $1.5 < |y| < 3.2$ and then decreases until it has negligible impact for $|y| > 4$. From these observations, it can be concluded that the Seed Extended time cut is preferable to the Seed cut because it is more effective in suppressing pile-up. It can also be seen that the Upper Limit $X_{\mathrm{UL}} = 10$ allows too much pile-up to remain in the event, so the lowest practical Upper Limit among those tested is $X_{\mathrm{UL}} = 20$.

6.2.4 Jet resolution

As discussed in Sect. 6.2.1, the time cut affects the jet calibration because of the different amount of pile-up remaining. To check for its impact on the performance, the jet energy resolution after calibration is compared for the different time cuts. The jet response is defined as the ratio of the calibrated energy of the reconstructed jet to the energy of the matching truth jet: $R = E_j^{\mathrm{calibrated}} / E_j^{\mathrm{truth}}$. Only those jets matched to a HS-truth jet are considered for this study. The response distribution is computed in bins of truth-jet p_{T} and rapidity ($|y|$), or truth-jet p_{T} and the event μ. For each bin, the response distribution is fitted with a Gaussian function. The jet resolution is then computed for each bin, as the ratio of the fitted standard deviation of the jet response R to its fitted mean value ($\sigma_R^{\mathrm{fit}} / \langle R \rangle^{\mathrm{fit}}$).

The estimated resolution is shown for two p_{T} bins in Fig. 9a, b as a function of the jet rapidity and in Fig. 9c, d as a function of μ. Some improvement in the jet resolution is visible, amounting to 5–10% for 20 GeV $\leq p_{\mathrm{T}} \leq$ 30 GeV, but no strong dependence on μ or $|y|$ is observed. A more accurate estimation of the jet resolution and calibration performance after the time cut is left for future studies, following the implementation of the algorithm in the standard ATLAS reconstruction chain.

7 Performance on ATLAS data

As a further probe of its performance, the time cut was tested on data collected by the ATLAS detector in 2017, corresponding to an integrated luminosity of $\mathcal{L} = 71 \pm 2\ \mathrm{pb}^{-1}$ after data quality requirements [23]. Single-jet triggers were used to collect the data, requiring at least one jet with sufficiently large p_{T}. Multiple triggers, listed in Table 1 and implementing different minimum p_{T} requirements, were studied independently. Relatively low minimum p_{T} requirements are considered, as the time cut is known to mostly effect low-energy jets. Triggers with different L1 seeds are also considered: events passing triggers seeded by random L1 triggers

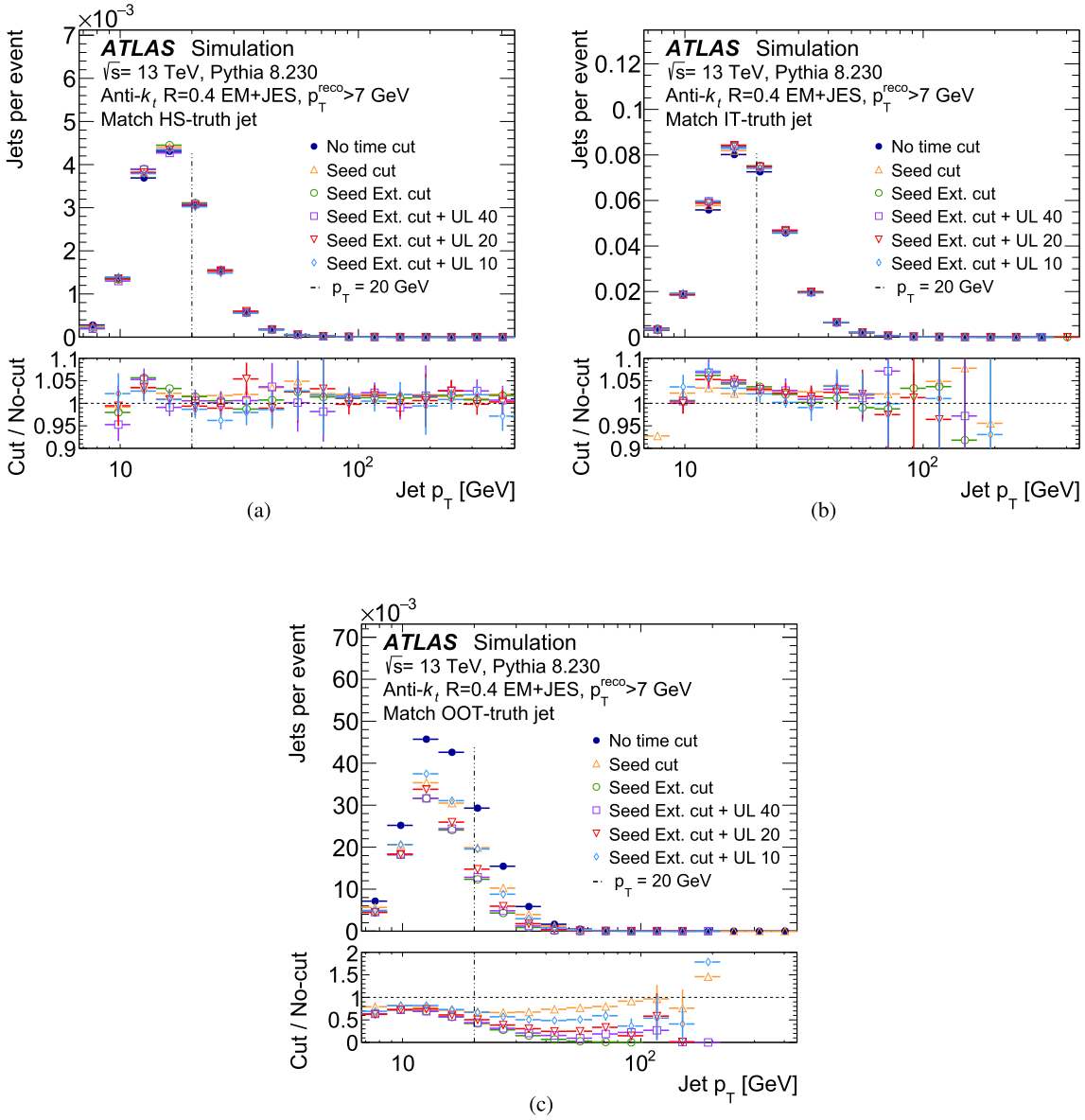

Fig. 7 Comparison between jet p_{T} spectra obtained when the Seed, Seed Extended, or no time cut is used. The Seed Extended cut is also shown in combination with the Upper Limit for $X_{\mathrm{UL}} = 40$, $X_{\mathrm{UL}} = 20$, and $X_{\mathrm{UL}} = 10$. **a** Jets matching HS-truth jets. **b** Jets matching IT-truth jets. **c** Jets matching OOT-truth jets. Uncertainties in the cut/no-cut ratios are obtained by splitting the available sample into subsamples and recomputing cut/no-cut ratio for each subsample. The standard deviation of the distribution of the ratio is used to estimate the ratio's uncertainty. The vertical dashed line represents the minimum jet p_{T} of 20 GeV normally required in ATLAS physics analyses

are expected to have a larger contamination from out-of-time pile-up than those triggered by single jet at L1. Since all the triggers in Table 1 are prescaled, the data were reweighted event-by-event by the respective trigger prescale factor.

Data and simulated events are required to contain at least one primary vertex; the one with the highest sum of squared track p_{T} is considered in this section. In addition, at least one jet must satisfy a minimum p_{T} requirement, as listed in Table 1. This requirement is needed to restrict selected events to a phase space where the trigger efficiency is within ∼20% of its plateau value. A fully efficient trigger is not necessary for this study, as the time cut is not applied at trigger level and a smaller trigger efficiency would not affect the comparison between the cut and no-cut scenarios. In order to properly compare data and MC events, jets are calibrated using the full calibration chain, including the in situ correction.[6] All jets are required to have $p_{\mathrm{T}} > 20$ GeV. The Seed Extended cut and Seed Extended plus $X_{\mathrm{UL}} = 20$ cut are compared

[6] As in Sect. 6, the residual pile-up correction is calculated after applying the time cut.

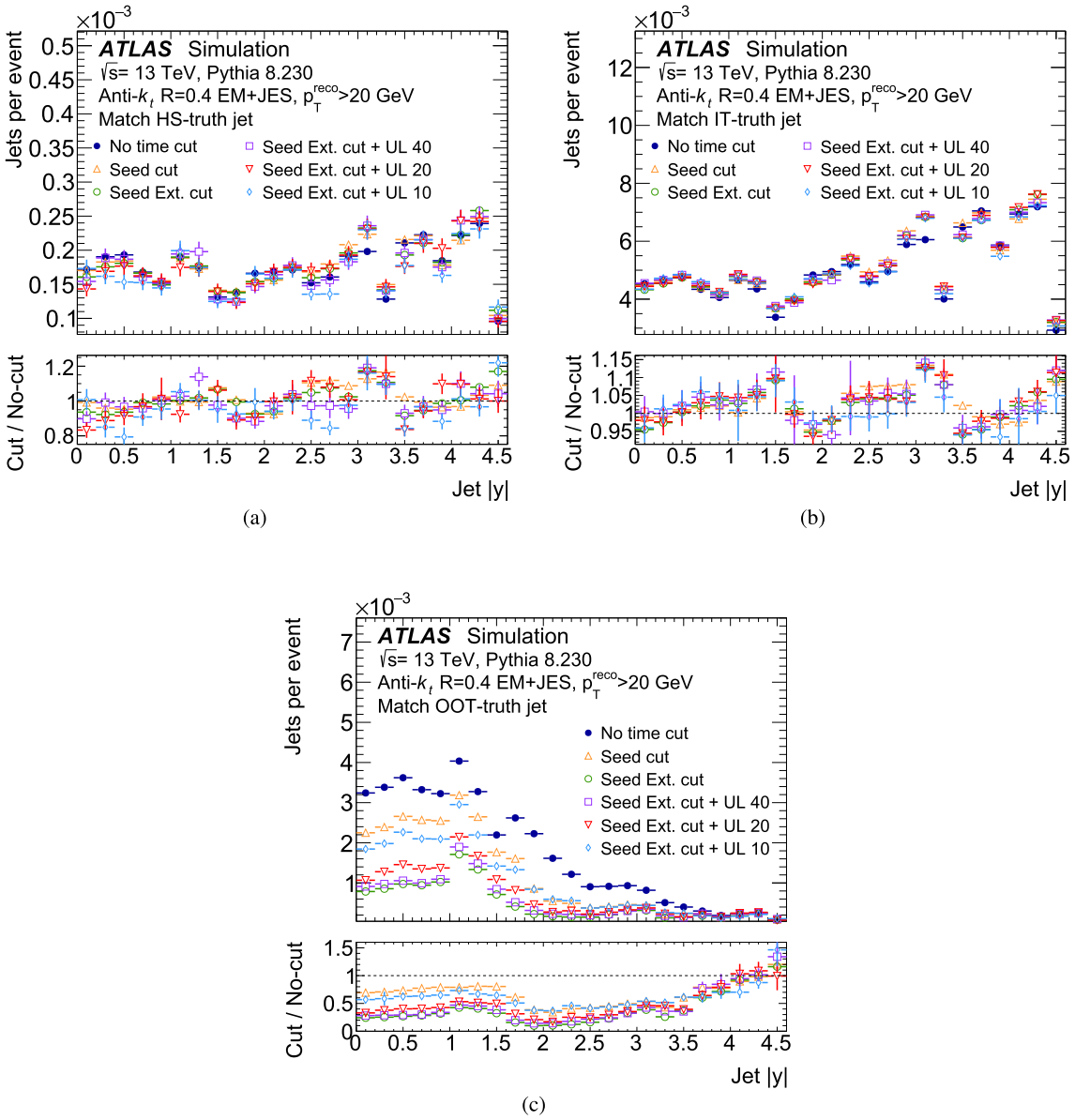

Fig. 8 Comparison between jet rapidity spectra obtained when the Seed, Seed Extended, or no time cut is used. The Seed Extended cut is also shown in combination with the Upper Limit for $X_{\mathrm{UL}} = 40$, $X_{\mathrm{UL}} = 20$, and $X_{\mathrm{UL}} = 10$. **a** Jets matching HS-truth jets. **b** Jets matching IT-truth jets. **c** Jets matching OOT-truth jets. Uncertainties in the cut/no-cut ratios are obtained by splitting the available sample into subsamples and recomputing the cut/no-cut ratio for each subsample. The standard deviation of the distribution of the ratio is used to estimate the ratio's uncertainty

with no-cut spectra for data and MC events. Figures 10, 11 and 12 show different jet kinematic properties, while topo-cluster properties are shown in Figs. 13, 14 and 15. Each histogram shows the distributions for events selected by a different trigger. Uncertainties shown for MC distributions are a combination of the MC statistical uncertainty and the luminosity uncertainty. The latter is based on the 2.4% luminosity uncertainty in 2017 [4]. Uncertainties shown for data are statistical only.

The data and MC distributions are not in perfect agreement, and exhibit relatively uniform differences of about 30–40%. This is to be expected as the MC sample used is a dijet simulation at leading order: even though the hadronisation and jet characteristics are well described by PYTHIA 8.230, the overall MC normalisation is likely to be too low due to

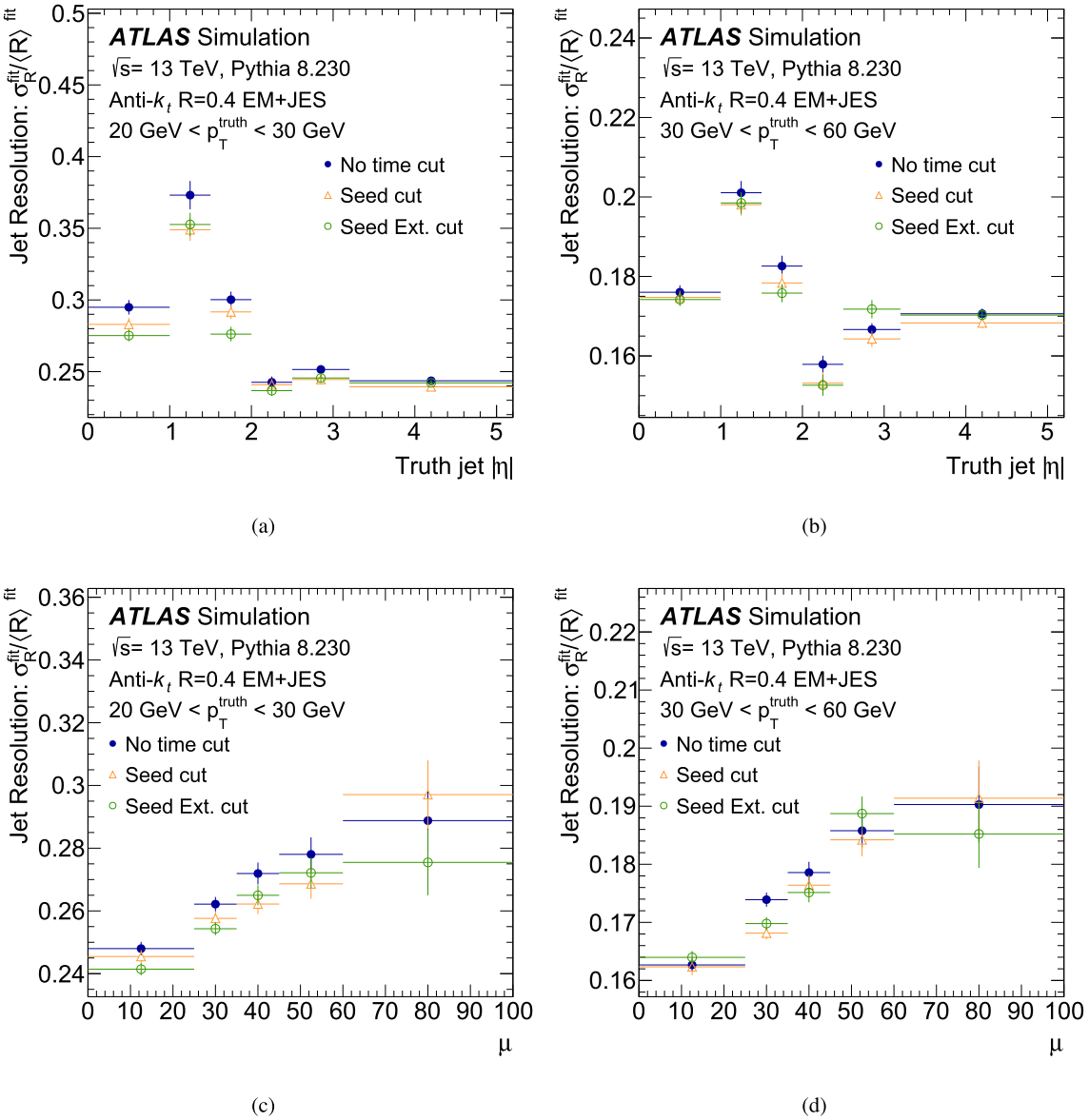

Fig. 9 Jet energy resolution after calibration as a function of **a**, **b** the jet $|\eta|$ and **c**, **d** the number of interactions per bunch-crossing (μ). Results are shown in bins of the jet p_{T} : **a**, **c** 20 GeV $< p_{\mathrm{T}}^{\mathrm{truth}} <$ 30 GeV; **b**, **d** 30 GeV $< p_{\mathrm{T}}^{\mathrm{truth}} <$ 60 GeV. The resolution is defined as the ratio of the standard deviation and mean of a Gaussian function fitted to the response distribution

Table 1 Triggers used for data selection

Trigger name	L1 trigger seed	Trigger minimum p_{T} ($\geq$ 1 jet with $p_{\mathrm{T}} \geq X$)	Offline minimum p_T ($\geq$ 1 jet with $p_{\mathrm{T}} \geq X$)
HLT_j15	Random for filled bunches	15 GeV	20 GeV
HLT_j25	Random for filled bunches	25 GeV	30 GeV
HLT_j45	$\geq$ 1 jet with $p_{\mathrm{T}} \geq$ 15 GeV	45 GeV	50 GeV
HLT_j45_L1RD0_FILLED	Random for filled bunches	45 GeV	50 GeV

the missing higher orders. Moreover, low-p_{T} events are dominated by soft QCD radiation, which is known to be difficult to model. A complete jet cross-section measurement would have to use an improved simulation and consider additional correction factors. Since this study only seeks to verify that the time cut's behaviour in data reflects what is observed in MC simulation, this level of agreement is considered acceptable.

The effect of the time cut depends on the trigger. Events passing HLT_j45, which has both a higher p_{T} threshold and a non-random L1 seed, are not affected at all by the time cut. The numbers of events passing the other three triggers exhibit a consistent reduction of ∼20% for values of the leading-jet p_{T} between 30 and 50 GeV (Fig. 10). Effects of similar size can be seen throughout the tested kinematic spectra.

Except for the HLT_j45 trigger, the time cut tends to have a more pronounced effect on data than on MC events, the difference being of $\mathcal{O}(10\%)$ in most of the phase space. This is most likely due to the simulation not accounting for events consisting exclusively of pile-up. Such events are expected to be present in non-negligible numbers for the other three triggers, which have relatively low p_{T} thresholds and are seeded by random events. In addition, the MC simulation does not reproduce bunch-to-bunch luminosity fluctuations, which have a more significant effect on the reconstruction of out-of-time signals [3].

7.1 Checks for time cut inefficiencies

The time cut relies on the accurate measurement of signal timing provided by the calorimeters. The precision of the calorimeter timing measurement is guaranteed by periodic realignment and constant monitoring, as discussed in Sect. 2.1. As a further safety check, the robustness of the cut against a local time miscalibration was tested. The events selected for this check were those in which one calorimeter channel had been flagged as producing fake out-of-time signals due to cross-talk. The effect of the time cut on particles hitting the affected region was then compared with the effect of the time cut on particles hitting unaffected regions of the same subdetector.

The affected channel was located in the second layer of the LAr EM endcap calorimeter, on the C-side (along the negative z-axis). As an example, Fig. 16 shows a combination of six events in which an electron from a $Z \to ee$ decay hit the affected area. Events were reconstructed with no cut, the Seed Extended cut and the Seed Extended plus $X_{\mathrm{UL}} = 20$ cut. These events were identified first by applying a standard $Z \to ee$ event selection. Events are required to pass photon triggers analogous to those used in diphoton resonance searches [48,49] and to contain at least two electrons with $p_{\mathrm{T}} > 10$ GeV and $|\eta| < 2.47$ (excluding the transition region $1.37 < |\eta| < 1.52$ between the LAr EM barrel and endcap calorimeters), satisfying the Medium identification selection and FCLoose isolation criteria [50]. The reconstructed track matched to each electron candidate must be consistent with having originated from the primary vertex: its longitudinal impact parameter z_0 and transverse impact parameter d_0 must satisfy $|z_0 \cdot \sin\theta| < 0.5$ mm and $|d_0|/\sigma_{d_0} < 5$ mm respectively. Furthermore, the dielectron pair is required to have an invariant mass m_{ee} satisfying $68\ \mathrm{GeV} < m_{ee} < 108\ \mathrm{GeV}$ and a pseudorapidity separation $|\Delta\eta(e_1, e_2)| > 0.1$. Electrons hitting the affected channel were then flagged by requiring that the most energetic cell in the second layer of the EM calorimeter has high enough energy ($E_{\mathrm{cell}}^{\mathrm{max}} > 5$ GeV) and its measured time satisfies $|t_{\mathrm{cell}}^{\mathrm{max}}| > 12.5$ ns. Figure 16 shows that the Seed Extended time cut does reject the energy from one spot in the centre of the topo-cluster. Despite this, the overall topo-cluster is not lost. Moreover, the addition of the Upper Limit restores most of the lost energy, so that no cell is entirely missing from the electron topo-cluster.

To better quantify the effect, the average $\eta \times \phi$ location of flagged $Z \to ee$ electrons was used to define a 3×3-cell *Test Region* containing the affected channel in the C-side LAr EM endcap's second layer. The $\eta \times \phi$ ranges corresponding to this area are listed in Table 2. In order to compare the time cut's effect in the Test Region with the normal time-cut behaviour, three *Control Regions* were also defined by inverting the sign of either η, ϕ or both in the Test Region's definition. The Control Regions' $\eta \times \phi$ boundaries are also listed in Table 2.

Events from one Luminosity Block of 2018 data, during which the Test Region was known to be affected by cross-talk, were used to test the time cut's behaviour. Rather than restricting the set of events to those passing a $Z \to ee$ selection, a more generic event selection is applied: for each region, events are considered if at least one cell of that region has a recorded transverse momentum of $p_{\mathrm{T}} > 10$ GeV.

Four variables of interest were considered. The cell occupancy N^{cells} and the cells' total energy E^{cells} are respectively defined as the number and total energy of cells in a given region that are part of a topo-cluster: they quantify whether single cells are lost due to the miscalibrated channel. The topo-cluster occupancy N^{clus} and topo-cluster total energy E^{clus} are the number and total energy of reconstructed topo-clusters that share at least one cell with a given region: they provide a way to evaluate whether entire topo-clusters are lost or their energy is significantly impacted by the time cut. In order to better quantify the effect of the time cut, the fraction $\mathcal{F}_{\mathrm{unchanged}}$ of events for which a given variable in a given region is unchanged by the cut is computed. For each event, N^{cells} (N^{clus}) is considered unchanged if the number of cells in the region (topo-clusters overlapping with the region) remains the same when applying the time cut. The total energies E^{cells} and E^{clus} are considered unchanged if

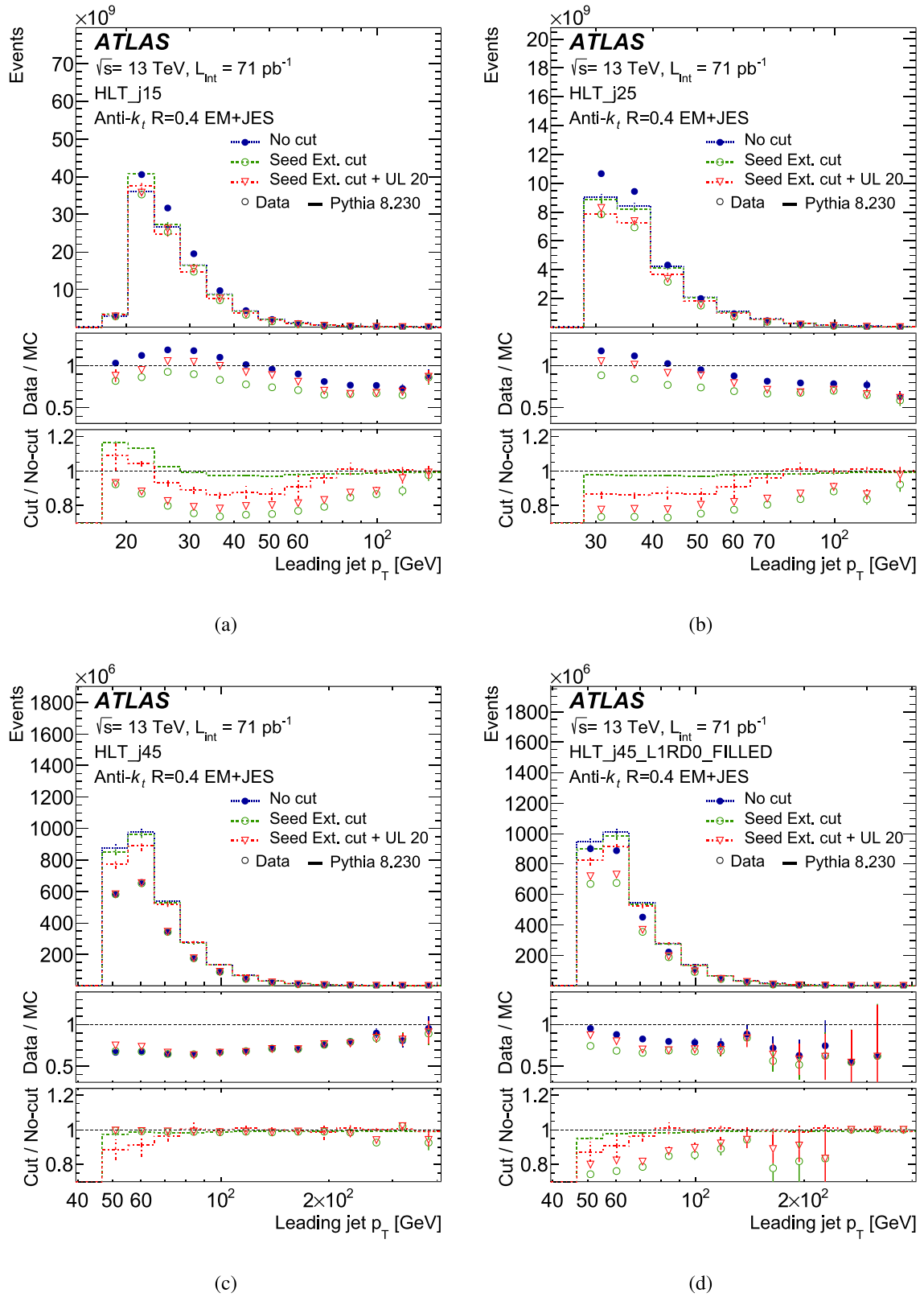

Fig. 10 Leading jet p_{T} spectrum in data and MC selected multi-jet events. Four triggers are compared: **a** HLT_j15, **b** HLT_j25, **c** HLT_j45, and **d** HLT_j45_L1RD0_FILLED. The error bars convey the statistical and luminosity uncertainties. Uncertainties in the cut/no-cut ratios are obtained by splitting the available sample into subsamples and recomputing the cut/no-cut ratio for each subsample. The standard deviation of the distribution of the ratio is used to estimate the ratio's uncertainty. The luminosity uncertainty does not apply to the cut/no-cut ratio. In the plots, lines represent MC events and markers represent data, different colours and styles represent different cuts

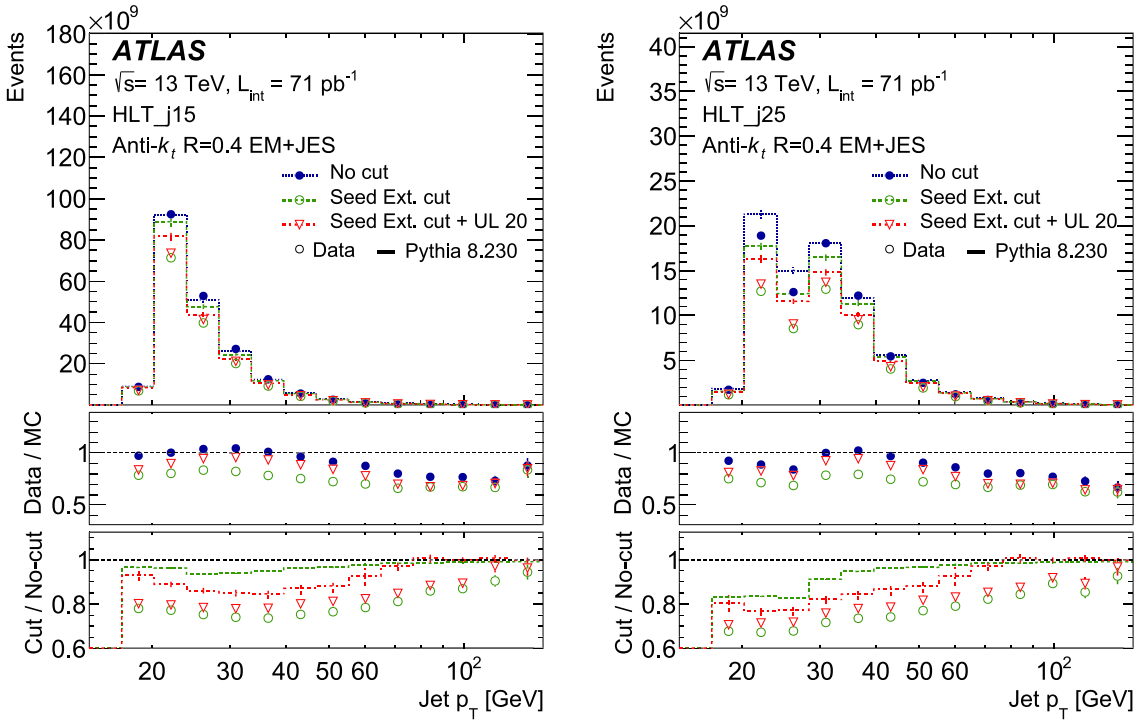

(a) (b)

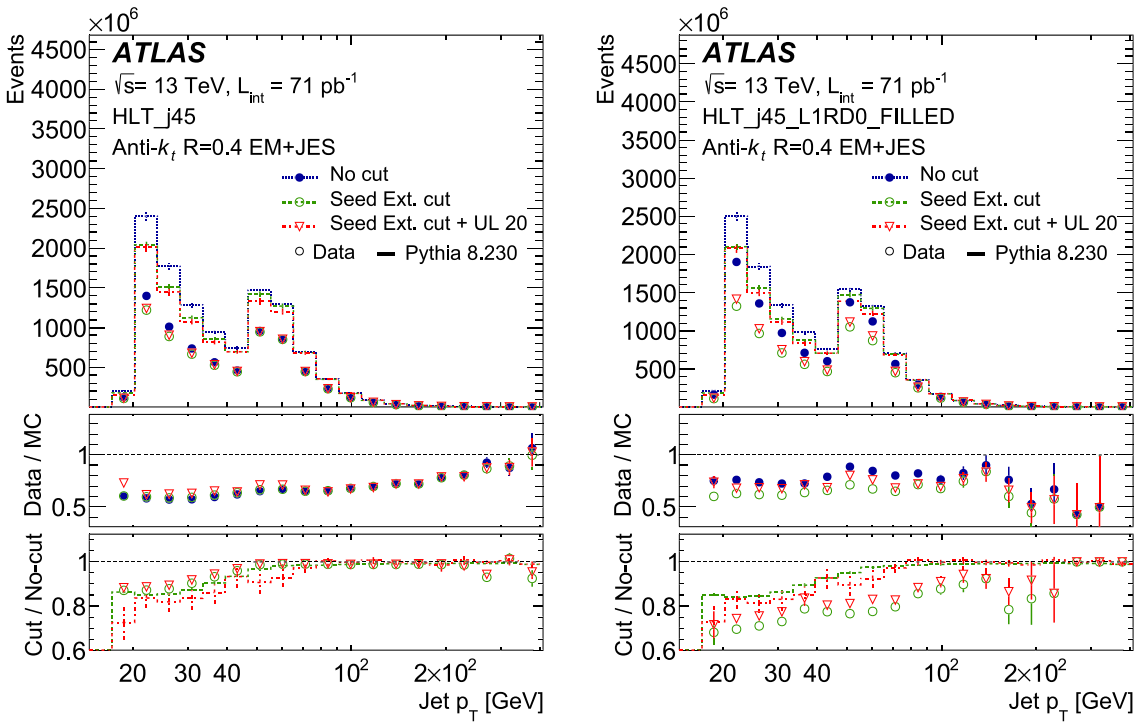

(c) (d)

Fig. 11 Jet p_{T} spectrum in data and MC selected multi-jet events. All jets passing the minimum p_{T} requirement ($p_{\mathrm{T}} > 20$ GeV) are shown. Four triggers are compared: **a** HLT_j15, **b** HLT_j25, **c** HLT_j45, and **d** HLT_j45_L1RD0_FILLED. The error bars convey the statistical and luminosity uncertainties. Uncertainties in the cut/no-cut ratios are obtained by splitting the available sample into subsamples and recomputing the cut/no-cut ratio for each subsample. The standard deviation of the distribution of the ratio is used to estimate the ratio's uncertainty. The luminosity uncertainty does not apply to the cut/no-cut ratio. In the plots, lines represent MC events and markers represent data, different colours and styles represent different cuts

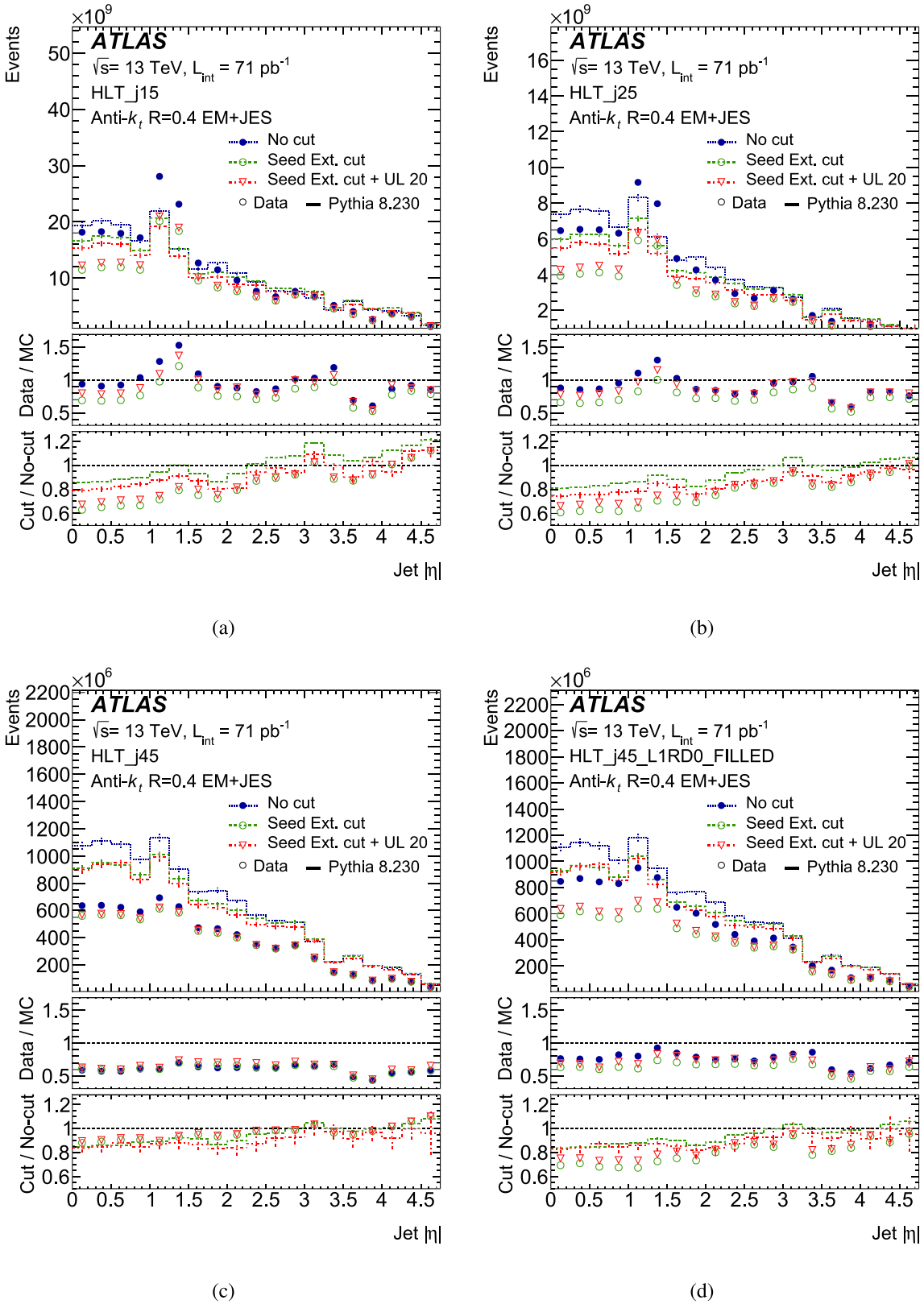

Fig. 12 Jet $|\eta|$ spectrum in data and MC selected multi-jet events. All jets passing the minimum p_{T} requirement ($p_{\mathrm{T}} > 20$ GeV) are shown. Four triggers are compared: **a** HLT_j15, **b** HLT_j25, **c** HLT_j45, and **d** HLT_j45_L1RD0_FILLED. The error bars convey the statistical and luminosity uncertainties. Uncertainties in the cut/no-cut ratios are obtained by splitting the available sample into subsamples and recomputing the cut/no-cut ratio for each subsample. The standard deviation of the distribution of the ratio is used to estimate the ratio's uncertainty. The luminosity uncertainty does not apply to the cut/no-cut ratio. In the plots, lines represent MC events and markers represent data, different colours and styles represent different cuts

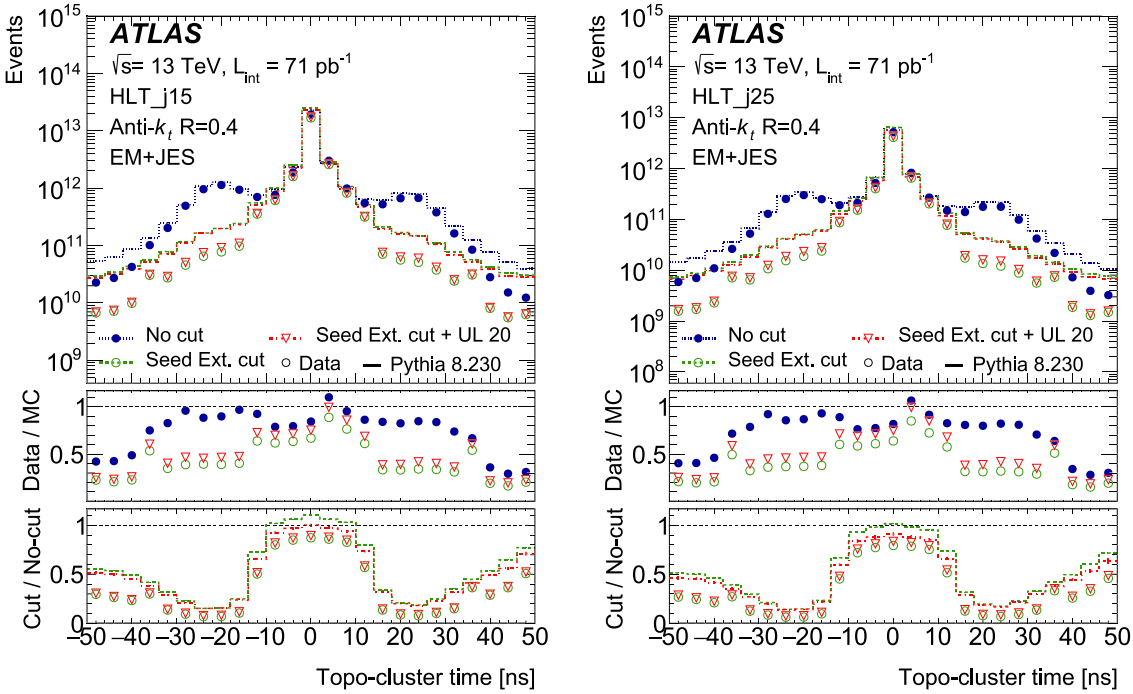

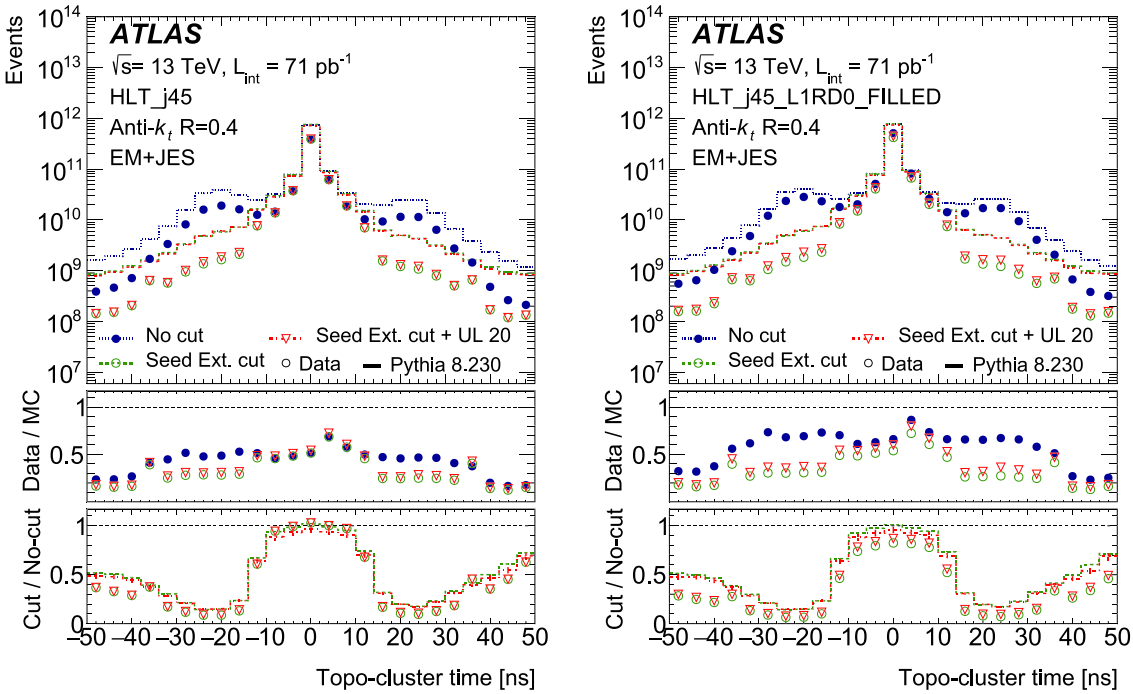

Fig. 13 Topo-cluster time spectrum in data and MC selected multi-jet events. Four triggers are compared: **a** HLT_j15, **b** HLT_j25, **c** HLT_j45, and (d) HLT_j45_L1RD0_FILLED. The error bars convey the statistical and luminosity uncertainties. Uncertainties in the cut/no-cut ratios are obtained by splitting the available sample into subsamples and recomputing the cut/no-cut ratio for each subsample. The standard deviation of the distribution of the ratio is used to estimate the ratio's uncertainty. The luminosity uncertainty does not apply to the cut/no-cut ratio. In the plots, lines represent MC events and markers represent data, different colours and styles represent different cuts

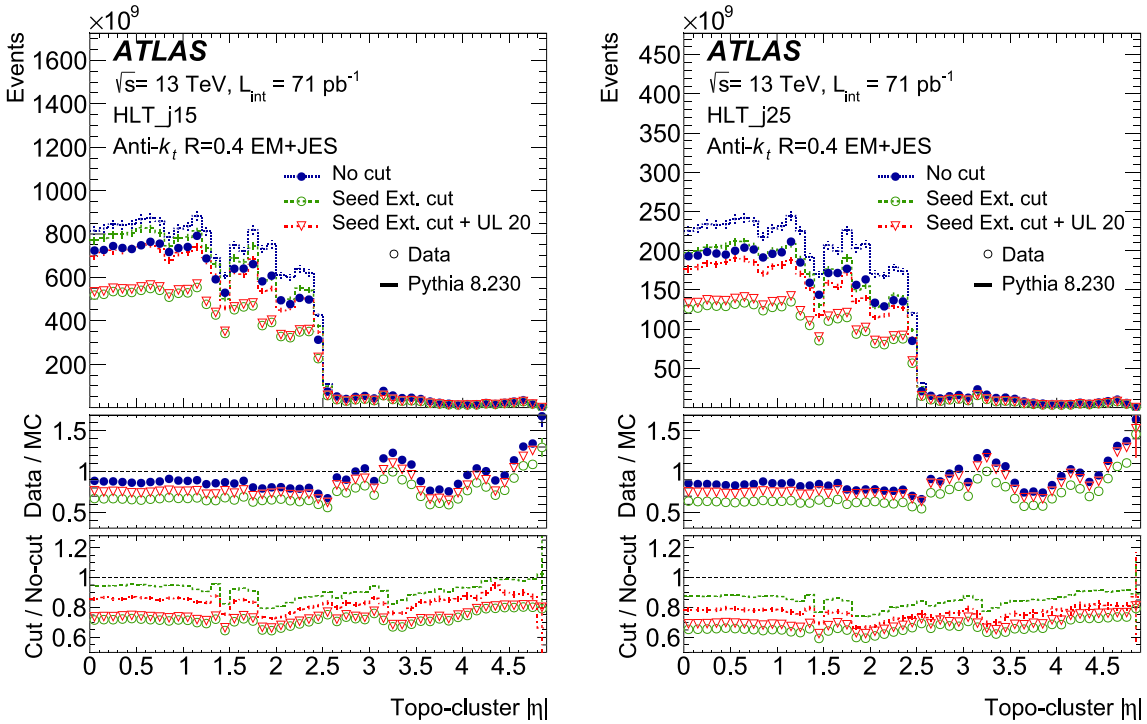

(a)

(b)

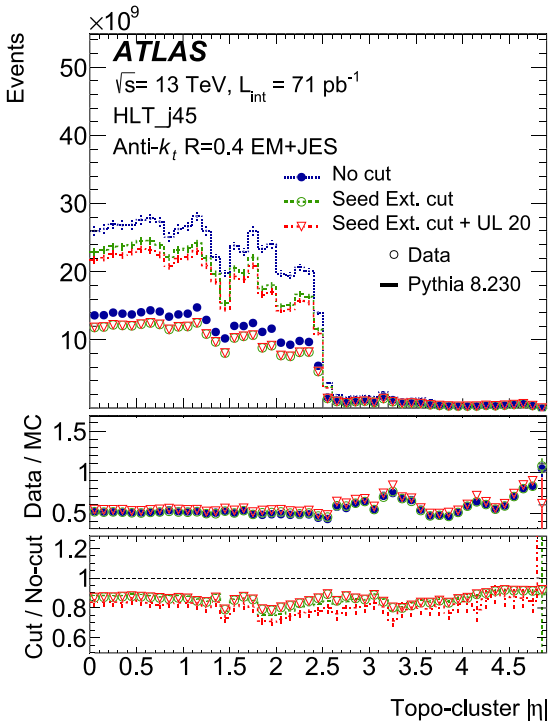

(c)

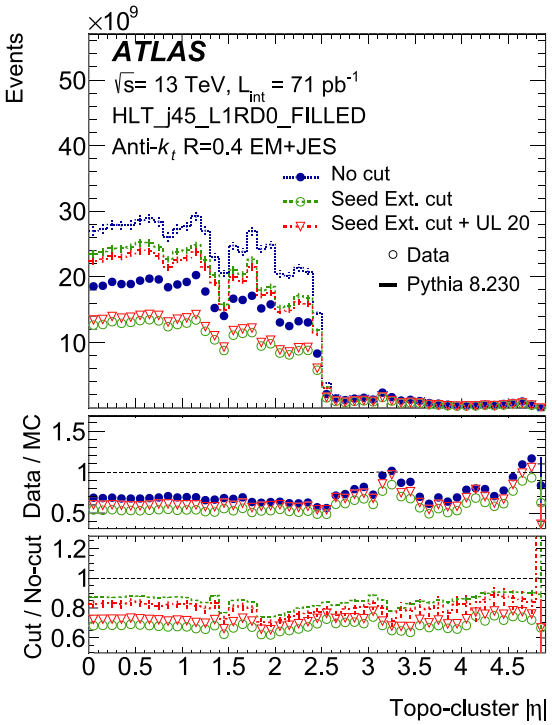

(d)

Fig. 14 Topo-cluster $|\eta|$ spectrum in data and MC selected multi-jet events. Four triggers are compared: **a** HLT_j15, **b** HLT_j25, **c** HLT_j45, and **d** HLT_j45_L1RD0_FILLED. The error bars convey the statistical and luminosity uncertainties. Uncertainties in the cut/no-cut ratios are obtained by splitting the available sample into subsamples and recomputing the cut/no-cut ratio for each subsample. The standard deviation of the distribution of the ratio is used to estimate the ratio's uncertainty. The luminosity uncertainty does not apply to the cut/no-cut ratio. In the plots, lines represent MC events and markers represent data, different colours and styles represent different cuts

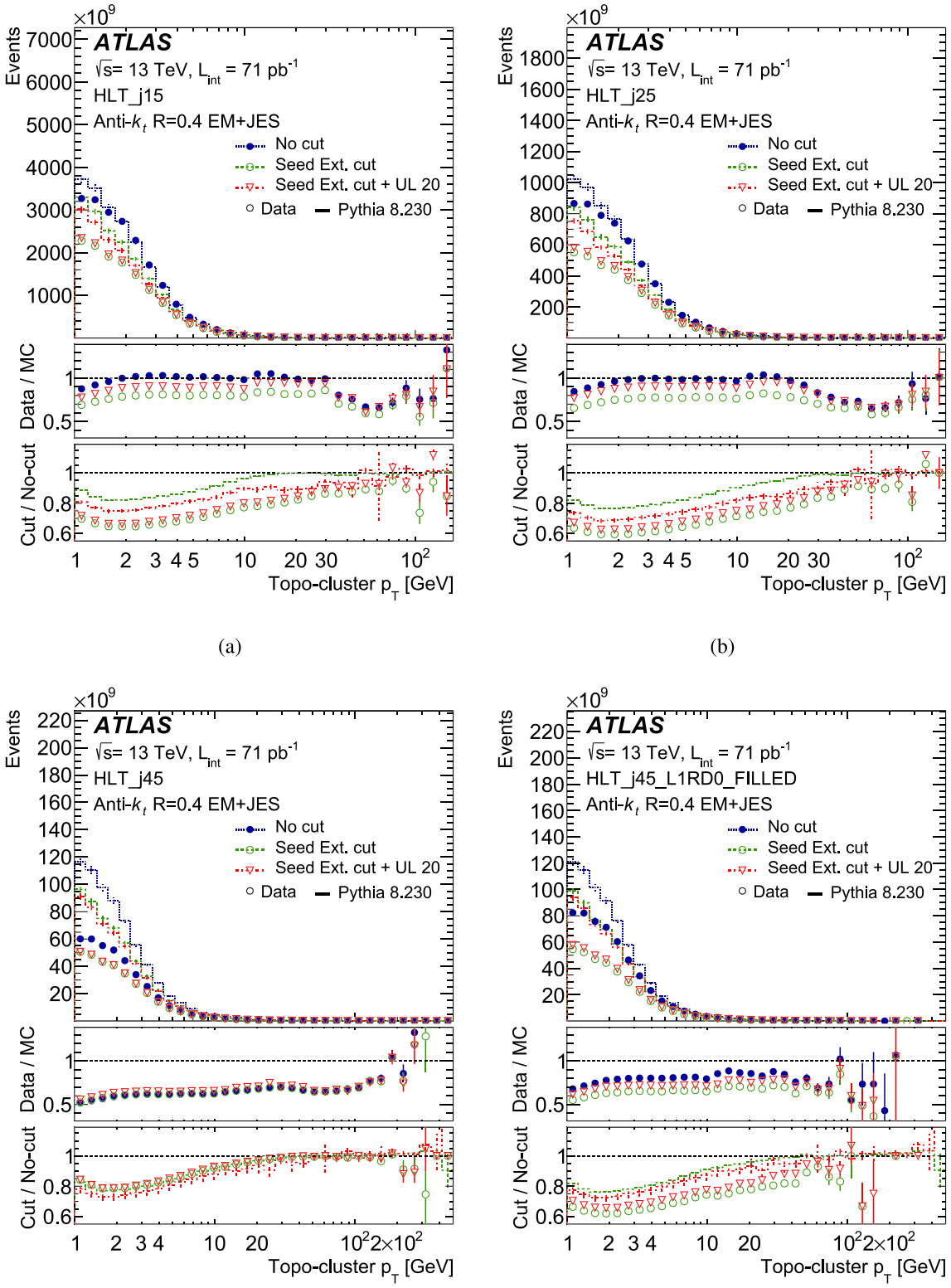

Fig. 15 Topo-cluster p_{T} spectrum in data and MC selected multi-jet events. Four triggers are compared: **a** HLT_j15, **b** HLT_j25, **c** HLT_j45, and **d** HLT_j45_L1RD0_FILLED. The error bars convey the statistical and luminosity uncertainties. Uncertainties in the cut/no-cut ratios are obtained by splitting the available sample into subsamples and recomputing the cut/no-cut ratio for each subsample. The standard deviation of the distribution of the ratio is used to estimate the ratio's uncertainty. The luminosity uncertainty does not apply to the cut/no-cut ratio. In the plots, lines represent MC events and markers represent data, different colours and styles represent different cuts

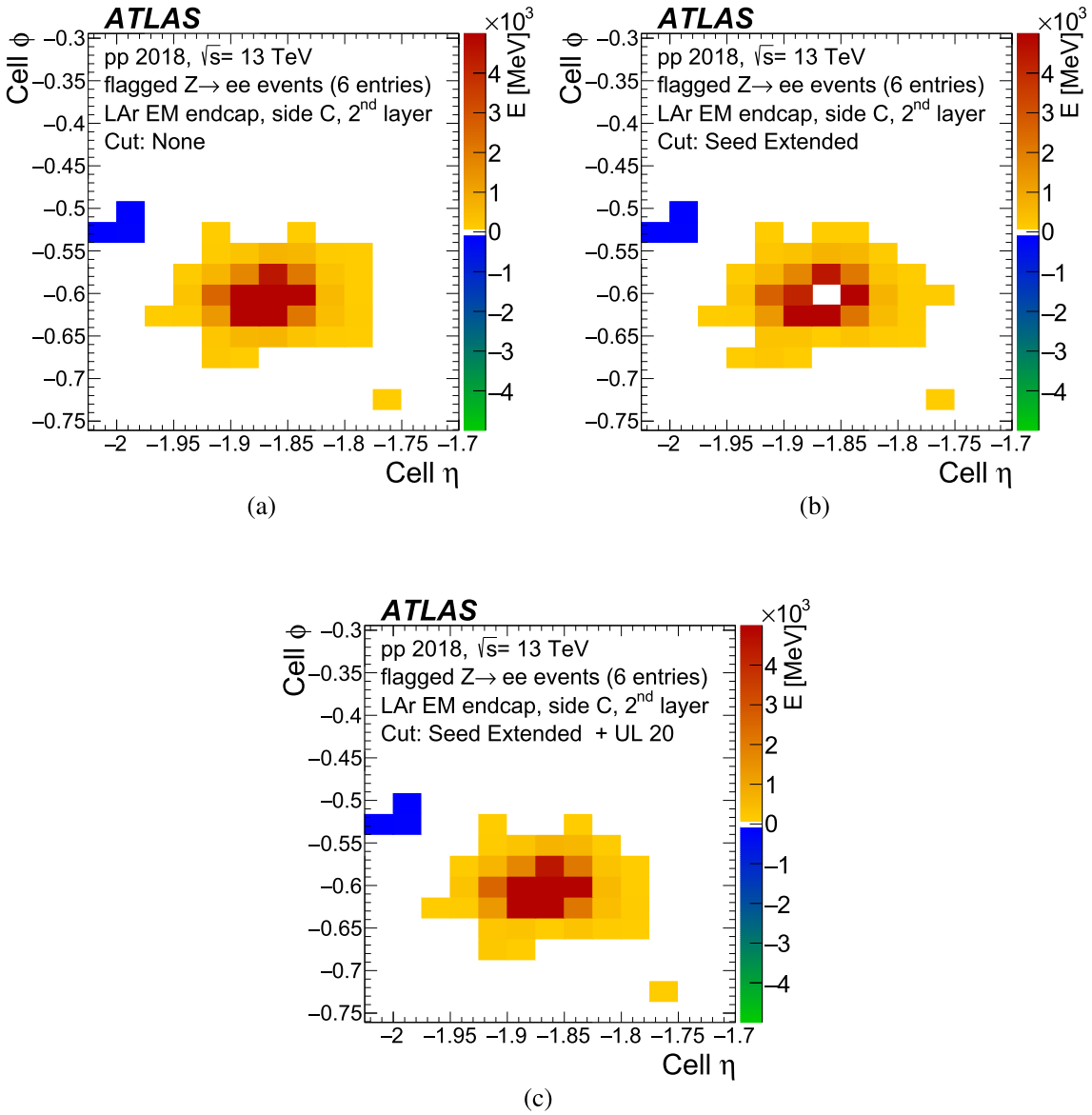

Fig. 16 The $\eta \times \phi$ distribution of cells belonging to topo-clusters in the second layer of the LAr EM endcap calorimeter, side C. The colour scale represents the recorded energy. Six events, in which $Z \to ee$ electrons hit the affected area, are averaged. The three panels show results with **a** no time cut, **b** the Seed Extended cut and **c** the Seed Extended plus $X_{\mathrm{UL}} = 20$ cut

the difference between the total energies computed with and without the time cut ($E_{\mathrm{cut}}^{\mathrm{cells(clus)}}$ and $E_{\mathrm{nocut}}^{\mathrm{cells(clus)}}$ respectively) satisfies:

$$|E_{\mathrm{cut}}^{\mathrm{cells(clus)}} - E_{\mathrm{nocut}}^{\mathrm{cells(clus)}}| < \sigma(E_{\mathrm{nocut}}^{\mathrm{cells(clus)}}),$$

where $\sigma(E_{\mathrm{nocut}}^{\mathrm{cells(clus)}})$ is the expected calorimeter resolution computed for either the cells' total energy (E^{cells}) or total cluster energy (E^{clus}) without any cut. The resolution is taken from Ref. [1] to be:

$$\frac{\sigma(E_{\mathrm{nocut}}^{\mathrm{cells(clus)}})}{E_{\mathrm{nocut}}^{\mathrm{cells(clus)}}} = \frac{10\%}{\sqrt{|E_{\mathrm{nocut}}^{\mathrm{cells(clus)}}|}} \oplus 0.7\%.$$

Figures 17 and 18 show $\mathcal{F}_{\mathrm{unchanged}}$ for the four variables of interest. Figure 17 is indicative of the time cut's impact on the cell content for clusters in the Test Region compared to that for clusters in the Control Regions. The fraction of events with unchanged N^{cells} is shown in Fig. 17a, b: for the Seed Extended cut, $\mathcal{F}_{\mathrm{unchanged}}$ in the Test Region is smaller than the average of the control values by slightly more than

Table 2 Definition of test and control regions

	η range	ϕ range
Test Region	$[-1.9, -1.825]$	$[-0.638, -0.565]$
Control Region 1	$[+1.9, +1.825]$	$[-0.638, -0.565]$
Control Region 2	$[-1.9, -1.825]$	$[+0.638, +0.565]$
Control Region 3	$[+1.9, +1.825]$	$[+0.638, +0.565]$

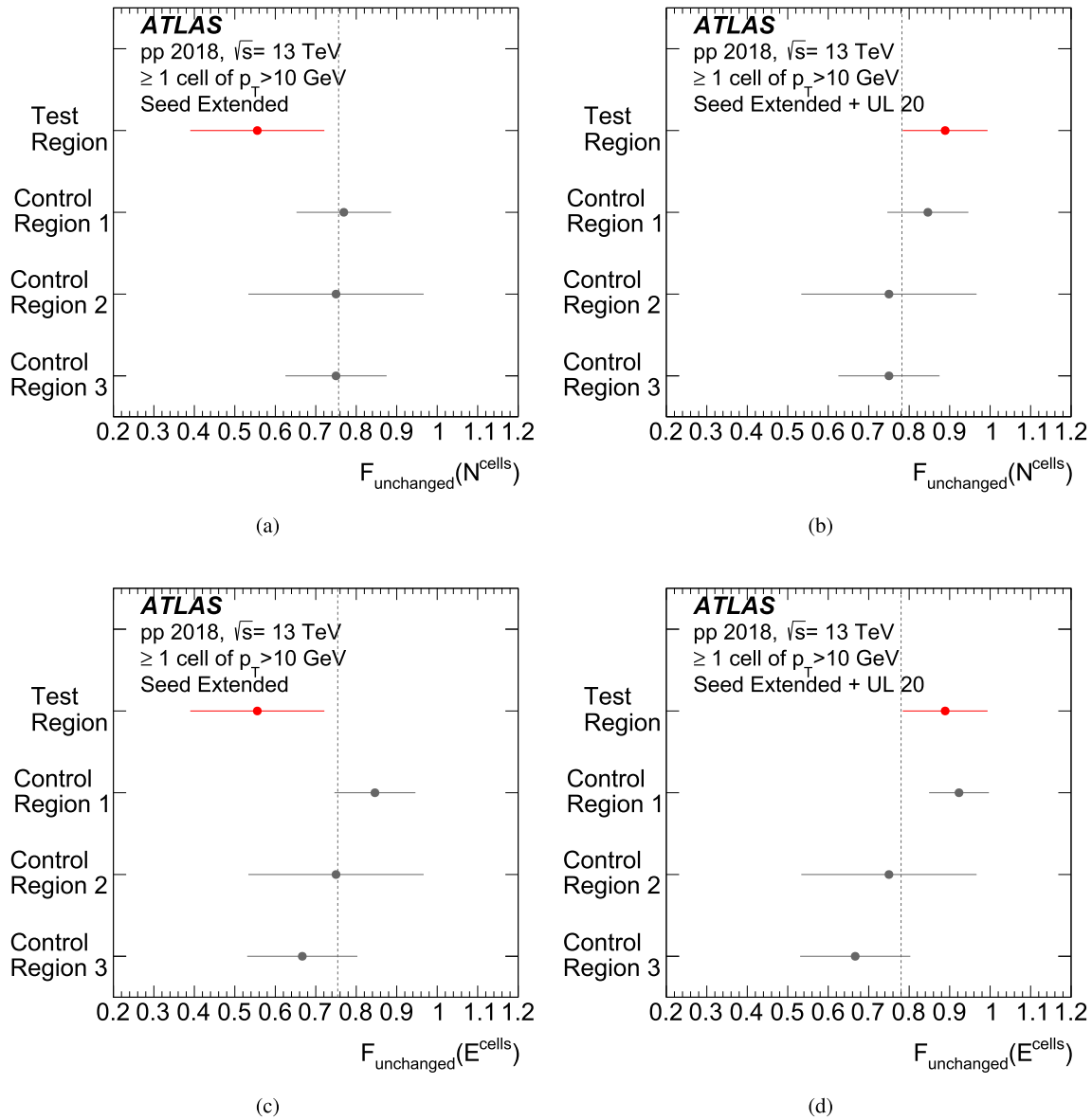

Fig. 17 Comparison between the Test Region and three Control Regions for **a** the fraction of events in which the cell occupancy N^{cells} is left unchanged by the Seed Extended cut, **b** the fraction of events in which N^{cells} is left unchanged by the Seed Extended plus $X_{\text{UL}} = 20$ cut, **c** the fraction of events in which the cells' total energy E^{cells} is left unchanged by the Seed Extended cut, and (d) the fraction of events in which E^{cells} is left unchanged by the Seed Extended plus $X_{\text{UL}} = 20$ cut. The cell occupancy (cells' total energy) in a given region is defined as the number (energy sum) of cells in the region that are included in a topo-cluster. Uncertainties on the event fractions are computed as the standard deviation of a binomial distribution. The dashed line represents the average of the three Control Regions

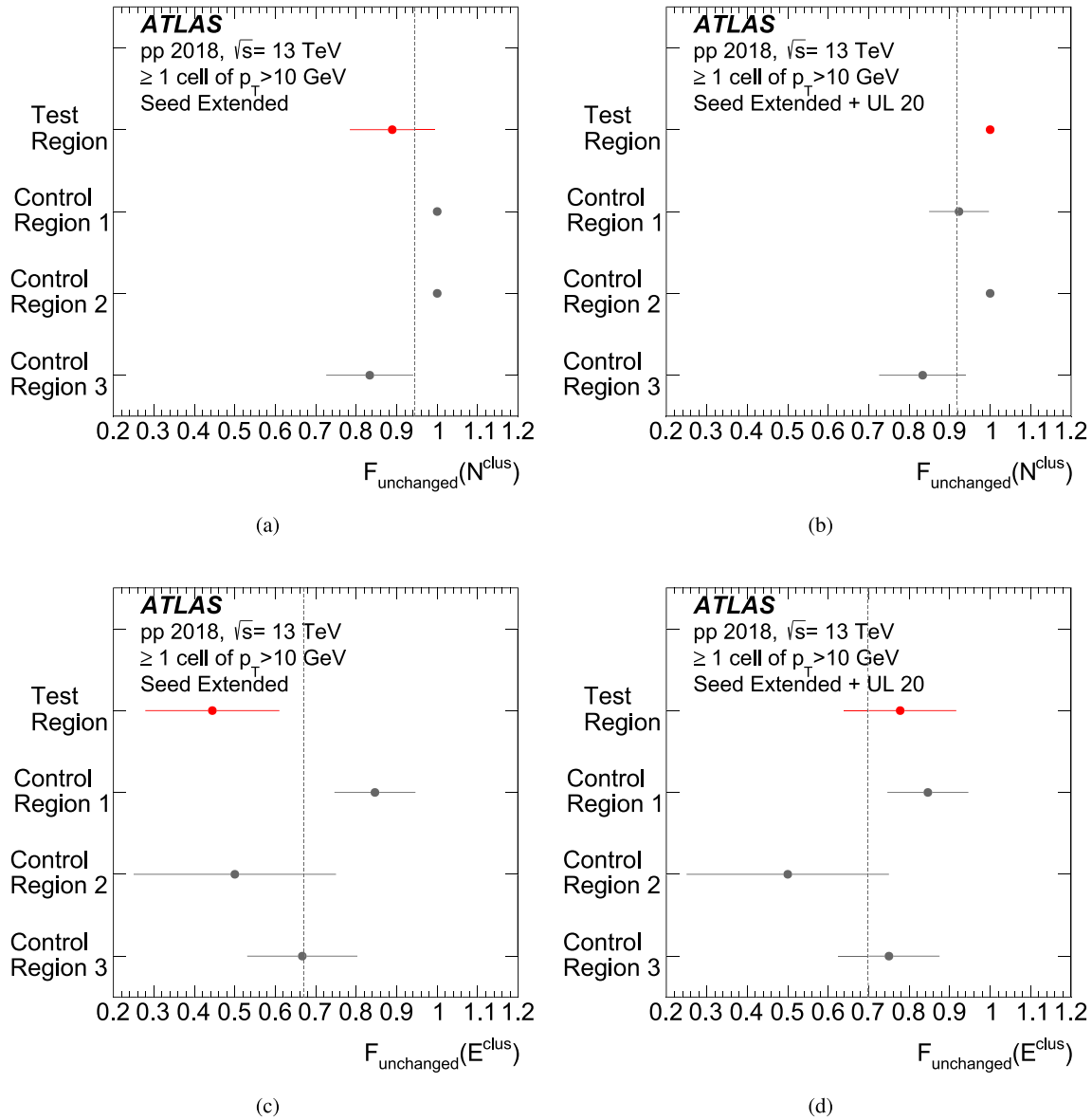

Fig. 18 Comparison between the Test Region and three Control Regions for **a** the fraction of events in which the topo-cluster occupancy N^{clus} is left unchanged by the Seed Extended cut, **b** the fraction of events in which N^{clus} is left unchanged by the Seed Extended plus $X_{\text{UL}} = 20$ cut, **c** the fraction of events in which the topo-cluster total energy E^{clus} is left unchanged by the Seed Extended cut, and **d** the fraction of events in which E^{clus} is left unchanged by the Seed Extended plus $X_{\text{UL}} = 20$ cut. The topo-cluster occupancy (total energy) in a given region is defined as the number (energy sum) of topo-clusters that contain at least one cell belonging to the region. Uncertainties on the event fractions are computed as the standard deviation of a binomial distribution. The dashed line represents the average of the three Control Regions

1σ. Even though the phenomenon has a small significance due to the limited sample size, the effect of the time cut can be seen to disappear when the same events are processed with the Seed Extended plus $X_{\text{UL}} = 20$ cut, confirming that cell losses are cured by the Upper Limit. The same behaviour is visible for E^{cells} (Fig. 17c, d), indicating that the loss of a cell, when it occurs, causes a significant energy variation, while no decrease in E^{cells} can be seen in the case of the Seed Extended plus $X_{\text{UL}} = 20$ cut. Figure 18 shows the fraction of events in which the topo-cluster occupancy and total energy are unchanged, thus investigating the effect of the time cut on topo-clusters as a whole, when they overlap the Test or Control Regions. The topo-cluster occupancy (Fig. 18a, b) remains consistent with the control values even for the Seed Extended cut, confirming that the signal topo-cluster is not entirely lost. The topo-cluster total energy E^{clus} is impacted by the Seed Extended cut (Fig. 18c), reflecting the loss of a cell in a way similar to that causing losses in the cells' total energy, while also being restored to its original value by applying the Upper Limit (Fig. 18d).

Table 3 Collection size changes for data events on disk with the introduction of the time cut. Changes of $\mathcal{O}(100\text{ b})$ are not significant for most categories since they can arise from changes in the alignment of the (otherwise unchanged) objects and the subsequent compression when writing to disk. Larger size changes are reported relative to the original size on disk. The "Cells in topo-clusters" line is limited to clusters matched to tracks, electrons and muons

Category	Fraction (before cut)	Size on disk before cut (kb)	Size on disk after cut (kb)	Size change (%)
Total	1.000	288.7	271.1	−6.1
Trigger	0.302	87.11	87.01	–
Tracking	0.218	62.95	62.84	–
Topo-clusters	0.150	43.21	35.95	−17
Particle-flow [42,43] objects	0.103	29.75	24.50	−18
τ-leptons	0.078	22.42	20.58	−8.2
Electrons/photons	0.071	20.37	18.79	−7.8
Cells in topo-clusters	0.057	16.60	15.13	−8.8
Muons	0.018	5.293	5.295	–
ATLAS forward proton detector [51,52]	0.003	0.810	0.810	–
Metadata	0.001	0.154	0.154	–

Table 4 Collection size changes for MC events on disk with the introduction of the time cut. Changes of $\mathcal{O}(100\text{ b})$ are not significant for most categories since they can arise from changes in the alignment of the (otherwise unchanged) objects and the subsequent compression when writing to disk. The "Cells in topo-clusters" line is limited to clusters matched to tracks, electrons and muons

Category	Fraction (before cut)	Disk size before cut (kb)	Disk size after cut (kb)	Size change (%)
Total	1.000	428.8	398.3	−7.1
Tracking	0.222	94.98	94.51	−0.5
Topo-clusters	0.160	68.79	57.34	−17
Particle-flow [42,43] objects	0.114	49.00	39.94	−18
τ-leptons	0.108	46.38	43.24	−6.8
Trigger	0.106	45.26	45.25	–
Generator-level event	0.103	44.28	44.29	–
Electrons/photons	0.086	36.94	33.74	−8.6
Cells in topo-clusters	0.082	34.98	31.80	−9.1
Muons	0.016	6.927	6.931	–
Metadata	0.003	1.201	1.202	–
ATLAS forward proton detector [51,52]	< 0.001	0.041	0.041	–

7.2 Impact on the ATLAS event size

Calorimeter topo-clusters are used as input to the reconstruction of particles other than jets, most notably electrons, photons and τ-leptons. The time cut will then have pile-up-suppressing effects on these particles as well. A complete discussion of the effects of the time cut on electrons, photons and τ-leptons is beyond the scope of this paper. However, the widespread usage of topo-clusters in the ATLAS event reconstruction implies that the time cut can have a large beneficial effect on the overall consumption of computing resources by ATLAS data and MC samples.

The change in the ATLAS event size due to the time cut was evaluated for the introduction of the Seed Extended plus $X_{\text{UL}} = 20$ time cut into the default ATLAS reconstruction at the beginning of Run 3, before the start of 2023 data-taking. The test is performed by reconstructing one data sample and one MC sample ($t\bar{t}$ production in the fully hadronic decay) before and after the introduction of the time cut and later comparing the average event sizes on disk. In both samples the detector conditions are those of Run 3. Results are shown in Tables 3 and 4. The principal particle collections are shown, together with their relative size change. As expected, the largest effects are observed for the particle-flow object and topo-cluster collections, which are reduced in size by ∼16% to ∼18%, while smaller differences are present for electrons/photons and τ-leptons.[7] The overall event size is reduced by about 6% in data and 7% in MC simulation.

[7] A very small difference in the 'Tracking' category is to be expected since specific information related to electron tracks is grouped in this category.

8 Conclusion

This paper presents the design and evaluation of a cell-level time criterion used in the ATLAS topo-cluster reconstruction algorithm. This criterion (the "time cut") removes cells compatible with out-of-time pile-up signals. A second requirement, the Upper Limit, is imposed to prevent cells with a large amount of energy from being removed, including those expected from long-lived particles. The impact of the time cut on the reconstruction of hadronic signals was studied at both cluster level and jet level, using a combination of MC samples and ATLAS data recorded in 2017 and 2018.

The time cut was found to significantly reduce the contribution from out-of-time pile-up while not hindering signal reconstruction. Studies of MC events indicate that the multiplicity of out-of-time pile-up jets is reduced by ∼50% at $p_{\mathrm{T}} \sim 20$ GeV and by ∼80% above $p_{\mathrm{T}} \sim 50$ GeV, across the rapidity region $|y| \lesssim 3.5$. Studies of data events found that the time cut has negligible effect on events accepted by a single-jet trigger, requiring one jet with $p_{\mathrm{T}} > 45$ GeV and seeded by a single jet at L1. On the other hand, the time cut does affect events enriched in out-of-time pile-up, typically those accepted by a random L1 trigger. In this case, the effect of the time cut is largest for $p_{\mathrm{T}} \lesssim 30$ GeV and it is found to have a stronger effect on data events than on MC events, typical differences being of $\mathcal{O}(10\%)$. The effect is believed to be caused by the absence of pile-up-only events in the MC simulation. Additional tests for signal inefficiency in data were carried out and show that the time cut would not cause a loss of clusters in the case of a calorimeter channel miscalibration. The addition of the Upper Limit is also found to prevent the loss of individual cells within clusters in such a case.

The time cut was also found to impact the jet calibration, a repetition of the pile-up correction step being necessary. The time cut provides percent-level improvement in the jet resolution at $p_t \lesssim 30$ GeV. More extensive investigation is needed to evaluate in detail the effect of the time cut on the jet energy resolution and jet energy scale uncertainty, e.g. the pile-up-related JES uncertainty components. The full calibration chain will be re-evaluated after the introduction of the time cut into the ATLAS reconstruction software.

The Seed Extended plus $X_{\mathrm{UL}} = 20$ cut was found to be the best option among those studied. This cut was adopted as the default for offline topo-cluster reconstruction in ATLAS Run 3 data. The introduction of the Seed Extended plus $X_{\mathrm{UL}} = 20$ cut into the ATLAS offline reconstruction is also found to reduce the ATLAS event size on disk by 6% in data and by 7% in MC simulation. Further studies are necessary before the cut can be introduced at trigger level.

Acknowledgements We thank CERN for the very successful operation of the LHC, as well as the support staff from our institutions without whom ATLAS could not be operated efficiently. We acknowledge the support of ANPCyT, Argentina; YerPhI, Armenia; ARC, Australia; BMWFW and FWF, Austria; ANAS, Azerbaijan; CNPq and FAPESP, Brazil; NSERC, NRC and CFI, Canada; CERN; ANID, Chile; CAS, MOST and NSFC, China; Minciencias, Colombia; MEYS CR, Czech Republic; DNRF and DNSRC, Denmark; IN2P3-CNRS and CEA-DRF/IRFU, France; SRNSFG, Georgia; BMBF, HGF and MPG, Germany; GSRI, Greece; RGC and Hong Kong SAR, China; ISF and Benoziyo Center, Israel; INFN, Italy; MEXT and JSPS, Japan; CNRST, Morocco; NWO, Netherlands; RCN, Norway; MEiN, Poland; FCT, Portugal; MNE/IFA, Romania; MESTD, Serbia; MSSR, Slovakia; ARRS and MIZŠ, Slovenia; DSI/NRF, South Africa; MICINN, Spain; SRC and Wallenberg Foundation, Sweden; SERI, SNSF and Cantons of Bern and Geneva, Switzerland; MOST, Taipei; TENMAK, Türkiye; STFC, United Kingdom; DOE and NSF, United States of America. In addition, individual groups and members have received support from BCKDF, CANARIE, CRC and DRAC, Canada; PRIMUS 21/SCI/017 and UNCE SCI/013, Czech Republic; COST, ERC, ERDF, Horizon 2020, ICSC-NextGenerationEU and Marie Skłodowska-Curie Actions, European Union; Investissements d'Avenir Labex, Investissements d'Avenir Idex and ANR, France; DFG and AvH Foundation, Germany; Herakleitos, Thales and Aristeia programmes co-financed by EU-ESF and the Greek NSRF, Greece; BSF-NSF and MINERVA, Israel; Norwegian Financial Mechanism 2014–2021, Norway; NCN and NAWA, Poland; La Caixa Banking Foundation, CERCA Programme Generalitat de Catalunya and PROMETEO and GenT Programmes Generalitat Valenciana, Spain; Göran Gustafssons Stiftelse, Sweden; The Royal Society and Leverhulme Trust, United Kingdom. The crucial computing support from all WLCG partners is acknowledged gratefully, in particular from CERN, the ATLAS Tier-1 facilities at TRIUMF/SFU (Canada), NDGF (Denmark, Norway, Sweden), CC-IN2P3 (France), KIT/GridKA (Germany), INFN-CNAF (Italy), NL-T1 (Netherlands), PIC (Spain), RAL (UK) and BNL (USA), the Tier-2 facilities worldwide and large non-WLCG resource providers. Major contributors of computing resources are listed in Ref. [53].

Data Availability Statement This manuscript has no associated data or the data will not be deposited. [Authors' comment: All ATLAS scientific output is published in journals, and preliminary results are made available in Conference Notes. All are openly available, without restriction on use by external parties beyond copyright law and the standard conditions agreed by CERN. Data associated with journal publications are also made available: tables and data from plots (e.g. cross section values, likelihood profiles, selection efficiencies, cross section limits, ...) are stored in appropriate repositories such as HEPDATA (http://hepdata.cedar.ac.uk/). ATLAS also strives to make additional material related to the paper available that allows a reinterpretation of the data in the context of new theoretical models. For example, an extended encapsulation of the analysis is often provided for measurements in the framework of RIVET (http://rivet.hepforge.org/). This information is taken from the ATLAS Data Access Policy, which is a public document that can be downloaded from http://opendata.cern.ch/record/413 [opendata.cern.ch]].

Open Access This article is licensed under a Creative Commons Attribution 4.0 International License, which permits use, sharing, adaptation, distribution and reproduction in any medium or format, as long as you give appropriate credit to the original author(s) and the source, provide a link to the Creative Commons licence, and indicate if changes were made. The images or other third party material in this article are included in the article's Creative Commons licence, unless indicated otherwise in a credit line to the material. If material is not included in the article's Creative Commons licence and your intended use is not permitted by statutory regulation or exceeds the permitted use, you will need to obtain permission directly from the copyright holder. To view a copy of this licence, visit http://creativecomm

ons.org/licenses/by/4.0/.
Funded by SCOAP[3].

References

1. ATLAS Collaboration, The ATLAS Experiment at the CERN Large Hadron Collider. JINST **3**, S08003 (2008). https://doi.org/10.1088/1748-0221/3/08/S08003
2. L. Evans, P. Bryant, L.H.C. Machine, JINST **3**, S08001 (2008). https://doi.org/10.1088/1748-0221/3/08/S08001
3. ATLAS Collaboration, Topological cell clustering in the ATLAS calorimeters and its performance in LHC Run 1. Eur. Phys. J. C **77**, 490 (2017). https://doi.org/10.1140/epjc/s10052-017-5004-5. arXiv:1603.02934 [hep-ex]
4. ATLAS Collaboration, Luminosity determination in pp collisions at $\sqrt{s} = 13$ TeV using the ATLAS detector at the LHC. Eur. Phys. J. C **83**, 982 (2023). https://doi.org/10.1140/epjc/s10052-023-11747-w. arXiv:2212.09379 [hep-ex]
5. D. Krohn, J. Thaler, L.-T. Wang, Jet trimming. JHEP **02**, 084 (2010). https://doi.org/10.1007/JHEP02(2010)084. arXiv:0912.1342 [hep-ph]
6. A.J. Larkoski, S. Marzani, G. Soyez, J. Thaler, Soft drop. JHEP **05**, 146 (2014). https://doi.org/10.1007/JHEP05(2014)146. arXiv:1402.2657 [hep-ph]
7. M. Dasgupta, A. Fregoso, S. Marzani, G.P. Salam, Towards an understanding of jet substructure. JHEP **09**, 029 (2013). https://doi.org/10.1007/JHEP09(2013)029. arXiv:1307.0007 [hep-ph]
8. P. Berta, M. Spousta, D.W. Miller, R. Leitner, Particle-level pileup subtraction for jets and jet shapes. JHEP **06**, 092 (2014). https://doi.org/10.1007/JHEP06(2014)092. arXiv:1403.3108 [hep-ex]
9. M. Cacciari, G.P. Salam, G. Soyez, SoftKiller, a particle-level pileup removal method. Eur. Phys. J. C **75**, 59 (2015). https://doi.org/10.1140/epjc/s10052-015-3267-2. arXiv:1407.0408 [hep-ph]
10. ATLAS Collaboration, Optimisation of large-radius jet reconstruction for the ATLAS detector in 13 TeV proton-proton collisions. Eur. Phys. J. C **81**, 334 (2021). https://doi.org/10.1140/epjc/s10052-021-09054-3. arXiv:2009.04986 [hep-ex]
11. ATLAS Collaboration, ATLAS Insertable B-Layer: Technical Design Report, ATLAS-TDR-19; CERN-LHCC-2010-013 (2010). https://cds.cern.ch/record/1291633 [Addendum: ATLAS-TDR-19-ADD-1; CERN-LHCC-2012-009 (2012). https://cds.cern.ch/record/1451888]
12. B. Abbott et al., Production and integration of the ATLAS Insertable B-Layer. JINST **13**, T05008 (2018). https://doi.org/10.1088/1748-0221/13/05/T05008. arXiv:1803.00844 [physics.ins-det]
13. ATLAS Collaboration, Performance of the ATLAS trigger system in 2015. Eur. Phys. J. C **77**, 317 (2017). https://doi.org/10.1140/epjc/s10052-017-4852-3. arXiv:1611.09661 [hep-ex]
14. ATLAS Collaboration, The ATLAS Collaboration Software and Firmware, ATL-SOFT-PUB-2021-001 (2021). https://cds.cern.ch/record/2767187
15. N.J. Buchanan et al., Design and implementation of the Front End Board for the readout of the ATLAS liquid argon calorimeters. JINST **3**, P03004 (2008). https://doi.org/10.1088/1748-0221/3/03/P03004
16. W.E. Cleland, E.G. Stern, Signal processing considerations for liquid ionization calorimeters in a high rate environment. Nucl. Instrum. Meth. A **338**, 467 (1994). https://doi.org/10.1016/0168-9002(94)91332-3
17. ATLAS Collaboration, Readiness of the ATLAS liquid argon calorimeter for LHC collisions. Eur. Phys. J. C **70**, 723 (2010). https://doi.org/10.1140/epjc/s10052-010-1354-y.arXiv:0912.2642 [hep-ex]
18. ATLAS Collaboration, LAr Time Resolution Plots for 2015 Data. https://twiki.cern.ch/twiki/bin/view/AtlasPublic/LArCaloPublicResults2015
19. ATLAS Collaboration, Monitoring and data quality assessment of the ATLAS liquid argon calorimeter. JINST **9**, P07024 (2014). https://doi.org/10.1088/1748-0221/9/07/P07024. arXiv:1405.3768 [hep-ex]
20. ATLAS Collaboration, Readiness of the ATLAS Tile Calorimeter for LHC collisions. Eur. Phys. J. C **70**, 1193 (2010). https://doi.org/10.1140/epjc/s10052-010-1508-y. arXiv:1007.5423 [hep-ex]
21. M.N. Agaras et al., Laser calibration of the ATLAS Tile Calorimeter during LHC Run 2. JINST **18**, P06023 (2023). https://doi.org/10.1088/1748-0221/18/06/P06023. arXiv:2303.00121 [physics.ins-det]
22. ATLAS Collaboration, Timing calibration and performance public plots. https://twiki.cern.ch/twiki/bin/view/AtlasPublic/TileCaloPublicResultsTiming
23. ATLAS Collaboration, ATLAS data quality operations and performance for 2015–2018 data-taking. JINST **15**, P04003 (2020). https://doi.org/10.1088/1748-0221/15/04/P04003. arXiv:1911.04632 [physics.ins-det]
24. G. Avoni et al., The new LUCID-2 detector for luminosity measurement and monitoring in ATLAS. JINST **13**, P07017 (2018). https://doi.org/10.1088/1748-0221/13/07/P07017
25. T. Sjöstrand et al., An introduction to PYTHIA 8.2. Comput. Phys. Commun. **191**, 159 (2015). https://doi.org/10.1016/j.cpc.2015.01.024. arXiv:1410.3012 [hep-ph]
26. NNPDF Collaboration, R. D. Ball et al., Parton distributions with LHC data. Nucl. Phys. B **867**, 244 (2013). https://doi.org/10.1016/j.nuclphysb.2012.10.003. arXiv:1207.1303 [hep-ph]
27. ATLAS Collaboration, ATLAS Pythia 8 tunes to 7 TeV data, ATL-PHYS-PUB-2014-021 (2014). https://cds.cern.ch/record/1966419
28. B. Andersson, G. Gustafson, G. Ingelman, T. Sjöstrand, Parton fragmentation and string dynamics. Phys. Rep. **97**, 31 (1983). https://doi.org/10.1016/0370-1573(83)90080-7
29. T. Sjöstrand, Jet fragmentation of multiparton configurations in a string framework. Nucl. Phys. B **248**, 469 (1984). https://doi.org/10.1016/0550-3213(84)90607-2
30. T. Sjöstrand, S. Mrenna, P. Skands, A brief introduction to PYTHIA 8.1. Comput. Phys. Commun. **178**, 852 (2008). https://doi.org/10.1016/j.cpc.2008.01.036. arXiv:0710.3820 [hep-ph]
31. ATLAS Collaboration, The Pythia 8 A3 tune description of ATLAS minimum bias and inelastic measurements incorporating the Donnachie–Landshoff diffractive model, ATL-PHYS-PUB-2016-017 (2016). https://cds.cern.ch/record/2206965
32. S. Frixione, G. Ridolfi, P. Nason, A positive-weight next-to-leading-order Monte Carlo for heavy flavour hadroproduction. JHEP **09**, 126 (2007). https://doi.org/10.1088/1126-6708/2007/09/126. arXiv:0707.3088 [hep-ph]
33. P. Nason, A new method for combining NLO QCD with shower Monte Carlo algorithms. JHEP **11**, 040 (2004). https://doi.org/10.1088/1126-6708/2004/11/040. arXiv:0409146 [hep-ph]
34. S. Frixione, P. Nason, C. Oleari, Matching NLO QCD computations with parton shower simulations: the POWHEG method. JHEP **11**, 070 (2007). https://doi.org/10.1088/1126-6708/2007/11/070. arXiv:0709.2092 [hep-ph]
35. S. Alioli, P. Nason, C. Oleari, E. Re, A general framework for implementing NLO calculations in shower Monte Carlo programs: the POWHEG BOX. JHEP **06**, 043 (2010). https://doi.org/10.1007/JHEP06(2010)043. arXiv:1002.2581 [hep-ph]
36. NNPDF Collaboration, R.D. Ball et al., Parton distributions for the LHC run II. JHEP **04**, 040 (2015). https://doi.org/10.1007/JHEP04(2015)040. arXiv:1410.8849 [hep-ph]
37. ATLAS Collaboration, Studies on top-quark Monte Carlo modelling for Top2016, ATL-PHYS-PUB-2016-020 (2016). https://cds.cern.ch/record/2216168

38. D.J. Lange, The EvtGen particle decay simulation package. Nucl. Instrum. Meth. A **462**, 152 (2001). https://doi.org/10.1016/S0168-9002(01)00089-4
39. J. Alimena et al., Searching for long-lived particles beyond the Standard Model at the Large Hadron Collider. J. Phys. G **47**, 090501 (2020). https://doi.org/10.1088/1361-6471/ab4574. arXiv:1903.04497 [hep-ex]
40. L. Lee, C. Ohm, A. Soffer and T.-T. Yu, Collider Searches for Long-Lived Particles Beyond the Standard Model. Prog. Part. Nucl. Phys. **106**, 210 (2019). https://doi.org/10.1016/j.ppnp.2019.02.006. arXiv:1810.12602 [hep-ph] [Erratum: Prog. Part. Nucl. Phys. **122**, 103912 (2022). issn: 0146-6410]
41. M. Cacciari, G.P. Salam, G. Soyez, The anti-k_t jet clustering algorithm. JHEP **04**, 063 (2008). https://doi.org/10.1088/1126-6708/2008/04/063. arXiv:0802.1189 [hep-ph]
42. ATLAS Collaboration, Jet reconstruction and performance using particle flow with the ATLAS Detector. Eur. Phys. J. C **77**, 466 (2017). https://doi.org/10.1140/epjc/s10052-017-5031-2. arXiv:1703.10485 [hep-ex]
43. ATLAS Collaboration, Jet energy scale and resolution measured in proton-proton collisions at $\sqrt{s} = 13$ TeV with the ATLAS detector. Eur. Phys. J. C **81**, 689 (2021). https://doi.org/10.1140/epjc/s10052-021-09402-3. arXiv:2007.02645 [hep-ex]
44. S.D. Ellis, D.E. Soper, Successive combination jet algorithm for hadron collisions. Phys. Rev. D **48**, 3160 (1993). https://doi.org/10.1103/PhysRevD.48.3160
45. S. Catani, Y. Dokshitzer, M. Seymour, B. Webber, Longitudinally-invariant $k_\perp$-clustering algorithms for hadron-hadron collisions. Nucl. Phys. B **406**, 187 (1993). https://doi.org/10.1016/0550-3213(93)90166-M, issn: 0550-3213
46. ATLAS Collaboration, Tagging and suppression of pileup jets with the ATLAS detector, ATLAS-CONF-2014-018 (2014). https://cds.cern.ch/record/1700870
47. ATLAS Collaboration, Emulating the impact of additional proton–proton interactions in the ATLAS simulation by pre-sampling sets of inelastic Monte Carlo events. Comput. Softw. Big Sci. **6**, 3 (2022). https://doi.org/10.1007/s41781-021-00062-2. arXiv:2102.09495 [hep-ex]
48. ATLAS Collaboration, Search for displaced photons produced in exotic decays of the Higgs boson using 13 TeV pp collisions with the ATLAS detector. Phys. Rev. D **108**, 032016 (2023). https://doi.org/10.1103/PhysRevD.108.032016. arXiv:2209.01029 [hep-ex]
49. ATLAS Collaboration, Search in diphoton and dielectron final states for displaced production of Higgs or Z bosons with the ATLAS detector in $\sqrt{s} = 13$ TeV pp collisions. Phys. Rev. D **108**, 012012 (2023). https://doi.org/10.1103/PhysRevD.108.012012. arXiv:2304.12885 [hep-ex]
50. ATLAS Collaboration, Electron and photon performance measurements with the ATLAS detector using the 2015–2017 LHC proton–proton collision data. JINST **14**, P12006 (2019). https://doi.org/10.1088/1748-0221/14/12/P12006. arXiv:1908.00005 [hep-ex]
51. ATLAS Collaboration, ATLAS Forward Proton Phase-I Upgrade: Technical Design Report, ATLAS-TDR-024; CERN-LHCC-2015-009 (2015). https://cds.cern.ch/record/2017378
52. ATLAS Collaboration, Proton tagging with the one arm AFP detector, ATL-PHYS-PUB-2017-012 (2017). https://cds.cern.ch/record/2273274
53. ATLAS Collaboration, ATLAS Computing Acknowledgements, ATL-SOFT-PUB-2023-001 (2023). https://cds.cern.ch/record/2869272

ATLAS Collaboration*

G. Aad[102], B. Abbott[120], K. Abeling[55], N. J. Abicht[49], S. H. Abidi[29], A. Aboulhorma[35e], H. Abramowicz[151], H. Abreu[150], Y. Abulaiti[117], B. S. Acharya[69a,69b,m], C. Adam Bourdarios[4], L. Adamczyk[86a], S. V. Addepalli[26], M. J. Addison[101], J. Adelman[115], A. Adiguzel[21c], T. Adye[134], A. A. Affolder[136], Y. Afik[36], M. N. Agaras[13], J. Agarwala[73a,73b], A. Aggarwal[100], C. Agheorghiesei[27c], A. Ahmad[36], F. Ahmadov[38,y], W. S. Ahmed[104], S. Ahuja[95], X. Ai[62a], G. Aielli[76a,76b], A. Aikot[163], M. Ait Tamlihat[35e], B. Aitbenchikh[35a], I. Aizenberg[169], M. Akbiyik[100], T. P. A. Åkesson[98], A. V. Akimov[37], D. Akiyama[168], N. N. Akolkar[24], S. Aktas[21a], K. Al Khoury[41], G. L. Alberghi[23b], J. Albert[165], P. Albicocco[53], G. L. Albouy[60], S. Alderweireldt[52], M. Aleksa[36], I. N. Aleksandrov[38], C. Alexa[27b], T. Alexopoulos[10], F. Alfonsi[23b], M. Algren[56], M. Alhroob[120], B. Ali[132], H. M. J. Ali[91], S. Ali[148], S. W. Alibocus[92], M. Aliev[145], G. Alimonti[71a], W. Alkakhi[55], C. Allaire[66], B. M. M. Allbrooke[146], J. F. Allen[52], C. A. Allendes Flores[137f], P. P. Allport[20], A. Aloisio[72a,72b], F. Alonso[90], C. Alpigiani[138], M. Alvarez Estevez[99], A. Alvarez Fernandez[100], M. Alves Cardoso[56], M. G. Alviggi[72a,72b], M. Aly[101], Y. Amaral Coutinho[83b], A. Ambler[104], C. Amelung[36], M. Amerl[101], C. G. Ames[109], D. Amidei[106], S. P. Amor Dos Santos[130a], K. R. Amos[163], V. Ananiev[125], C. Anastopoulos[139], T. Andeen[11], J. K. Anders[36], S. Y. Andrean[47a,47b], A. Andreazza[71a,71b], S. Angelidakis[9], A. Angerami[41,ab], A. V. Anisenkov[37], A. Annovi[74a], C. Antel[56], M. T. Anthony[139], E. Antipov[145], M. Antonelli[53], F. Anulli[75a], M. Aoki[84], T. Aoki[153], J. A. Aparisi Pozo[163], M. A. Aparo[146], L. Aperio Bella[48], C. Appelt[18], A. Apyan[26], N. Aranzabal[36], S. J. Arbiol Val[87], C. Arcangeletti[53], A. T. H. Arce[51], E. Arena[92], J.-F. Arguin[108], S. Argyropoulos[54], J.-H. Arling[48], O. Arnaez[4], H. Arnold[114], G. Artoni[75a,75b], H. Asada[111], K. Asai[118], S. Asai[153], N. A. Asbah[61], K. Assamagan[29], R. Astalos[28a], S. Atashi[160], R. J. Atkin[33a], M. Atkinson[162], H. Atmani[35f], P. A. Atmasiddha[128], K. Augsten[132], S. Auricchio[72a,72b], A. D. Auriol[20], V. A. Austrup[101], G. Avolio[36], K. Axiotis[56], G. Azuelos[108,af], D. Babal[28b], H. Bachacou[135], K. Bachas[152,p], A. Bachiu[34], F. Backman[47a,47b], A. Badea[61], T. M. Baer[106], P. Bagnaia[75a,75b], M. Bahmani[18], A. J. Bailey[163], V. R. Bailey[162], J. T. Baines[134], L. Baines[94], O. K. Baker[172], E. Bakos[15], D. Bakshi Gupta[8], V. Balakrishnan[120], R. Balasubramanian[114], E. M. Baldin[37],

P. Balek[86a], E. Ballabene[23a,23b], F. Balli[135], L. M. Baltes[63a], W. K. Balunas[32], J. Balz[100], E. Banas[87], M. Bandieramonte[129], A. Bandyopadhyay[24], S. Bansal[24], L. Barak[151], M. Barakat[48], E. L. Barberio[105], D. Barberis[57a,57b], M. Barbero[102], M. Z. Barel[114], K. N. Barends[33a], T. Barillari[110], M.-S. Barisits[36], T. Barklow[143], P. Baron[122], D. A. Baron Moreno[101], A. Baroncelli[62a], G. Barone[29], A. J. Barr[126], J. D. Barr[96], L. Barranco Navarro[47a,47b], F. Barreiro[99], J. Barreiro Guimarães da Costa[14a], U. Barron[151], M. G. Barros Teixeira[130a], S. Barsov[37], F. Bartels[63a], R. Bartoldus[143], A. E. Barton[91], P. Bartos[28a], A. Basan[100], M. Baselga[49], A. Bassalat[66,b], M. J. Basso[156a], C. R. Basson[101], R. L. Bates[59], S. Batlamous[35e], J. R. Batley[32], B. Batool[141], M. Battaglia[136], D. Battulga[18], M. Bauce[75a,75b], M. Bauer[36], P. Bauer[24], L. T. Bazzano Hurrell[30], J. B. Beacham[51], T. Beau[127], J. Y. Beaucamp[90], P. H. Beauchemin[158], F. Becherer[54], P. Bechtle[24], H. P. Beck[19,o], K. Becker[167], A. J. Beddall[82], V. A. Bednyakov[38], C. P. Bee[145], L. J. Beemster[15], T. A. Beermann[36], M. Begalli[83d], M. Begel[29], A. Behera[145], J. K. Behr[48], J. F. Beirer[36], F. Beisiegel[24], M. Belfkir[159], G. Bella[151], L. Bellagamba[23b], A. Bellerive[34], P. Bellos[20], K. Beloborodov[37], D. Benchekroun[35a], F. Bendebba[35a], Y. Benhammou[151], M. Benoit[29], J. R. Bensinger[26], S. Bentvelsen[114], L. Beresford[48], M. Beretta[53], E. Bergeaas Kuutmann[161], N. Berger[4], B. Bergmann[132], J. Beringer[17a], G. Bernardi[5], C. Bernius[143], F. U. Bernlochner[24], F. Bernon[36,102], A. Berrocal Guardia[13], T. Berry[95], P. Berta[133], A. Berthold[50], I. A. Bertram[91], S. Bethke[110], A. Betti[75a,75b], A. J. Bevan[94], N. K. Bhalla[54], M. Bhamjee[33c], S. Bhatta[145], D. S. Bhattacharya[166], P. Bhattarai[143], V. S. Bhopatkar[121], R. Bi[29,ai], R. M. Bianchi[129], G. Bianco[23a,23b], O. Biebel[109], R. Bielski[123], M. Biglietti[77a], M. Bindi[55], A. Bingul[21b], C. Bini[75a,75b], A. Biondini[92], C. J. Birch-sykes[101], G. A. Bird[20,134], M. Birman[169], M. Biros[133], S. Biryukov[146], T. Bisanz[49], E. Bisceglie[43a,43b], J. P. Biswal[134], D. Biswas[141], A. Bitadze[101], K. Bjørke[125], I. Bloch[48], A. Blue[59], U. Blumenschein[94], J. Blumenthal[100], G. J. Bobbink[114], V. S. Bobrovnikov[37], M. Boehler[54], B. Boehm[166], D. Bogavac[36], A. G. Bogdanchikov[37], C. Bohm[47a], V. Boisvert[95], P. Bokan[48], T. Bold[86a], M. Bomben[5], M. Bona[94], M. Boonekamp[135], C. D. Booth[95], A. G. Borbély[59], I. S. Bordulev[37], H. M. Borecka-Bielska[108], G. Borissov[91], D. Bortoletto[126], D. Boscherini[23b], M. Bosman[13], J. D. Bossio Sola[36], K. Bouaouda[35a], N. Bouchhar[163], J. Boudreau[129], E. V. Bouhova-Thacker[91], D. Boumediene[40], R. Bouquet[165], A. Boveia[119], J. Boyd[36], D. Boye[29], I. R. Boyko[38], J. Bracinik[20], N. Brahimi[62d], G. Brandt[171], O. Brandt[32], F. Braren[48], B. Brau[103], J. E. Brau[123], R. Brener[169], L. Brenner[114], R. Brenner[161], S. Bressler[169], D. Britton[59], D. Britzger[110], I. Brock[24], G. Brooijmans[41], W. K. Brooks[137f], E. Brost[29], L. M. Brown[165], L. E. Bruce[61], T. L. Bruckler[126], P. A. Bruckman de Renstrom[87], B. Brüers[48], A. Bruni[23b], G. Bruni[23b], M. Bruschi[23b], N. Bruscino[75a,75b], T. Buanes[16], Q. Buat[138], D. Buchin[110], A. G. Buckley[59], O. Bulekov[37], B. A. Bullard[143], S. Burdin[92], C. D. Burgard[49], A. M. Burger[40], B. Burghgrave[8], O. Burlayenko[54], J. T. P. Burr[32], C. D. Burton[11], J. C. Burzynski[142], E. L. Busch[41], V. Büscher[100], P. J. Bussey[59], J. M. Butler[25], C. M. Buttar[59], J. M. Butterworth[96], W. Buttinger[134], C. J. Buxo Vazquez[107], A. R. Buzykaev[37], S. Cabrera Urbán[163], L. Cadamuro[66], D. Caforio[58], H. Cai[129], Y. Cai[14a,14e], Y. Cai[14c], V. M. M. Cairo[36], O. Cakir[3a], N. Calace[36], P. Calafiura[17a], G. Calderini[127], P. Calfayan[68], G. Callea[59], L. P. Caloba[83b], D. Calvet[40], S. Calvet[40], T. P. Calvet[102], M. Calvetti[74a,74b], R. Camacho Toro[127], S. Camarda[36], D. Camarero Munoz[26], P. Camarri[76a,76b], M. T. Camerlingo[72a,72b], D. Cameron[36], C. Camincher[165], M. Campanelli[96], A. Camplani[42], V. Canale[72a,72b], A. Canesse[104], J. Cantero[163], Y. Cao[162], F. Capocasa[26], M. Capua[43a,43b], A. Carbone[71a,71b], R. Cardarelli[76a], J. C. J. Cardenas[8], F. Cardillo[163], G. Carducci[43a,43b], T. Carli[36], G. Carlino[72a], J. I. Carlotto[13], B. T. Carlson[129,q], E. M. Carlson[156a,165], L. Carminati[71a,71b], A. Carnelli[135], M. Carnesale[75a,75b], S. Caron[113], E. Carquin[137f], S. Carrá[71a], G. Carratta[23a,23b], F. Carrio Argos[33g], J. W. S. Carter[155], T. M. Carter[52], M. P. Casado[13,i], M. Caspar[48], F. L. Castillo[4], L. Castillo Garcia[13], V. Castillo Gimenez[163], N. F. Castro[130a,130e], A. Catinaccio[36], J. R. Catmore[125], V. Cavaliere[29], N. Cavalli[23a,23b], V. Cavasinni[74a,74b], Y. C. Cekmecelioglu[48], E. Celebi[21a], F. Celli[126], M. S. Centonze[70a,70b], V. Cepaitis[56], K. Cerny[122], A. S. Cerqueira[83a], A. Cerri[146], L. Cerrito[76a,76b], F. Cerutti[17a], B. Cervato[141], A. Cervelli[23b], G. Cesarini[53], S. A. Cetin[82], D. Chakraborty[115], J. Chan[170], W. Y. Chan[153], J. D. Chapman[32], E. Chapon[135], B. Chargeishvili[149b], D. G. Charlton[20], T. P. Charman[94], M. Chatterjee[19], C. Chauhan[133], S. Chekanov[6], S. V. Chekulaev[156a], G. A. Chelkov[38,a], A. Chen[106], B. Chen[151], B. Chen[165], H. Chen[14c], H. Chen[29], J. Chen[62c], J. Chen[142], M. Chen[126], S. Chen[153], S. J. Chen[14c], X. Chen[62c,135], X. Chen[14b,ae], Y. Chen[62a], C. L. Cheng[170], H. C. Cheng[64a], S. Cheong[143], A. Cheplakov[38], E. Cheremushkina[48], E. Cherepanova[114], R. Cherkaoui El Moursli[35e], E. Cheu[7], K. Cheung[65], L. Chevalier[135], V. Chiarella[53], G. Chiarelli[74a], N. Chiedde[102], G. Chiodini[70a], A. S. Chisholm[20], A. Chitan[27b],

M. Chitishvili[163], M. V. Chizhov[38], K. Choi[11], A. R. Chomont[75a,75b], Y. Chou[103], E. Y. S. Chow[113], T. Chowdhury[33g], K. L. Chu[169], M. C. Chu[64a], X. Chu[14a,14e], J. Chudoba[131], J. J. Chwastowski[87], D. Cieri[110], K. M. Ciesla[86a], V. Cindro[93], A. Ciocio[17a], F. Cirotto[72a,72b], Z. H. Citron[169,k], M. Citterio[71a], D. A. Ciubotaru[27b], A. Clark[56], P. J. Clark[52], C. Clarry[155], J. M. Clavijo Columbie[48], S. E. Clawson[48], C. Clement[47a,47b], J. Clercx[48], Y. Coadou[102], M. Cobal[69a,69c], A. Coccaro[57b], R. F. Coelho Barrue[130a], R. Coelho Lopes De Sa[103], S. Coelli[71a], A. E. C. Coimbra[71a,71b], B. Cole[41], J. Collot[60], P. Conde Muiño[130a,130g], M. P. Connell[33c], S. H. Connell[33c], I. A. Connelly[59], E. I. Conroy[126], F. Conventi[72a,ag], H. G. Cooke[20], A. M. Cooper-Sarkar[126], A. Cordeiro Oudot Choi[127], L. D. Corpe[40], M. Corradi[75a,75b], F. Corriveau[104,w], A. Cortes-Gonzalez[18], M. J. Costa[163], F. Costanza[4], D. Costanzo[139], B. M. Cote[119], G. Cowan[95], K. Cranmer[170], D. Cremonini[23a,23b], S. Crépé-Renaudin[60], F. Crescioli[127], M. Cristinziani[141], M. Cristoforetti[78a,78b], V. Croft[114], J. E. Crosby[121], G. Crosetti[43a,43b], A. Cueto[99], T. Cuhadar Donszelmann[160], H. Cui[14a,14e], Z. Cui[7], W. R. Cunningham[59], F. Curcio[43a,43b], P. Czodrowski[36], M. M. Czurylo[63b], M. J. Da Cunha Sargedas De Sousa[57a,57b], J. V. Da Fonseca Pinto[83b], C. Da Via[101], W. Dabrowski[86a], T. Dado[49], S. Dahbi[33g], T. Dai[106], D. Dal Santo[19], C. Dallapiccola[103], M. Dam[42], G. D'amen[29], V. D'Amico[109], J. Damp[100], J. R. Dandoy[34], M. F. Daneri[30], M. Danninger[142], V. Dao[36], G. Darbo[57b], S. Darmora[6], S. J. Das[29,ai], S. D'Auria[71a,71b], C. David[156b], T. Davidek[133], B. Davis-Purcell[34], I. Dawson[94], H. A. Day-hall[132], K. De[8], R. De Asmundis[72a], N. De Biase[48], S. De Castro[23a,23b], N. De Groot[113], P. de Jong[114], H. De la Torre[115], A. De Maria[14c], A. De Salvo[75a], U. De Sanctis[76a,76b], A. De Santo[146], J. B. De Vivie De Regie[60], D. V. Dedovich[38], J. Degens[114], A. M. Deiana[44], F. Del Corso[23a,23b], J. Del Peso[99], F. Del Rio[63a], F. Deliot[135], C. M. Delitzsch[49], M. Della Pietra[72a,72b], D. Della Volpe[56], A. Dell'Acqua[36], L. Dell'Asta[71a,71b], M. Delmastro[4], P. A. Delsart[60], S. Demers[172], M. Demichev[38], S. P. Denisov[37], L. D'Eramo[40], D. Derendarz[87], F. Derue[127], P. Dervan[92], K. Desch[24], C. Deutsch[24], F. A. Di Bello[57a,57b], A. Di Ciaccio[76a,76b], L. Di Ciaccio[4], A. Di Domenico[75a,75b], C. Di Donato[72a,72b], A. Di Girolamo[36], G. Di Gregorio[36], A. Di Luca[78a,78b], B. Di Micco[77a,77b], R. Di Nardo[77a,77b], C. Diaconu[102], M. Diamantopoulou[34], F. A. Dias[114], T. Dias Do Vale[142], M. A. Diaz[137a,137b], F. G. Diaz Capriles[24], M. Didenko[163], E. B. Diehl[106], L. Diehl[54], S. Díez Cornell[48], C. Diez Pardos[141], C. Dimitriadi[24,161], A. Dimitrievska[17a], J. Dingfelder[24], I.-M. Dinu[27b], S. J. Dittmeier[63b], F. Dittus[36], F. Djama[102], T. Djobava[149b], J. I. Djuvsland[16], C. Doglioni[98,101], A. Dohnalova[28a], J. Dolejsi[133], Z. Dolezal[133], K. M. Dona[39], M. Donadelli[83c], B. Dong[107], J. Donini[40], A. D'Onofrio[72a,72b], M. D'Onofrio[92], J. Dopke[134], A. Doria[72a], N. Dos Santos Fernandes[130a], P. Dougan[101], M. T. Dova[90], A. T. Doyle[59], M. A. Draguet[126], E. Dreyer[169], I. Drivas-koulouris[10], M. Drnevich[117], A. S. Drobac[158], M. Drozdova[56], D. Du[62a], T. A. du Pree[114], F. Dubinin[37], M. Dubovsky[28a], E. Duchovni[169], G. Duckeck[109], O. A. Ducu[27b], D. Duda[52], A. Dudarev[36], E. R. Duden[26], M. D'uffizi[101], L. Duflot[66], M. Dührssen[36], C. Dülsen[171], A. E. Dumitriu[27b], M. Dunford[63a], S. Dungs[49], K. Dunne[47a,47b], A. Duperrin[102], H. Duran Yildiz[3a], M. Düren[58], A. Durglishvili[149b], B. L. Dwyer[115], G. I. Dyckes[17a], M. Dyndal[86a], B. S. Dziedzic[87], Z. O. Earnshaw[146], G. H. Eberwein[126], B. Eckerova[28a], S. Eggebrecht[55], E. Egidio Purcino De Souza[127], L. F. Ehrke[56], G. Eigen[16], K. Einsweiler[17a], T. Ekelof[161], P. A. Ekman[98], S. El Farkh[35b], Y. El Ghazali[35b], H. El Jarrari[36], A. El Moussaouy[108], V. Ellajosyula[161], M. Ellert[161], F. Ellinghaus[171], N. Ellis[36], J. Elmsheuser[29], M. Elsing[36], D. Emeliyanov[134], Y. Enari[153], I. Ene[17a], S. Epari[13], J. Erdmann[49], P. A. Erland[87], M. Errenst[171], M. Escalier[66], C. Escobar[163], E. Etzion[151], G. Evans[130a], H. Evans[68], L. S. Evans[95], M. O. Evans[146], A. Ezhilov[37], S. Ezzarqtouni[35a], F. Fabbri[59], L. Fabbri[23a,23b], G. Facini[96], V. Fadeyev[136], R. M. Fakhrutdinov[37], S. Falciano[75a], L. F. Falda Ulhoa Coelho[36], P. J. Falke[24], J. Faltova[133], C. Fan[162], Y. Fan[14a], Y. Fang[14a,14e], M. Fanti[71a,71b], M. Faraj[69a,69b], Z. Farazpay[97], A. Farbin[8], A. Farilla[77a], T. Farooque[107], S. M. Farrington[52], F. Fassi[35e], D. Fassouliotis[9], M. Faucci Giannelli[76a,76b], W. J. Fawcett[32], L. Fayard[66], P. Federic[133], P. Federicova[131], O. L. Fedin[37,a], G. Fedotov[37], M. Feickert[170], L. Feligioni[102], D. E. Fellers[123], C. Feng[62b], M. Feng[14b], Z. Feng[114], M. J. Fenton[160], A. B. Fenyuk[37], L. Ferencz[48], R. A. M. Ferguson[91], S. I. Fernandez Luengo[137f], P. Fernandez Martinez[13], M. J. V. Fernoux[102], J. Ferrando[48], A. Ferrari[161], P. Ferrari[113,114], R. Ferrari[73a], D. Ferrere[56], C. Ferretti[106], F. Fiedler[100], P. Fiedler[132], A. Filipčič[93], E. K. Filmer[1], F. Filthaut[113], M. C. N. Fiolhais[130a,130c,c], L. Fiorini[163], W. C. Fisher[107], T. Fitschen[101], P. M. Fitzhugh[135], I. Fleck[141], P. Fleischmann[106], T. Flick[171], M. Flores[33d,ac], L. R. Flores Castillo[64a], L. Flores Sanz De Acedo[36], F. M. Follega[78a,78b], N. Fomin[16], J. H. Foo[155], B. C. Forland[68], A. Formica[135], A. C. Forti[101], E. Fortin[36], A. W. Fortman[61], M. G. Foti[17a], L. Fountas[9,j], D. Fournier[66], H. Fox[91], P. Francavilla[74a,74b], S. Francescato[61], S. Franchellucci[56], M. Franchini[23a,23b],

S. Franchino[63a], D. Francis[36], L. Franco[113], V. Franco Lima[36], L. Franconi[48], M. Franklin[61], G. Frattari[26], A. C. Freegard[94], W. S. Freund[83b], Y. Y. Frid[151], J. Friend[59], N. Fritzsche[50], A. Froch[54], D. Froidevaux[36], J. A. Frost[126], Y. Fu[62a], S. Fuenzalida Garrido[137f], M. Fujimoto[102], K. Y. Fung[64a], E. Furtado De Simas Filho[83b], M. Furukawa[153], J. Fuster[163], A. Gabrielli[23a,23b], A. Gabrielli[155], P. Gadow[36], G. Gagliardi[57a,57b], L. G. Gagnon[17a], E. J. Gallas[126], B. J. Gallop[134], K. K. Gan[119], S. Ganguly[153], Y. Gao[52], F. M. Garay Walls[137a,137b], B. Garcia[29], C. García[163], A. Garcia Alonso[114], A. G. Garcia Caffaro[172], J. E. García Navarro[163], M. Garcia-Scivetes[17a], G. L. Gardner[128], R. W. Gardner[39], N. Garelli[158], D. Garg[80], R. B. Garg[143,n], J. M. Gargan[52], C. A. Garner[155], C. M. Garvey[33a], P. Gaspar[83b], V. K. Gassmann[158], G. Gaudio[73a], V. Gautam[13], P. Gauzzi[75a,75b], I. L. Gavrilenko[37], A. Gavrilyuk[37], C. Gay[164], G. Gaycken[48], E. N. Gazis[10], A. A. Geanta[27b], C. M. Gee[136], A. Gekow[119], C. Gemme[57b], M. H. Genest[60], S. Gentile[75a,75b], A. D. Gentry[112], S. George[95], W. F. George[20], T. Geralis[46], P. Gessinger-Befurt[36], M. E. Geyik[171], M. Ghani[167], M. Ghneimat[141], K. Ghorbanian[94], A. Ghosal[141], A. Ghosh[160], A. Ghosh[7], B. Giacobbe[23b], S. Giagu[75a,75b], T. Giani[114], P. Giannetti[74a], A. Giannini[62a], S. M. Gibson[95], M. Gignac[136], D. T. Gil[86b], A. K. Gilbert[86a], B. J. Gilbert[41], D. Gillberg[34], G. Gilles[114], N. E. K. Gillwald[48], L. Ginabat[127], D. M. Gingrich[2,af], M. P. Giordani[69a,69c], P. F. Giraud[135], G. Giugliarelli[69a,69c], D. Giugni[71a], F. Giuli[36], I. Gkialas[9,j], L. K. Gladilin[37], C. Glasman[99], G. R. Gledhill[123], G. Glemža[48], M. Glisic[123], I. Gnesi[43b,f], Y. Go[29,ai], M. Goblirsch-Kolb[36], B. Gocke[49], D. Godin[108], B. Gokturk[21a], S. Goldfarb[105], T. Golling[56], M. G. D. Gololo[33g], D. Golubkov[37], J. P. Gombas[107], A. Gomes[130a,130b], G. Gomes Da Silva[141], A. J. Gomez Delegido[163], R. Gonçalo[130a,130c], G. Gonella[123], L. Gonella[20], A. Gongadze[149c], F. Gonnella[20], J. L. Gonski[41], R. Y. González Andana[52], S. González de la Hoz[163], S. Gonzalez Fernandez[13], R. Gonzalez Lopez[92], C. Gonzalez Renteria[17a], M. V. Gonzalez Rodrigues[48], R. Gonzalez Suarez[161], S. Gonzalez-Sevilla[56], G. R. Gonzalvo Rodriguez[163], L. Goossens[36], B. Gorini[36], E. Gorini[70a,70b], A. Gorišek[93], T. C. Gosart[128], A. T. Goshaw[51], M. I. Gostkin[38], S. Goswami[121], C. A. Gottardo[36], S. A. Gotz[109], M. Gouighri[35b], V. Goumarre[48], A. G. Goussiou[138], N. Govender[33c], I. Grabowska-Bold[86a], K. Graham[34], E. Gramstad[125], S. Grancagnolo[70a,70b], M. Grandi[146], C. M. Grant[1,135], P. M. Gravila[27f], F. G. Gravili[70a,70b], H. M. Gray[17a], M. Greco[70a,70b], C. Grefe[24], I. M. Gregor[48], P. Grenier[143], S. G. Grewe[110], C. Grieco[13], A. A. Grillo[136], K. Grimm[31], S. Grinstein[13,s], J.-F. Grivaz[66], E. Gross[169], J. Grosse-Knetter[55], C. Grud[106], J. C. Grundy[126], L. Guan[106], W. Guan[29], C. Gubbels[164], J. G. R. Guerrero Rojas[163], G. Guerrieri[69a,69c], F. Guescini[110], R. Gugel[100], J. A. M. Guhit[106], A. Guida[18], E. Guilloton[134,167], S. Guindon[36], F. Guo[14a,14e], J. Guo[62c], L. Guo[48], Y. Guo[106], R. Gupta[48], R. Gupta[129], S. Gurbuz[24], S. S. Gurdasani[54], G. Gustavino[36], M. Guth[56], P. Gutierrez[120], L. F. Gutierrez Zagazeta[128], M. Gutsche[50], C. Gutschow[96], C. Gwenlan[126], C. B. Gwilliam[92], E. S. Haaland[125], A. Haas[117], M. Habedank[48], C. Haber[17a], H. K. Hadavand[8], A. Hadef[50], S. Hadzic[110], A. I. Hagan[91], J. J. Hahn[141], E. H. Haines[96], M. Haleem[166], J. Haley[121], J. J. Hall[139], G. D. Hallewell[102], L. Halser[19], K. Hamano[165], M. Hamer[24], G. N. Hamity[52], E. J. Hampshire[95], J. Han[62b], K. Han[62a], L. Han[14c], L. Han[62a], S. Han[17a], Y. F. Han[155], K. Hanagaki[84], M. Hance[136], D. A. Hangal[41,ab], H. Hanif[142], M. D. Hank[128], R. Hankache[101], J. B. Hansen[42], J. D. Hansen[42], P. H. Hansen[42], K. Hara[157], D. Harada[56], T. Harenberg[171], S. Harkusha[37], M. L. Harris[103], Y. T. Harris[126], J. Harrison[13], N. M. Harrison[119], P. F. Harrison[167], N. M. Hartman[110], N. M. Hartmann[109], Y. Hasegawa[140], R. Hauser[107], C. M. Hawkes[20], R. J. Hawkings[36], Y. Hayashi[153], S. Hayashida[111], D. Hayden[107], C. Hayes[106], R. L. Hayes[114], C. P. Hays[126], J. M. Hays[94], H. S. Hayward[92], F. He[62a], M. He[14a,14e], Y. He[154], Y. He[48], N. B. Heatley[94], V. Hedberg[98], A. L. Heggelund[125], N. D. Hehir[94,*], C. Heidegger[54], K. K. Heidegger[54], W. D. Heidorn[81], J. Heilman[34], S. Heim[48], T. Heim[17a], J. G. Heinlein[128], J. J. Heinrich[123], L. Heinrich[110,ad], J. Hejbal[131], L. Helary[48], A. Held[170], S. Hellesund[16], C. M. Helling[164], S. Hellman[47a,47b], R. C. W. Henderson[91], L. Henkelmann[32], A. M. Henriques Correia[36], H. Herde[98], Y. Hernández Jiménez[145], L. M. Herrmann[24], T. Herrmann[50], G. Herten[54], R. Hertenberger[109], L. Hervas[36], M. E. Hesping[100], N. P. Hessey[156a], H. Hibi[85], E. Hill[155], S. J. Hillier[20], J. R. Hinds[107], F. Hinterkeuser[24], M. Hirose[124], S. Hirose[157], D. Hirschbuehl[171], T. G. Hitchings[101], B. Hiti[93], J. Hobbs[145], R. Hobincu[27e], N. Hod[169], M. C. Hodgkinson[139], B. H. Hodkinson[32], A. Hoecker[36], D. D. Hofer[106], J. Hofer[48], T. Holm[24], M. Holzbock[110], L. B. A. H. Hommels[32], B. P. Honan[101], J. Hong[62c], T. M. Hong[129], B. H. Hooberman[162], W. H. Hopkins[6], Y. Horii[111], S. Hou[148], A. S. Howard[93], J. Howarth[59], J. Hoya[6], M. Hrabovsky[122], A. Hrynevich[48], T. Hryn'ova[4], P. J. Hsu[65], S.-C. Hsu[138], Q. Hu[62a], Y. F. Hu[14a,14e], S. Huang[64b], X. Huang[14c], X. Huang[14a,14e], Y. Huang[139], Y. Huang[14a], Z. Huang[101], Z. Hubacek[132], M. Huebner[24], F. Huegging[24], T. B. Huffman[126], C. A. Hugli[48], M. Huhtinen[36], S. K. Huiberts[16],

R. Hulsken[104], N. Huseynov[12], J. Huston[107], J. Huth[61], R. Hyneman[143], G. Iacobucci[56], G. Iakovidis[29], I. Ibragimov[141], L. Iconomidou-Fayard[66], P. Iengo[72a,72b], R. Iguchi[153], T. Iizawa[126], Y. Ikegami[84], N. Ilic[155], H. Imam[35a], M. Ince Lezki[56], T. Ingebretsen Carlson[47a,47b], G. Introzzi[73a,73b], M. Iodice[77a], V. Ippolito[75a,75b], R. K. Irwin[92], M. Ishino[153], W. Islam[170], C. Issever[18,48], S. Istin[21a,ak], H. Ito[168], J. M. Iturbe Ponce[64a], R. Iuppa[78a,78b], A. Ivina[169], J. M. Izen[45], V. Izzo[72a], P. Jacka[131,132], P. Jackson[1], R. M. Jacobs[48], B. P. Jaeger[142], C. S. Jagfeld[109], G. Jain[156a], P. Jain[54], K. Jakobs[54], T. Jakoubek[169], J. Jamieson[59], K. W. Janas[86a], M. Javurkova[103], F. Jeanneau[135], L. Jeanty[123], J. Jejelava[149a,z], P. Jenni[54,g], C. E. Jessiman[34], S. Jézéquel[4], C. Jia[62b], J. Jia[145], X. Jia[61], X. Jia[14a,14e], Z. Jia[14c], S. Jiggins[48], J. Jimenez Pena[13], S. Jin[14c], A. Jinaru[27b], O. Jinnouchi[154], P. Johansson[139], K. A. Johns[7], J. W. Johnson[136], D. M. Jones[32], E. Jones[48], P. Jones[32], R. W. L. Jones[91], T. J. Jones[92], H. L. Joos[36,55], R. Joshi[119], J. Jovicevic[15], X. Ju[17a], J. J. Junggeburth[103], T. Junkermann[63a], A. Juste Rozas[13,s], M. K. Juzek[87], S. Kabana[137e], A. Kaczmarska[87], M. Kado[110], H. Kagan[119], M. Kagan[143], A. Kahn[41], A. Kahn[128], C. Kahra[100], T. Kaji[153], E. Kajomovitz[150], N. Kakati[169], I. Kalaitzidou[54], C. W. Kalderon[29], A. Kamenshchikov[155], N. J. Kang[136], D. Kar[33g], K. Karava[126], M. J. Kareem[156b], E. Karentzos[54], I. Karkanias[152], O. Karkout[114], S. N. Karpov[38], Z. M. Karpova[38], V. Kartvelishvili[91], A. N. Karyukhin[37], E. Kasimi[152], J. Katzy[48], S. Kaur[34], K. Kawade[140], M. P. Kawale[120], C. Kawamoto[88], T. Kawamoto[62a], E. F. Kay[36], F. I. Kaya[158], S. Kazakos[107], V. F. Kazanin[37], Y. Ke[145], J. M. Keaveney[33a], R. Keeler[165], G. V. Kehris[61], J. S. Keller[34], A. S. Kelly[96], J. J. Kempster[146], K. E. Kennedy[41], P. D. Kennedy[100], O. Kepka[131], B. P. Kerridge[167], S. Kersten[171], B. P. Kerševan[93], S. Keshri[66], L. Keszeghova[28a], S. Ketabchi Haghighat[155], R. A. Khan[129], M. Khandoga[127], A. Khanov[121], A. G. Kharlamov[37], T. Kharlamova[37], E. E. Khoda[138], M. Kholodenko[37], T. J. Khoo[18], G. Khoriauli[166], J. Khubua[149b], Y. A. R. Khwaira[66], A. Kilgallon[123], D. W. Kim[47a,47b], Y. K. Kim[39], N. Kimura[96], M. K. Kingston[55], A. Kirchhoff[55], C. Kirfel[24], F. Kirfel[24], J. Kirk[134], A. E. Kiryunin[110], C. Kitsaki[10], O. Kivernyk[24], M. Klassen[63a], C. Klein[34], L. Klein[166], M. H. Klein[106], M. Klein[92], S. B. Klein[56], U. Klein[92], P. Klimek[36], A. Klimentov[29], T. Klioutchnikova[36], P. Kluit[114], S. Kluth[110], E. Kneringer[79], T. M. Knight[155], A. Knue[49], R. Kobayashi[88], D. Kobylianskii[169], S. F. Koch[126], M. Kocian[143], P. Kodyš[133], D. M. Koeck[123], P. T. Koenig[24], T. Koffas[34], O. Kolay[50], I. Koletsou[4], T. Komarek[122], K. Köneke[54], A. X. Y. Kong[1], T. Kono[118], N. Konstantinidis[96], P. Kontaxakis[56], B. Konya[98], R. Kopeliansky[68], S. Koperny[86a], K. Korcyl[87], K. Kordas[152,e], G. Koren[151], A. Korn[96], S. Korn[55], I. Korolkov[13], N. Korotkova[37], B. Kortman[114], O. Kortner[110], S. Kortner[110], W. H. Kostecka[115], V. V. Kostyukhin[141], A. Kotsokechagia[135], A. Kotwal[51], A. Koulouris[36], A. Kourkoumeli-Charalampidi[73a,73b], C. Kourkoumelis[9], E. Kourlitis[110,ad], O. Kovanda[146], R. Kowalewski[165], W. Kozanecki[135], A. S. Kozhin[37], V. A. Kramarenko[37], G. Kramberger[93], P. Kramer[100], M. W. Krasny[127], A. Krasznahorkay[36], J. W. Kraus[171], J. A. Kremer[48], T. Kresse[50], J. Kretzschmar[92], K. Kreul[18], P. Krieger[155], S. Krishnamurthy[103], M. Krivos[133], K. Krizka[20], K. Kroeninger[49], H. Kroha[110], J. Kroll[131], J. Kroll[128], K. S. Krowpman[107], U. Kruchonak[38], H. Krüger[24], N. Krumnack[81], M. C. Kruse[51], O. Kuchinskaia[37], S. Kuday[3a], S. Kuehn[36], R. Kuesters[54], T. Kuhl[48], V. Kukhtin[38], Y. Kulchitsky[37,a], S. Kuleshov[137b,137d], M. Kumar[33g], N. Kumari[48], A. Kupco[131], T. Kupfer[49], A. Kupich[37], O. Kuprash[54], H. Kurashige[85], L. L. Kurchaninov[156a], O. Kurdysh[66], Y. A. Kurochkin[37], A. Kurova[37], M. Kuze[154], A. K. Kvam[103], J. Kvita[122], T. Kwan[104], N. G. Kyriacou[106], L. A. O. Laatu[102], C. Lacasta[163], F. Lacava[75a,75b], H. Lacker[18], D. Lacour[127], N. N. Lad[96], E. Ladygin[38], B. Laforge[127], T. Lagouri[137e], F. Z. Lahbabi[35a], S. Lai[55], I. K. Lakomiec[86a], N. Lalloue[60], J. E. Lambert[165], S. Lammers[68], W. Lampl[7], C. Lampoudis[152,e], A. N. Lancaster[115], E. Lançon[29], U. Landgraf[54], M. P. J. Landon[94], V. S. Lang[54], R. J. Langenberg[103], O. K. B. Langrekken[125], A. J. Lankford[160], F. Lanni[36], K. Lantzsch[24], A. Lanza[73a], A. Lapertosa[57a,57b], J. F. Laporte[135], T. Lari[71a], F. Lasagni Manghi[23b], M. Lassnig[36], V. Latonova[131], A. Laudrain[100], A. Laurier[150], S. D. Lawlor[139], Z. Lawrence[101], R. Lazaridou[167], M. Lazzaroni[71a,71b], B. Le[101], E. M. Le Boulicaut[51], B. Leban[93], A. Lebedev[81], M. LeBlanc[101], F. Ledroit-Guillon[60], A. C. A. Lee[96], S. C. Lee[148], S. Lee[47a,47b], T. F. Lee[92], L. L. Leeuw[33c], H. P. Lefebvre[95], M. Lefebvre[165], C. Leggett[17a], G. Lehmann Miotto[36], M. Leigh[56], W. A. Leight[103], W. Leinonen[113], A. Leisos[152,r], M. A. L. Leite[83c], C. E. Leitgeb[48], R. Leitner[133], K. J. C. Leney[44], T. Lenz[24], S. Leone[74a], C. Leonidopoulos[52], A. Leopold[144], C. Leroy[108], R. Les[107], C. G. Lester[32], M. Levchenko[37], J. Levêque[4], D. Levin[106], L. J. Levinson[169], M. P. Lewicki[87], D. J. Lewis[4], A. Li[5], B. Li[62b], C. Li[62a], C.-Q. Li[110], H. Li[62a], H. Li[62b], H. Li[14c], H. Li[14b], H. Li[62b], J. Li[62c], K. Li[138], L. Li[62c], M. Li[14a,14e], Q. Y. Li[62a], S. Li[14a,14e], S. Li[62c,62d,d], T. Li[5], X. Li[104], Z. Li[126], Z. Li[104], Z. Li[92], Z. Li[14a,14e], S. Liang[14a,14e], Z. Liang[14a], M. Liberatore[135],

B. Liberti[76a], K. Lie[64c], J. Lieber Marin[83b], H. Lien[68], K. Lin[107], R. E. Lindley[7], J. H. Lindon[2], E. Lipeles[128], A. Lipniacka[16], A. Lister[164], J. D. Little[4], B. Liu[14a], B. X. Liu[142], D. Liu[62c,62d], J. B. Liu[62a], J. K. K. Liu[32], K. Liu[62c,62d], M. Liu[62a], M. Y. Liu[62a], P. Liu[14a], Q. Liu[62c,62d,138], X. Liu[62a], Y. Liu[14d,14e], Y. L. Liu[62b], Y. W. Liu[62a], J. Llorente Merino[142], S. L. Lloyd[94], E. M. Lobodzinska[48], P. Loch[7], T. Lohse[18], K. Lohwasser[139], E. Loiacono[48], M. Lokajicek[131,*], J. D. Lomas[20], J. D. Long[162], I. Longarini[160], L. Longo[70a,70b], R. Longo[162], I. Lopez Paz[67], A. Lopez Solis[48], N. Lorenzo Martinez[4], A. M. Lory[109], G. Löschcke Centeno[146], O. Loseva[37], X. Lou[47a,47b], X. Lou[14a,14e], A. Lounis[66], J. Love[6], P. A. Love[91], G. Lu[14a,14e], M. Lu[80], S. Lu[128], Y. J. Lu[65], H. J. Lubatti[138], C. Luci[75a,75b], F. L. Lucio Alves[14c], A. Lucotte[60], F. Luehring[68], I. Luise[145], O. Lukianchuk[66], O. Lundberg[144], B. Lund-Jensen[144], N. A. Luongo[6], M. S. Lutz[151], A. B. Lux[25], D. Lynn[29], H. Lyons[92], R. Lysak[131], E. Lytken[98], V. Lyubushkin[38], T. Lyubushkina[38], M. M. Lyukova[145], H. Ma[29], K. Ma[62a], L. L. Ma[62b], W. Ma[62a], Y. Ma[121], D. M. Mac Donell[165], G. Maccarrone[53], J. C. MacDonald[100], P. C. Machado De Abreu Farias[83b], R. Madar[40], W. F. Mader[50], T. Madula[96], J. Maeda[85], T. Maeno[29], H. Maguire[139], V. Maiboroda[135], A. Maio[130a,130b,130d], K. Maj[86a], O. Majersky[48], S. Majewski[123], N. Makovec[66], V. Maksimovic[15], B. Malaescu[127], Pa. Malecki[87], V. P. Maleev[37], F. Malek[60], M. Mali[93], D. Malito[95], U. Mallik[80], S. Maltezos[10], S. Malyukov[38], J. Mamuzic[13], G. Mancini[53], G. Manco[73a,73b], J. P. Mandalia[94], I. Mandić[93], L. Manhaes de Andrade Filho[83a], I. M. Maniatis[169], J. Manjarres Ramos[102,aa], D. C. Mankad[169], A. Mann[109], B. Mansoulie[135], S. Manzoni[36], L. Mao[62c], X. Mapekula[33c], A. Marantis[152,r], G. Marchiori[5], M. Marcisovsky[131], C. Marcon[71a], M. Marinescu[20], S. Marium[48], M. Marjanovic[120], E. J. Marshall[91], Z. Marshall[17a], S. Marti-Garcia[163], T. A. Martin[167], V. J. Martin[52], B. Martin dit Latour[16], L. Martinelli[75a,75b], M. Martinez[13,s], P. Martinez Agullo[163], V. I. Martinez Outschoorn[103], P. Martinez Suarez[13], S. Martin-Haugh[134], V. S. Martoiu[27b], A. C. Martyniuk[96], A. Marzin[36], D. Mascione[78a,78b], L. Masetti[100], T. Mashimo[153], J. Masik[101], A. L. Maslennikov[37], L. Massa[23b], P. Massarotti[72a,72b], P. Mastrandrea[74a,74b], A. Mastroberardino[43a,43b], T. Masubuchi[153], T. Mathisen[161], J. Matousek[133], N. Matsuzawa[153], J. Maurer[27b], B. Maček[93], D. A. Maximov[37], R. Mazini[148], I. Maznas[152], M. Mazza[107], S. M. Mazza[136], E. Mazzeo[71a,71b], C. Mc Ginn[29], J. P. Mc Gowan[104], S. P. Mc Kee[106], E. F. McDonald[105], A. E. McDougall[114], J. A. Mcfayden[146], R. P. McGovern[128], G. Mchedlidze[149b], R. P. Mckenzie[33g], T. C. Mclachlan[48], D. J. Mclaughlin[96], S. J. McMahon[134], C. M. Mcpartland[92], R. A. McPherson[165,w], S. Mehlhase[109], A. Mehta[92], D. Melini[150], B. R. Mellado Garcia[33g], A. H. Melo[55], F. Meloni[48], A. M. Mendes Jacques Da Costa[101], H. Y. Meng[155], L. Meng[91], S. Menke[110], M. Mentink[36], E. Meoni[43a,43b], G. Mercado[115], C. Merlassino[69a,69c], L. Merola[72a,72b], C. Meroni[71a,71b], G. Merz[106], O. Meshkov[37], J. Metcalfe[6], A. S. Mete[6], C. Meyer[68], J.-P. Meyer[135], R. P. Middleton[134], L. Mijović[52], G. Mikenberg[169], M. Mikestikova[131], M. Mikuž[93], H. Mildner[100], A. Milic[36], C. D. Milke[44], D. W. Miller[39], L. S. Miller[34], A. Milov[169], D. A. Milstead[47a,47b], T. Min[14c], A. A. Minaenko[37], I. A. Minashvili[149b], L. Mince[59], A. I. Mincer[117], B. Mindur[86a], M. Mineev[38], Y. Mino[88], L. M. Mir[13], M. Miralles Lopez[163], M. Mironova[17a], A. Mishima[153], M. C. Missio[113], A. Mitra[167], V. A. Mitsou[163], Y. Mitsumori[111], O. Miu[155], P. S. Miyagawa[94], T. Mkrtchyan[63a], M. Mlinarevic[96], T. Mlinarevic[96], M. Mlynarikova[36], S. Mobius[19], P. Moder[48], P. Mogg[109], A. F. Mohammed[14a,14e], S. Mohapatra[41], G. Mokgatitswane[33g], L. Moleri[169], B. Mondal[141], S. Mondal[132], K. Mönig[48], E. Monnier[102], L. Monsonis Romero[163], J. Montejo Berlingen[13], M. Montella[119], F. Montereali[77a,77b], F. Monticelli[90], S. Monzani[69a,69c], N. Morange[66], A. L. Moreira De Carvalho[130a], M. Moreno Llácer[163], C. Moreno Martinez[56], P. Morettini[57b], S. Morgenstern[36], M. Morii[61], M. Morinaga[153], A. K. Morley[36], F. Morodei[75a,75b], L. Morvaj[36], P. Moschovakos[36], B. Moser[36], M. Mosidze[149b], T. Moskalets[54], P. Moskvitina[113], J. Moss[31,l], E. J. W. Moyse[103], O. Mtintsilana[33g], S. Muanza[102], J. Mueller[129], D. Muenstermann[91], R. Müller[19], G. A. Mullier[161], A. J. Mullin[32], J. J. Mullin[128], D. P. Mungo[155], D. Munoz Perez[163], F. J. Munoz Sanchez[101], M. Murin[101], W. J. Murray[134,167], A. Murrone[71a,71b], M. Muškinja[17a], C. Mwewa[29], A. G. Myagkov[37,a], A. J. Myers[8], G. Myers[68], M. Myska[132], B. P. Nachman[17a], O. Nackenhorst[49], A. Nag[50], K. Nagai[126], K. Nagano[84], J. L. Nagle[29,ai], E. Nagy[102], A. M. Nairz[36], Y. Nakahama[84], K. Nakamura[84], K. Nakkalil[5], H. Nanjo[124], R. Narayan[44], E. A. Narayanan[112], I. Naryshkin[37], M. Naseri[34], S. Nasri[159], C. Nass[24], G. Navarro[22a], J. Navarro-Gonzalez[163], R. Nayak[151], A. Nayaz[18], P. Y. Nechaeva[37], F. Nechansky[48], L. Nedic[126], T. J. Neep[20], A. Negri[73a,73b], M. Negrini[23b], C. Nellist[114], C. Nelson[104], K. Nelson[106], S. Nemecek[131], M. Nessi[36,h], M. S. Neubauer[162], F. Neuhaus[100], J. Neundorf[48], R. Newhouse[164], P. R. Newman[20], C. W. Ng[129], Y. W. Y. Ng[48], B. Ngair[35e], H. D. N. Nguyen[108], R. B. Nickerson[126],

R. Nicolaidou[135], J. Nielsen[136], M. Niemeyer[55], J. Niermann[36,55], N. Nikiforou[36], V. Nikolaenko[37,a], I. Nikolic-Audit[127], K. Nikolopoulos[20], P. Nilsson[29], I. Ninca[48], H. R. Nindhito[56], G. Ninio[151], A. Nisati[75a], N. Nishu[2], R. Nisius[110], J.-E. Nitschke[50], E. K. Nkadimeng[33g], T. Nobe[153], D. L. Noel[32], T. Nommensen[147], M. B. Norfolk[139], R. R. B. Norisam[96], B. J. Norman[34], M. Noury[35a], J. Novak[93], T. Novak[48], L. Novotny[132], R. Novotny[112], L. Nozka[122], K. Ntekas[160], N. M. J. Nunes De Moura Junior[83b], E. Nurse[96], J. Ocariz[127], A. Ochi[85], I. Ochoa[130a], S. Oerdek[48], J. T. Offermann[39], A. Ogrodnik[133], A. Oh[101], C. C. Ohm[144], H. Oide[84], R. Oishi[153], M. L. Ojeda[48], M. W. O'Keefe[92], Y. Okumura[153], L. F. Oleiro Seabra[130a], S. A. Olivares Pino[137d], D. Oliveira Damazio[29], D. Oliveira Goncalves[83a], J. L. Oliver[160], Ö. O. Öncel[54], A. P. O'Neill[19], A. Onofre[130a,130e], P. U. E. Onyisi[11], M. J. Oreglia[39], G. E. Orellana[90], D. Orestano[77a,77b], N. Orlando[13], R. S. Orr[155], V. O'Shea[59], L. M. Osojnak[128], R. Ospanov[62a], G. Otero y Garzon[30], H. Otono[89], P. S. Ott[63a], G. J. Ottino[17a], M. Ouchrif[35d], J. Ouellette[29], F. Ould-Saada[125], M. Owen[59], R. E. Owen[134], K. Y. Oyulmaz[21a], V. E. Ozcan[21a], F. Ozturk[87], N. Ozturk[8], S. Ozturk[82], H. A. Pacey[126], A. Pacheco Pages[13], C. Padilla Aranda[13], G. Padovano[75a,75b], S. Pagan Griso[17a], G. Palacino[68], A. Palazzo[70a,70b], S. Palestini[36], J. Pan[172], T. Pan[64a], D. K. Panchal[11], C. E. Pandini[114], J. G. Panduro Vazquez[95], H. D. Pandya[1], H. Pang[14b], P. Pani[48], G. Panizzo[69a,69c], L. Paolozzi[56], C. Papadatos[108], S. Parajuli[44], A. Paramonov[6], C. Paraskevopoulos[10], D. Paredes Hernandez[64b], K. R. Park[41], T. H. Park[155], M. A. Parker[32], F. Parodi[57a,57b], E. W. Parrish[115], V. A. Parrish[52], J. A. Parsons[41], U. Parzefall[54], B. Pascual Dias[108], L. Pascual Dominguez[151], E. Pasqualucci[75a], S. Passaggio[57b], F. Pastore[95], P. Pasuwan[47a,47b], P. Patel[87], U. M. Patel[51], J. R. Pater[101], T. Pauly[36], J. Pearkes[143], M. Pedersen[125], R. Pedro[130a], S. V. Peleganchuk[37], O. Penc[36], E. A. Pender[52], K. E. Penski[109], M. Penzin[37], B. S. Peralva[83d], A. P. Pereira Peixoto[60], L. Pereira Sanchez[47a,47b], D. V. Perepelitsa[29,ai], E. Perez Codina[156a], M. Perganti[10], L. Perini[71a,71b,*], H. Pernegger[36], O. Perrin[40], K. Peters[48], R. F. Y. Peters[101], B. A. Petersen[36], T. C. Petersen[42], E. Petit[102], V. Petousis[132], C. Petridou[152,e], A. Petrukhin[141], M. Pettee[17a], N. E. Pettersson[36], A. Petukhov[37], K. Petukhova[133], R. Pezoa[137f], L. Pezzotti[36], G. Pezzullo[172], T. M. Pham[170], T. Pham[105], P. W. Phillips[134], G. Piacquadio[145], E. Pianori[17a], F. Piazza[123], R. Piegaia[30], D. Pietreanu[27b], A. D. Pilkington[101], M. Pinamonti[69a,69c], J. L. Pinfold[2], B. C. Pinheiro Pereira[130a], A. E. Pinto Pinoargote[100,135], L. Pintucci[69a,69c], K. M. Piper[146], A. Pirttikoski[56], D. A. Pizzi[34], L. Pizzimento[64b], A. Pizzini[114], M.-A. Pleier[29], V. Plesanovs[54], V. Pleskot[133], E. Plotnikova[38], G. Poddar[4], R. Poettgen[98], L. Poggioli[127], I. Pokharel[55], S. Polacek[133], G. Polesello[73a], A. Poley[142,156a], R. Polifka[132], A. Polini[23b], C. S. Pollard[167], Z. B. Pollock[119], V. Polychronakos[29], E. Pompa Pacchi[75a,75b], D. Ponomarenko[113], L. Pontecorvo[36], S. Popa[27a], G. A. Popeneciu[27d], A. Poreba[36], D. M. Portillo Quintero[156a], S. Pospisil[132], M. A. Postill[139], P. Postolache[27c], K. Potamianos[167], P. A. Potepa[86a], I. N. Potrap[38], C. J. Potter[32], H. Potti[1], T. Poulsen[48], J. Poveda[163], M. E. Pozo Astigarraga[36], A. Prades Ibanez[163], J. Pretel[54], D. Price[101], M. Primavera[70a], M. A. Principe Martin[99], R. Privara[122], T. Procter[59], M. L. Proffitt[138], N. Proklova[128], K. Prokofiev[64c], G. Proto[110], S. Protopopescu[29], J. Proudfoot[6], M. Przybycien[86a], W. W. Przygoda[86b], J. E. Puddefoot[139], D. Pudzha[37], D. Pyatiizbyantseva[37], J. Qian[106], D. Qichen[101], Y. Qin[101], T. Qiu[52], A. Quadt[55], M. Queitsch-Maitland[101], G. Quetant[56], R. P. Quinn[164], G. Rabanal Bolanos[61], D. Rafanoharana[54], F. Ragusa[71a,71b], J. L. Rainbolt[39], J. A. Raine[56], S. Rajagopalan[29], E. Ramakoti[37], I. A. Ramirez-Berend[34], K. Ran[14e,48], N. P. Rapheeha[33g], H. Rasheed[27b], V. Raskina[127], D. F. Rassloff[63a], S. Rave[100], B. Ravina[55], I. Ravinovich[169], M. Raymond[36], A. L. Read[125], N. P. Readioff[139], D. M. Rebuzzi[73a,73b], G. Redlinger[29], A. S. Reed[110], K. Reeves[26], J. A. Reidelsturz[171], D. Reikher[151], A. Rej[49], C. Rembser[36], A. Renardi[48], M. Renda[27b], M. B. Rendel[110], F. Renner[48], A. G. Rennie[160], A. L. Rescia[48], S. Resconi[71a], M. Ressegotti[57a,57b], S. Rettie[36], J. G. Reyes Rivera[107], E. Reynolds[17a], O. L. Rezanova[37], P. Reznicek[133], N. Ribaric[91], E. Ricci[78a,78b], R. Richter[110], S. Richter[47a,47b], E. Richter-Was[86b], M. Ridel[127], S. Ridouani[35d], P. Rieck[117], P. Riedler[36], E. M. Riefel[47a,47b], J. O. Rieger[114], M. Rijssenbeek[145], A. Rimoldi[73a,73b], M. Rimoldi[36], L. Rinaldi[23a,23b], T. T. Rinn[29], M. P. Rinnagel[109], G. Ripellino[161], I. Riu[13], P. Rivadeneira[48], J. C. Rivera Vergara[165], F. Rizatdinova[121], E. Rizvi[94], B. A. Roberts[167], B. R. Roberts[17a], S. H. Robertson[104,w], D. Robinson[32], C. M. Robles Gajardo[137f], M. Robles Manzano[100], A. Robson[59], A. Rocchi[76a,76b], C. Roda[74a,74b], S. Rodriguez Bosca[63a], Y. Rodriguez Garcia[22a], A. Rodriguez Rodriguez[54], A. M. Rodríguez Vera[156b], S. Roe[36], J. T. Roemer[160], A. R. Roepe-Gier[136], J. Roggel[171], O. Røhne[125], R. A. Rojas[103], C. P. A. Roland[127], J. Roloff[29], A. Romaniouk[37], E. Romano[73a,73b], M. Romano[23b], A. C. Romero Hernandez[162], N. Rompotis[92], L. Roos[127], S. Rosati[75a], B. J. Rosser[39], E. Rossi[126],

E. Rossi[72a,72b], L. P. Rossi[57b], L. Rossini[54], R. Rosten[119], M. Rotaru[27b], B. Rottler[54], C. Rougier[102,aa], D. Rousseau[66], D. Rousso[32], A. Roy[162], S. Roy-Garand[155], A. Rozanov[102], Z. M. A. Rozario[59], Y. Rozen[150], X. Ruan[33g], A. Rubio Jimenez[163], A. J. Ruby[92], V. H. Ruelas Rivera[18], T. A. Ruggeri[1], A. Ruggiero[126], A. Ruiz-Martinez[163], A. Rummler[36], Z. Rurikova[54], N. A. Rusakovich[38], H. L. Russell[165], G. Russo[75a,75b], J. P. Rutherfoord[7], S. Rutherford Colmenares[32], K. Rybacki[91], M. Rybar[133], E. B. Rye[125], A. Ryzhov[44], J. A. Sabater Iglesias[56], P. Sabatini[163], H. F.-W. Sadrozinski[136], F. Safai Tehrani[75a], B. Safarzadeh Samani[134], M. Safdari[143], S. Saha[165], M. Sahinsoy[110], A. Saibel[163], M. Saimpert[135], M. Saito[153], T. Saito[153], D. Salamani[36], A. Salnikov[143], J. Salt[163], A. Salvador Salas[151], D. Salvatore[43a,43b], F. Salvatore[146], A. Salzburger[36], D. Sammel[54], D. Sampsonidis[152,e], D. Sampsonidou[123], J. Sánchez[163], A. Sanchez Pineda[4], V. Sanchez Sebastian[163], H. Sandaker[125], C. O. Sander[48], J. A. Sandesara[103], M. Sandhoff[171], C. Sandoval[22b], D. P. C. Sankey[134], T. Sano[88], A. Sansoni[53], L. Santi[75a,75b], C. Santoni[40], H. Santos[130a,130b], S. N. Santpur[17a], A. Santra[169], K. A. Saoucha[116b], J. G. Saraiva[130a,130d], J. Sardain[7], O. Sasaki[84], K. Sato[157], C. Sauer[63b], F. Sauerburger[54], E. Sauvan[4], P. Savard[155,af], R. Sawada[153], C. Sawyer[134], L. Sawyer[97], I. Sayago Galvan[163], C. Sbarra[23b], A. Sbrizzi[23a,23b], T. Scanlon[96], J. Schaarschmidt[138], P. Schacht[110], U. Schäfer[100], A. C. Schaffer[44,66], D. Schaile[109], R. D. Schamberger[145], C. Scharf[18], M. M. Schefer[19], V. A. Schegelsky[37], D. Scheirich[133], F. Schenck[18], M. Schernau[160], C. Scheulen[55], C. Schiavi[57a,57b], E. J. Schioppa[70a,70b], M. Schioppa[43a,43b], B. Schlag[143,n], K. E. Schleicher[54], S. Schlenker[36], J. Schmeing[171], M. A. Schmidt[171], K. Schmieden[100], C. Schmitt[100], N. Schmitt[100], S. Schmitt[48], L. Schoeffel[135], A. Schoening[63b], P. G. Scholer[54], E. Schopf[126], M. Schott[100], J. Schovancova[36], S. Schramm[56], F. Schroeder[171], T. Schroer[56], H.-C. Schultz-Coulon[63a], M. Schumacher[54], B. A. Schumm[136], Ph. Schune[135], A. J. Schuy[138], H. R. Schwartz[136], A. Schwartzman[143], T. A. Schwarz[106], Ph. Schwemling[135], R. Schwienhorst[107], A. Sciandra[136], G. Sciolla[26], F. Scuri[74a], C. D. Sebastiani[92], K. Sedlaczek[115], P. Seema[18], S. C. Seidel[112], A. Seiden[136], B. D. Seidlitz[41], C. Seitz[48], J. M. Seixas[83b], G. Sekhniaidze[72a], S. J. Sekula[44], L. Selem[60], N. Semprini-Cesari[23a,23b], D. Sengupta[56], V. Senthilkumar[163], L. Serin[66], L. Serkin[69a,69b], M. Sessa[76a,76b], H. Severini[120], F. Sforza[57a,57b], A. Sfyrla[56], E. Shabalina[55], R. Shaheen[144], J. D. Shahinian[128], D. Shaked Renous[169], L. Y. Shan[14a], M. Shapiro[17a], A. Sharma[36], A. S. Sharma[164], P. Sharma[80], S. Sharma[48], P. B. Shatalov[37], K. Shaw[146], S. M. Shaw[101], A. Shcherbakova[37], Q. Shen[5,62c], D. J. Sheppard[142], P. Sherwood[96], L. Shi[96], X. Shi[14a], C. O. Shimmin[172], J. D. Shinner[95], I. P. J. Shipsey[126], S. Shirabe[56,h], M. Shiyakova[38,u], J. Shlomi[169], M. J. Shochet[39], J. Shojaii[105], D. R. Shope[125], B. Shrestha[120], S. Shrestha[119,aj], E. M. Shrif[33g], M. J. Shroff[165], P. Sicho[131], A. M. Sickles[162], E. Sideras Haddad[33g], A. Sidoti[23b], F. Siegert[50], Dj. Sijacki[15], F. Sili[90], J. M. Silva[20], M. V. Silva Oliveira[29], S. B. Silverstein[47a], S. Simion[66], R. Simoniello[36], E. L. Simpson[59], H. Simpson[146], L. R. Simpson[106], N. D. Simpson[98], S. Simsek[82], S. Sindhu[55], P. Sinervo[155], S. Singh[155], S. Sinha[48], S. Sinha[101], M. Sioli[23a,23b], I. Siral[36], E. Sitnikova[48], S. Yu. Sivoklokov[37,*], J. Sjölin[47a,47b], A. Skaf[55], E. Skorda[20], P. Skubic[120], M. Slawinska[87], V. Smakhtin[169], B. H. Smart[134], J. Smiesko[36], S. Yu. Smirnov[37], Y. Smirnov[37], L. N. Smirnova[37,a], O. Smirnova[98], A. C. Smith[41], E. A. Smith[39], H. A. Smith[126], J. L. Smith[92], R. Smith[143], M. Smizanska[91], K. Smolek[132], A. A. Snesarev[37], S. R. Snider[155], H. L. Snoek[114], S. Snyder[29], R. Sobie[165,w], A. Soffer[151], C. A. Solans Sanchez[36], E. Yu. Soldatov[37], U. Soldevila[163], A. A. Solodkov[37], S. Solomon[26], A. Soloshenko[38], K. Solovieva[54], O. V. Solovyanov[40], V. Solovyev[37], P. Sommer[36], A. Sonay[13], W. Y. Song[156b], J. M. Sonneveld[114], A. Sopczak[132], A. L. Sopio[96], F. Sopkova[28b], I. R. Sotarriva Alvarez[154], V. Sothilingam[63a], O. J. Soto Sandoval[137b,137c], S. Sottocornola[68], R. Soualah[116b], Z. Soumaimi[35e], D. South[48], N. Soybelman[169], S. Spagnolo[70a,70b], M. Spalla[110], D. Sperlich[54], G. Spigo[36], S. Spinali[91], D. P. Spiteri[59], M. Spousta[133], E. J. Staats[34], A. Stabile[71a,71b], R. Stamen[63a], A. Stampekis[20], M. Standke[24], E. Stanecka[87], M. V. Stange[50], B. Stanislaus[17a], M. M. Stanitzki[48], B. Stapf[48], E. A. Starchenko[37], G. H. Stark[136], J. Stark[102,aa], D. M. Starko[156b], P. Staroba[131], P. Starovoitov[63a], S. Stärz[104], R. Staszewski[87], G. Stavropoulos[46], J. Steentoft[161], P. Steinberg[29], B. Stelzer[142,156a], H. J. Stelzer[129], O. Stelzer-Chilton[156a], H. Stenzel[58], T. J. Stevenson[146], G. A. Stewart[36], J. R. Stewart[121], M. C. Stockton[36], G. Stoicea[27b], M. Stolarski[130a], S. Stonjek[110], A. Straessner[50], J. Strandberg[144], S. Strandberg[47a,47b], M. Stratmann[171], M. Strauss[120], T. Strebler[102], P. Strizenec[28b], R. Ströhmer[166], D. M. Strom[123], R. Stroynowski[44], A. Strubig[47a,47b], S. A. Stucci[29], B. Stugu[16], J. Stupak[120], N. A. Styles[48], D. Su[143], S. Su[62a], W. Su[62d], X. Su[62a,66], K. Sugizaki[153], V. V. Sulin[37], M. J. Sullivan[92], D. M. S. Sultan[78a,78b], L. Sultanaliyeva[37], S. Sultansoy[3b], T. Sumida[88], S. Sun[106], S. Sun[170], O. Sunneborn Gudnadottir[161], N. Sur[102], M. R. Sutton[146], H. Suzuki[157],

M. Svatos[131], M. Swiatlowski[156a], T. Swirski[166], I. Sykora[28a], M. Sykora[133], T. Sykora[133], D. Ta[100], K. Tackmann[48,t], A. Taffard[160], R. Tafirout[156a], J. S. Tafoya Vargas[66], E. P. Takeva[52], Y. Takubo[84], M. Talby[102], A. A. Talyshev[37], K. C. Tam[64b], N. M. Tamir[151], A. Tanaka[153], J. Tanaka[153], R. Tanaka[66], M. Tanasini[57a,57b], Z. Tao[164], S. Tapia Araya[137f], S. Tapprogge[100], A. Tarek Abouelfadl Mohamed[107], S. Tarem[150], K. Tariq[14a], G. Tarna[27b,102], G. F. Tartarelli[71a], P. Tas[133], M. Tasevsky[131], E. Tassi[43a,43b], A. C. Tate[162], G. Tateno[153], Y. Tayalati[35e,v], G. N. Taylor[105], W. Taylor[156b], A. S. Tee[170], R. Teixeira De Lima[143], P. Teixeira-Dias[95], J. J. Teoh[155], K. Terashi[153], J. Terron[99], S. Terzo[13], M. Testa[53], R. J. Teuscher[155,w], A. Thaler[79], O. Theiner[56], N. Themistokleous[52], T. Theveneaux-Pelzer[102], O. Thielmann[171], D. W. Thomas[95], J. P. Thomas[20], E. A. Thompson[17a], P. D. Thompson[20], E. Thomson[128], Y. Tian[55], V. Tikhomirov[37,a], Yu. A. Tikhonov[37], S. Timoshenko[37], D. Timoshyn[133], E. X. L. Ting[1], P. Tipton[172], S. H. Tlou[33g], A. Tnourji[40], K. Todome[154], S. Todorova-Nova[133], S. Todt[50], M. Togawa[84], J. Tojo[89], S. Tokár[28a], K. Tokushuku[84], O. Toldaiev[68], R. Tombs[32], M. Tomoto[84,111], L. Tompkins[143,n], K. W. Topolnicki[86b], E. Torrence[123], H. Torres[102,aa], E. Torró Pastor[163], M. Toscani[30], C. Tosciri[39], M. Tost[11], D. R. Tovey[139], A. Traeet[16], I. S. Trandafir[27b], T. Trefzger[166], A. Tricoli[29], I. M. Trigger[156a], S. Trincaz-Duvoid[127], D. A. Trischuk[26], B. Trocmé[60], C. Troncon[71a], L. Truong[33c], M. Trzebinski[87], A. Trzupek[87], F. Tsai[145], M. Tsai[106], A. Tsiamis[152,e], P. V. Tsiareshka[37], S. Tsigaridas[156a], A. Tsirigotis[152,r], V. Tsiskaridze[155], E. G. Tskhadadze[149a], M. Tsopoulou[152,e], Y. Tsujikawa[88], I. I. Tsukerman[37], V. Tsulaia[17a], S. Tsuno[84], K. Tsuri[118], D. Tsybychev[145], Y. Tu[64b], A. Tudorache[27b], V. Tudorache[27b], A. N. Tuna[61], S. Turchikhin[57a,57b], I. Turk Cakir[3a], R. Turra[71a], T. Turtuvshin[38,x], P. M. Tuts[41], S. Tzamarias[152,e], P. Tzanis[10], E. Tzovara[100], F. Ukegawa[157], P. A. Ulloa Poblete[137b,137c], E. N. Umaka[29], G. Unal[36], M. Unal[11], A. Undrus[29], G. Unel[160], J. Urban[28b], P. Urquijo[105], P. Urrejola[137a], G. Usai[8], R. Ushioda[154], M. Usman[108], Z. Uysal[21b], V. Vacek[132], B. Vachon[104], K. O. H. Vadla[125], T. Vafeiadis[36], A. Vaitkus[96], C. Valderanis[109], E. Valdes Santurio[47a,47b], M. Valente[156a], S. Valentinetti[23a,23b], A. Valero[163], E. Valiente Moreno[163], A. Vallier[102,aa], J. A. Valls Ferrer[163], D. R. Van Arneman[114], T. R. Van Daalen[138], A. Van Der Graaf[49], P. Van Gemmeren[6], M. Van Rijnbach[36,125], S. Van Stroud[96], I. Van Vulpen[114], M. Vanadia[76a,76b], W. Vandelli[36], M. Vandenbroucke[135], E. R. Vandewall[121], D. Vannicola[151], L. Vannoli[57a,57b], R. Vari[75a], E. W. Varnes[7], C. Varni[17b], T. Varol[148], D. Varouchas[66], L. Varriale[163], K. E. Varvell[147], M. E. Vasile[27b], L. Vaslin[84], G. A. Vasquez[165], A. Vasyukov[38], F. Vazeille[40], T. Vazquez Schroeder[36], J. Veatch[31], V. Vecchio[101], M. J. Veen[103], I. Veliscek[126], L. M. Veloce[155], F. Veloso[130a,130c], S. Veneziano[75a], A. Ventura[70a,70b], S. Ventura Gonzalez[135], A. Verbytskyi[110], M. Verducci[74a,74b], C. Vergis[24], M. Verissimo De Araujo[83b], W. Verkerke[114], J. C. Vermeulen[114], C. Vernieri[143], M. Vessella[103], M. C. Vetterli[142,af], A. Vgenopoulos[152,e], N. Viaux Maira[137f], T. Vickey[139], O. E. Vickey Boeriu[139], G. H. A. Viehhauser[126], L. Vigani[63b], M. Villa[23a,23b], M. Villaplana Perez[163], E. M. Villhauer[52], E. Vilucchi[53], M. G. Vincter[34], G. S. Virdee[20], A. Vishwakarma[52], A. Visibile[114], C. Vittori[36], I. Vivarelli[146], E. Voevodina[110], F. Vogel[109], J. C. Voigt[50], P. Vokac[132], Yu. Volkotrub[86a], J. Von Ahnen[48], E. Von Toerne[24], B. Vormwald[36], V. Vorobel[133], K. Vorobev[37], M. Vos[163], K. Voss[141], J. H. Vossebeld[92], M. Vozak[114], L. Vozdecky[94], N. Vranjes[15], M. Vranjes Milosavljevic[15], M. Vreeswijk[114], R. Vuillermet[36], O. Vujinovic[100], I. Vukotic[39], S. Wada[157], C. Wagner[103], J. M. Wagner[17a], W. Wagner[171], S. Wahdan[171], H. Wahlberg[90], M. Wakida[111], J. Walder[134], R. Walker[109], W. Walkowiak[141], A. Wall[128], T. Wamorkar[6], A. Z. Wang[136], C. Wang[100], C. Wang[62c], H. Wang[17a], J. Wang[64a], R.-J. Wang[100], R. Wang[61], R. Wang[6], S. M. Wang[148], S. Wang[62b], T. Wang[62a], W. T. Wang[80], W. Wang[14a], X. Wang[14c], X. Wang[162], X. Wang[62c], Y. Wang[62d], Y. Wang[14c], Z. Wang[106], Z. Wang[51,62c,62d], Z. Wang[106], A. Warburton[104], R. J. Ward[20], N. Warrack[59], A. T. Watson[20], H. Watson[59], M. F. Watson[20], E. Watton[59,134], G. Watts[138], B. M. Waugh[96], C. Weber[29], H. A. Weber[18], M. S. Weber[19], S. M. Weber[63a], C. Wei[62a], Y. Wei[126], A. R. Weidberg[126], E. J. Weik[117], J. Weingarten[49], M. Weirich[100], C. Weiser[54], C. J. Wells[48], T. Wenaus[29], B. Wendland[49], T. Wengler[36], N. S. Wenke[110], N. Wermes[24], M. Wessels[63a], A. M. Wharton[91], A. S. White[61], A. White[8], M. J. White[1], D. Whiteson[160], L. Wickremasinghe[124], W. Wiedenmann[170], C. Wiel[50], M. Wielers[134], C. Wiglesworth[42], D. J. Wilbern[120], H. G. Wilkens[36], D. M. Williams[41], H. H. Williams[128], S. Williams[32], S. Willocq[103], B. J. Wilson[101], P. J. Windischhofer[39], F. I. Winkel[30], F. Winklmeier[123], B. T. Winter[54], J. K. Winter[101], M. Wittgen[143], M. Wobisch[97], Z. Wolffs[114], J. Wollrath[160], M. W. Wolter[87], H. Wolters[130a,130c], A. F. Wongel[48], E. L. Woodward[41], S. D. Worm[48], B. K. Wosiek[87], K. W. Woźniak[87], S. Wozniewski[55], K. Wraight[59], C. Wu[20], J. Wu[14a,14e], M. Wu[64a], M. Wu[113], S. L. Wu[170], X. Wu[56], Y. Wu[62a], Z. Wu[135], J. Wuerzinger[110,ad], T. R. Wyatt[101], B. M. Wynne[52], S. Xella[42], L. Xia[14c], M. Xia[14b],

J. Xiang[64c], M. Xie[62a], X. Xie[62a], S. Xin[14a,14e], A. Xiong[123], J. Xiong[17a], D. Xu[14a], H. Xu[62a], L. Xu[62a], R. Xu[128], T. Xu[106], Y. Xu[14b], Z. Xu[52], Z. Xu[14c], B. Yabsley[147], S. Yacoob[33a], Y. Yamaguchi[154], E. Yamashita[153], H. Yamauchi[157], T. Yamazaki[17a], Y. Yamazaki[85], J. Yan[62c], S. Yan[126], Z. Yan[25], H. J. Yang[62c,62d], H. T. Yang[62a], S. Yang[62a], T. Yang[64c], X. Yang[36], X. Yang[14a], Y. Yang[44], Y. Yang[62a], Z. Yang[62a], W.-M. Yao[17a], Y. C. Yap[48], H. Ye[14c], H. Ye[55], J. Ye[14a], S. Ye[29], X. Ye[62a], Y. Yeh[96], I. Yeletskikh[38], B. K. Yeo[17b], M. R. Yexley[96], P. Yin[41], K. Yorita[168], S. Younas[27b], C. J. S. Young[36], C. Young[143], C. Yu[14a,14e,ah], Y. Yu[62a], M. Yuan[106], R. Yuan[62b], L. Yue[96], M. Zaazoua[62a], B. Zabinski[87], E. Zaid[52], Z. K. Zak[87], T. Zakareishvili[149b], N. Zakharchuk[34], S. Zambito[56], J. A. Zamora Saa[137b,137d], J. Zang[153], D. Zanzi[54], O. Zaplatilek[132], C. Zeitnitz[171], H. Zeng[14a], J. C. Zeng[162], D. T. Zenger Jr[26], O. Zenin[37], T. Ženiš[28a], S. Zenz[94], S. Zerradi[35a], D. Zerwas[66], M. Zhai[14a,14e], B. Zhang[14c], D. F. Zhang[139], J. Zhang[62b], J. Zhang[6], K. Zhang[14a,14e], L. Zhang[14c], P. Zhang[14a,14e], R. Zhang[170], S. Zhang[106], S. Zhang[44], T. Zhang[153], X. Zhang[62c], X. Zhang[62b], Y. Zhang[5,62c], Y. Zhang[96], Y. Zhang[14c], Z. Zhang[17a], Z. Zhang[66], H. Zhao[138], T. Zhao[62b], Y. Zhao[136], Z. Zhao[62a], A. Zhemchugov[38], J. Zheng[14c], K. Zheng[162], X. Zheng[62a], Z. Zheng[143], D. Zhong[162], B. Zhou[106], H. Zhou[7], N. Zhou[62c], Y. Zhou[7], C. G. Zhu[62b], J. Zhu[106], Y. Zhu[62c], Y. Zhu[62a], X. Zhuang[14a], K. Zhukov[37], V. Zhulanov[37], N. I. Zimine[38], J. Zinsser[63b], M. Ziolkowski[141], L. Živković[15], A. Zoccoli[23a,23b], K. Zoch[61], T. G. Zorbas[139], O. Zormpa[46], W. Zou[41], L. Zwalinski[36]

[1] Department of Physics, University of Adelaide, Adelaide, Australia
[2] Department of Physics, University of Alberta, Edmonton, AB, Canada
[3] [(a)]Department of Physics, Ankara University, Ankara, Türkiye; [(b)]Division of Physics, TOBB University of Economics and Technology, Ankara, Türkiye
[4] LAPP, Université Savoie Mont Blanc, CNRS/IN2P3, Annecy, France
[5] APC, Université Paris Cité, CNRS/IN2P3, Paris, France
[6] High Energy Physics Division, Argonne National Laboratory, Argonne, IL, USA
[7] Department of Physics, University of Arizona, Tucson, AZ, USA
[8] Department of Physics, University of Texas at Arlington, Arlington, TX, USA
[9] Physics Department, National and Kapodistrian University of Athens, Athens, Greece
[10] Physics Department, National Technical University of Athens, Zografou, Greece
[11] Department of Physics, University of Texas at Austin, Austin, TX, USA
[12] Institute of Physics, Azerbaijan Academy of Sciences, Baku, Azerbaijan
[13] Institut de Física d'Altes Energies (IFAE), Barcelona Institute of Science and Technology, Barcelona, Spain
[14] [(a)]Institute of High Energy Physics, Chinese Academy of Sciences, Beijing, China; [(b)]Physics Department, Tsinghua University, Beijing, China; [(c)]Department of Physics, Nanjing University, Nanjing, China; [(d)]School of Science, Shenzhen Campus of Sun Yat-sen University, Shenzhen, China; [(e)]University of Chinese Academy of Science (UCAS), Beijing, China
[15] Institute of Physics, University of Belgrade, Belgrade, Serbia
[16] Department for Physics and Technology, University of Bergen, Bergen, Norway
[17] [(a)]Physics Division, Lawrence Berkeley National Laboratory, Berkeley, CA, USA; [(b)]University of California, Berkeley, CA, USA
[18] Institut für Physik, Humboldt Universität zu Berlin, Berlin, Germany
[19] Albert Einstein Center for Fundamental Physics and Laboratory for High Energy Physics, University of Bern, Bern, Switzerland
[20] School of Physics and Astronomy, University of Birmingham, Birmingham, UK
[21] [(a)]Department of Physics, Bogazici University, Istanbul, Türkiye; [(b)]Department of Physics Engineering, Gaziantep University, Gaziantep, Türkiye; [(c)]Department of Physics, Istanbul University, Istanbul, Türkiye
[22] [(a)]Facultad de Ciencias y Centro de Investigaciónes, Universidad Antonio Nariño, Bogotá, Colombia; [(b)]Departamento de Física, Universidad Nacional de Colombia, Bogotá, Colombia
[23] [(a)]Dipartimento di Fisica e Astronomia A. Righi, Università di Bologna, Bologna, Italy; [(b)]INFN Sezione di Bologna, Bologna, Italy
[24] Physikalisches Institut, Universität Bonn, Bonn, Germany
[25] Department of Physics, Boston University, Boston, MA, USA
[26] Department of Physics, Brandeis University, Waltham, MA, USA

[27] [(a)]Transilvania University of Brasov, Brasov, Romania; [(b)]Horia Hulubei National Institute of Physics and Nuclear Engineering, Bucharest, Romania; [(c)]Department of Physics, Alexandru Ioan Cuza University of Iasi, Iasi, Romania; [(d)]Physics Department, National Institute for Research and Development of Isotopic and Molecular Technologies, Cluj-Napoca, Romania; [(e)]National University of Science and Technology Politechnica, Bucharest, Romania; [(f)]West University in Timisoara, Timisoara, Romania; [(g)]Faculty of Physics, University of Bucharest, Bucharest, Romania
[28] [(a)]Faculty of Mathematics, Physics and Informatics, Comenius University, Bratislava, Slovak Republic; [(b)]Department of Subnuclear Physics, Institute of Experimental Physics of the Slovak Academy of Sciences, Kosice, Slovak Republic
[29] Physics Department, Brookhaven National Laboratory, Upton, NY, USA
[30] Departamento de Física, y CONICET, Facultad de Ciencias Exactas y Naturales, Instituto de Física de Buenos Aires (IFIBA), Universidad de Buenos Aires, Buenos Aires, Argentina
[31] California State University, Fresno, CA, USA
[32] Cavendish Laboratory, University of Cambridge, Cambridge, UK
[33] [(a)]Department of Physics, University of Cape Town, Cape Town, South Africa; [(b)]iThemba Labs, Western Cape, South Africa; [(c)]Department of Mechanical Engineering Science, University of Johannesburg, Johannesburg, South Africa; [(d)]National Institute of Physics, University of the Philippines Diliman, Quezon City, Philippines; [(e)]Department of Physics, University of South Africa, Pretoria, South Africa; [(f)]University of Zululand, KwaDlangezwa, South Africa; [(g)]School of Physics, University of the Witwatersrand, Johannesburg, South Africa
[34] Department of Physics, Carleton University, Ottawa, ON, Canada
[35] [(a)]Faculté des Sciences Ain Chock, Réseau Universitaire de Physique des Hautes Energies-Université Hassan II, Casablanca, Morocco; [(b)]Faculté des Sciences, Université Ibn-Tofail, Kénitra, Morocco; [(c)]Faculté des Sciences Semlalia, Université Cadi Ayyad, LPHEA-Marrakech, Morocco; [(d)]LPMR, Faculté des Sciences, Université Mohamed Premier, Oujda, Morocco; [(e)]Faculté des sciences, Université Mohammed V, Rabat, Morocco; [(f)]Institute of Applied Physics, Mohammed VI Polytechnic University, Ben Guerir, Morocco
[36] CERN, Geneva, Switzerland
[37] Affiliated with an Institute Covered by a Cooperation Agreement with CERN, Geneva, Switzerland
[38] Affiliated with an International Laboratory Covered by a Cooperation Agreement with CERN, Geneva, Switzerland
[39] Enrico Fermi Institute, University of Chicago, Chicago, IL, USA
[40] LPC, Université Clermont Auvergne, CNRS/IN2P3, Clermont-Ferrand, France
[41] Nevis Laboratory, Columbia University, Irvington, NY, USA
[42] Niels Bohr Institute, University of Copenhagen, Copenhagen, Denmark
[43] [(a)]Dipartimento di Fisica, Università della Calabria, Rende, Italy; [(b)]INFN Gruppo Collegato di Cosenza, Laboratori Nazionali di Frascati, Frascati, Italy
[44] Physics Department, Southern Methodist University, Dallas, TX, USA
[45] Physics Department, University of Texas at Dallas, Richardson, TX, USA
[46] National Centre for Scientific Research "Demokritos", Agia Paraskevi, Greece
[47] [(a)]Department of Physics, Stockholm University, Stockholm, Sweden; [(b)]Oskar Klein Centre, Stockholm, Sweden
[48] Deutsches Elektronen-Synchrotron DESY, Hamburg and Zeuthen, Germany
[49] Fakultät Physik, Technische Universität Dortmund, Dortmund, Germany
[50] Institut für Kern- und Teilchenphysik, Technische Universität Dresden, Dresden, Germany
[51] Department of Physics, Duke University, Durham, NC, USA
[52] SUPA-School of Physics and Astronomy, University of Edinburgh, Edinburgh, UK
[53] INFN e Laboratori Nazionali di Frascati, Frascati, Italy
[54] Physikalisches Institut, Albert-Ludwigs-Universität Freiburg, Freiburg, Germany
[55] II. Physikalisches Institut, Georg-August-Universität Göttingen, Göttingen, Germany
[56] Département de Physique Nucléaire et Corpusculaire, Université de Genève, Geneva, Switzerland
[57] [(a)]Dipartimento di Fisica, Università di Genova, Genoa, Italy; [(b)]INFN Sezione di Genova, Genoa, Italy
[58] II. Physikalisches Institut, Justus-Liebig-Universität Giessen, Giessen, Germany
[59] SUPA-School of Physics and Astronomy, University of Glasgow, Glasgow, UK
[60] LPSC, Université Grenoble Alpes, CNRS/IN2P3, Grenoble INP, Grenoble, France
[61] Laboratory for Particle Physics and Cosmology, Harvard University, Cambridge, MA, USA
[62] [(a)]Department of Modern Physics and State Key Laboratory of Particle Detection and Electronics, University of Science and Technology of China, Hefei, China; [(b)]Institute of Frontier and Interdisciplinary Science and Key Laboratory of

Particle Physics and Particle Irradiation (MOE), Shandong University, Qingdao, China; [c]School of Physics and Astronomy, Shanghai Jiao Tong University, Key Laboratory for Particle Astrophysics and Cosmology (MOE), SKLPPC, Shanghai, China; [d]Tsung-Dao Lee Institute, Shanghai, China; [e]School of Physics and Microelectronics, Zhengzhou University, Zhengzhou, China
63 [a]Kirchhoff-Institut für Physik, Ruprecht-Karls-Universität Heidelberg, Heidelberg, Germany; [b]Physikalisches Institut, Ruprecht-Karls-Universität Heidelberg, Heidelberg, Germany
64 [a]Department of Physics, Chinese University of Hong Kong, Shatin, N.T., Hong Kong, China; [b]Department of Physics, University of Hong Kong, Hong Kong, China; [c]Department of Physics and Institute for Advanced Study, Hong Kong University of Science and Technology, Clear Water Bay, Kowloon, Hong Kong, China
65 Department of Physics, National Tsing Hua University, Hsinchu, Taiwan
66 IJCLab, Université Paris-Saclay, CNRS/IN2P3, 91405 Orsay, France
67 Centro Nacional de Microelectrónica (IMB-CNM-CSIC), Barcelona, Spain
68 Department of Physics, Indiana University, Bloomington, IN, USA
69 [a]INFN Gruppo Collegato di Udine, Sezione di Trieste, Udine, Italy; [b]ICTP, Trieste, Italy; [c]Dipartimento Politecnico di Ingegneria e Architettura, Università di Udine, Udine, Italy
70 [a]INFN Sezione di Lecce, Lecce, Italy; [b]Dipartimento di Matematica e Fisica, Università del Salento, Lecce, Italy
71 [a]INFN Sezione di Milano, Milan, Italy; [b]Dipartimento di Fisica, Università di Milano, Milan, Italy
72 [a]INFN Sezione di Napoli, Naples, Italy; [b]Dipartimento di Fisica, Università di Napoli, Naples, Italy
73 [a]INFN Sezione di Pavia, Pavia, Italy; [b]Dipartimento di Fisica, Università di Pavia, Pavia, Italy
74 [a]INFN Sezione di Pisa, Pisa, Italy; [b]Dipartimento di Fisica E. Fermi, Università di Pisa, Pisa, Italy
75 [a]INFN Sezione di Roma, Rome, Italy; [b]Dipartimento di Fisica, Sapienza Università di Roma, Rome, Italy
76 [a]INFN Sezione di Roma Tor Vergata, Rome, Italy; [b]Dipartimento di Fisica, Università di Roma Tor Vergata, Rome, Italy
77 [a]INFN Sezione di Roma Tre, Rome, Italy; [b]Dipartimento di Matematica e Fisica, Università Roma Tre, Rome, Italy
78 [a]INFN-TIFPA, Povo, Italy; [b]Università degli Studi di Trento, Trento, Italy
79 Universität Innsbruck, Department of Astro and Particle Physics, Innsbruck, Austria
80 University of Iowa, Iowa City, IA, USA
81 Department of Physics and Astronomy, Iowa State University, Ames, IA, USA
82 Istinye University, Sariyer, Istanbul, Türkiye
83 [a]Departamento de Engenharia Elétrica, Universidade Federal de Juiz de Fora (UFJF), Juiz de Fora, Brazil; [b]Universidade Federal do Rio De Janeiro COPPE/EE/IF, Rio de Janeiro, Brazil; [c]Instituto de Física, Universidade de São Paulo, São Paulo, Brazil; [d]Rio de Janeiro State University, Rio de Janeiro, Brazil
84 KEK, High Energy Accelerator Research Organization, Tsukuba, Japan
85 Graduate School of Science, Kobe University, Kobe, Japan
86 [a]Faculty of Physics and Applied Computer Science, AGH University of Krakow, Krakow, Poland; [b]Marian Smoluchowski Institute of Physics, Jagiellonian University, Krakow, Poland
87 Institute of Nuclear Physics Polish Academy of Sciences, Krakow, Poland
88 Faculty of Science, Kyoto University, Kyoto, Japan
89 Research Center for Advanced Particle Physics and Department of Physics, Kyushu University, Fukuoka , Japan
90 Instituto de Física La Plata, Universidad Nacional de La Plata and CONICET, La Plata, Argentina
91 Physics Department, Lancaster University, Lancaster, UK
92 Oliver Lodge Laboratory, University of Liverpool, Liverpool, UK
93 Department of Experimental Particle Physics, Jožef Stefan Institute and Department of Physics, University of Ljubljana, Ljubljana, Slovenia
94 School of Physics and Astronomy, Queen Mary University of London, London, UK
95 Department of Physics, Royal Holloway University of London, Egham, UK
96 Department of Physics and Astronomy, University College London, London, UK
97 Louisiana Tech University, Ruston, LA, USA
98 Fysiska Institutionen, Lunds Universitet, Lund, Sweden
99 Departamento de Física Teorica C-15 and CIAFF, Universidad Autónoma de Madrid, Madrid, Spain
100 Institut für Physik, Universität Mainz, Mainz, Germany
101 School of Physics and Astronomy, University of Manchester, Manchester, UK
102 CPPM, Aix-Marseille Université, CNRS/IN2P3, Marseille, France

[103] Department of Physics, University of Massachusetts, Amherst, MA, USA
[104] Department of Physics, McGill University, Montreal, QC, Canada
[105] School of Physics, University of Melbourne, Victoria, Australia
[106] Department of Physics, University of Michigan, Ann Arbor, MI, USA
[107] Department of Physics and Astronomy, Michigan State University, East Lansing, MI, USA
[108] Group of Particle Physics, University of Montreal, Montreal, QC, Canada
[109] Fakultät für Physik, Ludwig-Maximilians-Universität München, Munich, Germany
[110] Max-Planck-Institut für Physik (Werner-Heisenberg-Institut), Munich, Germany
[111] Graduate School of Science and Kobayashi-Maskawa Institute, Nagoya University, Nagoya, Japan
[112] Department of Physics and Astronomy, University of New Mexico, Albuquerque, NM, USA
[113] Institute for Mathematics, Astrophysics and Particle Physics, Radboud University/Nikhef, Nijmegen, The Netherlands
[114] Nikhef National Institute for Subatomic Physics and University of Amsterdam, Amsterdam, The Netherlands
[115] Department of Physics, Northern Illinois University, DeKalb, IL, USA
[116] [(a)]New York University Abu Dhabi, Abu Dhabi, United Arab Emirates; [(b)]University of Sharjah, Sharjah, United Arab Emirates
[117] Department of Physics, New York University, New York, NY, USA
[118] Ochanomizu University, Otsuka, Bunkyo-ku, Tokyo, Japan
[119] Ohio State University, Columbus, OH, USA
[120] Homer L. Dodge Department of Physics and Astronomy, University of Oklahoma, Norman, OK, USA
[121] Department of Physics, Oklahoma State University, Stillwater, OK, USA
[122] Joint Laboratory of Optics, Palacký University, Olomouc, Czech Republic
[123] Institute for Fundamental Science, University of Oregon, Eugene, OR, USA
[124] Graduate School of Science, Osaka University, Osaka, Japan
[125] Department of Physics, University of Oslo, Oslo, Norway
[126] Department of Physics, Oxford University, Oxford, UK
[127] LPNHE, Sorbonne Université, Université Paris Cité, CNRS/IN2P3, Paris, France
[128] Department of Physics, University of Pennsylvania, Philadelphia, PA, USA
[129] Department of Physics and Astronomy, University of Pittsburgh, Pittsburgh, PA, USA
[130] [(a)]Laboratório de Instrumentação e Física Experimental de Partículas-LIP, Lisbon, Portugal; [(b)]Departamento de Física, Faculdade de Ciências, Universidade de Lisboa, Lisbon, Portugal; [(c)]Departamento de Física, Universidade de Coimbra, Coimbra, Portugal; [(d)]Centro de Física Nuclear da Universidade de Lisboa, Lisbon, Portugal; [(e)]Departamento de Física, Universidade do Minho, Braga, Portugal; [(f)]Departamento de Física Teórica y del Cosmos, Universidad de Granada, Granada, Spain; [(g)]Departamento de Física, Instituto Superior Técnico, Universidade de Lisboa, Lisbon, Portugal
[131] Institute of Physics of the Czech Academy of Sciences, Prague, Czech Republic
[132] Czech Technical University in Prague, Prague, Czech Republic
[133] Faculty of Mathematics and Physics, Charles University, Prague, Czech Republic
[134] Particle Physics Department, Rutherford Appleton Laboratory, Didcot, UK
[135] IRFU, CEA, Université Paris-Saclay, Gif-sur-Yvette, France
[136] Santa Cruz Institute for Particle Physics, University of California Santa Cruz, Santa Cruz, CA, USA
[137] [(a)]Departamento de Física, Pontificia Universidad Católica de Chile, Santiago, Chile; [(b)]Millennium Institute for Subatomic physics at high energy frontier (SAPHIR), Santiago, Chile; [(c)]Instituto de Investigación Multidisciplinario en Ciencia y Tecnología, y Departamento de Física, Universidad de La Serena, La Serena, Chile; [(d)]Department of Physics, Universidad Andres Bello, Santiago, Chile; [(e)]Instituto de Alta Investigación, Universidad de Tarapacá, Arica, Chile; [(f)]Departamento de Física, Universidad Técnica Federico Santa María, Valparaíso, Chile
[138] Department of Physics, University of Washington, Seattle, WA, USA
[139] Department of Physics and Astronomy, University of Sheffield, Sheffield, UK
[140] Department of Physics, Shinshu University, Nagano, Japan
[141] Department Physik, Universität Siegen, Siegen, Germany
[142] Department of Physics, Simon Fraser University, Burnaby, BC, Canada
[143] SLAC National Accelerator Laboratory, Stanford, CA, USA
[144] Department of Physics, Royal Institute of Technology, Stockholm, Sweden
[145] Departments of Physics and Astronomy, Stony Brook University, Stony Brook, NY, USA
[146] Department of Physics and Astronomy, University of Sussex, Brighton, UK

[147] School of Physics, University of Sydney, Sydney, Australia
[148] Institute of Physics, Academia Sinica, Taipei, Taiwan
[149] [(a)]E. Andronikashvili Institute of Physics, Iv. Javakhishvili Tbilisi State University, Tbilisi, Georgia; [(b)]High Energy Physics Institute, Tbilisi State University, Tbilisi, Georgia; [(c)]University of Georgia, Tbilisi, Georgia
[150] Department of Physics, Technion, Israel Institute of Technology, Haifa, Israel
[151] Raymond and Beverly Sackler School of Physics and Astronomy, Tel Aviv University, Tel Aviv, Israel
[152] Department of Physics, Aristotle University of Thessaloniki, Thessaloniki, Greece
[153] International Center for Elementary Particle Physics and Department of Physics, University of Tokyo, Tokyo, Japan
[154] Department of Physics, Tokyo Institute of Technology, Tokyo, Japan
[155] Department of Physics, University of Toronto, Toronto, ON, Canada
[156] [(a)]TRIUMF, Vancouver, BC, Canada; [(b)]Department of Physics and Astronomy, York University, Toronto, ON, Canada
[157] Division of Physics and Tomonaga Center for the History of the Universe, Faculty of Pure and Applied Sciences, University of Tsukuba, Tsukuba, Japan
[158] Department of Physics and Astronomy, Tufts University, Medford, MA, USA
[159] United Arab Emirates University, Al Ain, United Arab Emirates
[160] Department of Physics and Astronomy, University of California Irvine, Irvine, CA, USA
[161] Department of Physics and Astronomy, University of Uppsala, Uppsala, Sweden
[162] Department of Physics, University of Illinois, Urbana, IL, USA
[163] Instituto de Física Corpuscular (IFIC), Centro Mixto Universidad de Valencia-CSIC, Valencia, Spain
[164] Department of Physics, University of British Columbia, Vancouver, BC, Canada
[165] Department of Physics and Astronomy, University of Victoria, Victoria, BC, Canada
[166] Fakultät für Physik und Astronomie, Julius-Maximilians-Universität Würzburg, Würzburg, Germany
[167] Department of Physics, University of Warwick, Coventry, UK
[168] Waseda University, Tokyo, Japan
[169] Department of Particle Physics and Astrophysics, Weizmann Institute of Science, Rehovot, Israel
[170] Department of Physics, University of Wisconsin, Madison, WI, USA
[171] Fakultät für Mathematik und Naturwissenschaften, Fachgruppe Physik, Bergische Universität Wuppertal, Wuppertal, Germany
[172] Department of Physics, Yale University, New Haven, CT, USA

[a] Also Affiliated with an Institute Covered by a Cooperation Agreement with CERN, Geneva, Switzerland
[b] Also at An-Najah National University, Nablus, Palestine
[c] Also at Borough of Manhattan Community College, City University of New York, New York, NY, USA
[d] Also at Center for High Energy Physics, Peking University, Beijing, China
[e] Also at Center for Interdisciplinary Research and Innovation (CIRI-AUTH), Thessaloniki, Greece
[f] Also at Centro Studi e Ricerche Enrico Fermi, Rome, Italy
[g] Also at CERN, Geneva, Switzerland
[h] Also at Département de Physique Nucléaire et Corpusculaire, Université de Genève, Geneva, Switzerland
[i] Also at Departament de Fisica de la Universitat Autonoma de Barcelona, Barcelona, Spain
[j] Also at Department of Financial and Management Engineering, University of the Aegean, Chios, Greece
[k] Also at Department of Physics, Ben Gurion University of the Negev, Beer Sheva, Israel
[l] Also at Department of Physics, California State University, Sacramento, USA
[m] Also at Department of Physics, King's College London, London, UK
[n] Also at Department of Physics, Stanford University, Stanford, CA, USA
[o] Also at Department of Physics, University of Fribourg, Fribourg, Switzerland
[p] Also at Department of Physics, University of Thessaly, Thessaly, Greece
[q] Also at Department of Physics, Westmont College, Santa Barbara, USA
[r] Also at Hellenic Open University, Patras, Greece
[s] Also at Institucio Catalana de Recerca i Estudis Avancats, ICREA, Barcelona, Spain
[t] Also at Institut für Experimentalphysik, Universität Hamburg, Hamburg, Germany
[u] Also at Institute for Nuclear Research and Nuclear Energy (INRNE) of the Bulgarian Academy of Sciences, Sofia, Bulgaria
[v] Also at Institute of Applied Physics, Mohammed VI Polytechnic University, Ben Guerir, Morocco

[w] Also at Institute of Particle Physics (IPP), Canada
[x] Also at Institute of Physics and Technology, Mongolian Academy of Sciences, Ulaanbaatar, Mongolia
[y] Also at Institute of Physics, Azerbaijan Academy of Sciences, Baku, Azerbaijan
[z] Also at Institute of Theoretical Physics, Ilia State University, Tbilisi, Georgia
[aa] Also at L2IT, Université de Toulouse, CNRS/IN2P3, UPS, Toulouse, France
[ab] Also at Lawrence Livermore National Laboratory, Livermore, USA
[ac] Also at National Institute of Physics, University of the Philippines Diliman, Quezon City, Philippines
[ad] Also at Technical University of Munich, Munich, Germany
[ae] Also at The Collaborative Innovation Center of Quantum Matter (CICQM), Beijing, China
[af] Also at TRIUMF, Vancouver, BC, Canada
[ag] Also at Università di Napoli Parthenope, Naples, Italy
[ah] Also at University of Chinese Academy of Sciences (UCAS), Beijing, China
[ai] Also at Department of Physics, University of Colorado Boulder, Boulder, CO, USA
[aj] Also at Washington College, Chestertown, MD, USA
[ak] Also at Physics Department, Yeditepe University, Istanbul, Türkiye
* Deceased